

Washington University in St. Louis

## Washington University Open Scholarship

---

Arts & Sciences Electronic Theses and  
Dissertations

Arts & Sciences

---

Summer 8-15-2018

### Identification of Bhlhe40 and Irg1 as essential regulators of the inflammatory response to *Mycobacterium tuberculosis*

Jeremy Peter Huynh  
*Washington University in St. Louis*

Follow this and additional works at: [https://openscholarship.wustl.edu/art\\_sci\\_etds](https://openscholarship.wustl.edu/art_sci_etds)



Part of the [Allergy and Immunology Commons](#), [Immunology and Infectious Disease Commons](#), [Medical Immunology Commons](#), and the [Microbiology Commons](#)

---

#### Recommended Citation

Huynh, Jeremy Peter, "Identification of Bhlhe40 and Irg1 as essential regulators of the inflammatory response to *Mycobacterium tuberculosis*" (2018). *Arts & Sciences Electronic Theses and Dissertations*. 1628.

[https://openscholarship.wustl.edu/art\\_sci\\_etds/1628](https://openscholarship.wustl.edu/art_sci_etds/1628)

This Dissertation is brought to you for free and open access by the Arts & Sciences at Washington University Open Scholarship. It has been accepted for inclusion in Arts & Sciences Electronic Theses and Dissertations by an authorized administrator of Washington University Open Scholarship. For more information, please contact [digital@wumail.wustl.edu](mailto:digital@wumail.wustl.edu).

WASHINGTON UNIVERSITY IN ST. LOUIS

Division of Biology and Biomedical Sciences Program in  
Molecular Microbiology and Microbial Pathogenesis

Dissertation Examination Committee:

Christina L. Stallings, Chair

Adrianus C.M. Boon

Brian T. Edelson

Michael J. Holtzman

Shabaana A. Khader

L. David Sibley

Identification of Bhlhe40 and Irg1 as Essential Regulators of the Inflammatory Response to  
*Mycobacterium tuberculosis*

by

Jeremy P. Huynh

A dissertation presented to  
The Graduate School  
of Washington University in Saint Louis in  
partial fulfillment of the  
requirements for the degree  
of Doctor of Philosophy

August 2018  
Saint Louis, Missouri

© 2018, Jeremy P. Huynh

## Table of Contents

List of Figures .....	iv
List of Tables .....	vi
List of Abbreviations .....	vii
Acknowledgments.....	ix
Abstract of the Dissertation .....	xi
<b>Chapter 1: Introduction</b> .....	1
Tuberculosis.....	2
The immune response to <i>Mycobacterium tuberculosis</i> .....	4
Bhlhe40 .....	10
Irg1 .....	12
<b>Chapter 2: the role of Bhlhe40 in control of <i>Mycobacterium tuberculosis</i> infection</b> .....	17
Introduction.....	18
Results.....	20
Lower <i>BHLHE40</i> expression is associated with active tuberculosis .....	20
Bhlhe40 is required to control mycobacterial infection .....	20
Bhlhe40 deficiency leads to severe lung inflammation .....	22
Neutrophil and monocyte inflammation do not drive susceptibility in <i>Bhlhe40</i> <sup>-/-</sup> mice. ....	26
Bhlhe40 is required within hematopoietic cells .....	28
Bhlhe40 enables control of <i>Mtb</i> in the context of T cell deficiency .....	31
Bhlhe40 is required in CD11c <sup>+</sup> , Zbtb46 <sup>+</sup> , and T cells.....	32
Bhlhe40 deficiency alters cytokine transcription after exposure to <i>Mtb</i> .....	37
Bhlhe40 suppresses IL-10 production during <i>in vivo</i> <i>Mtb</i> infection.....	40
Bhlhe40 suppresses IL-10 expression in myeloid cells <i>in vitro</i> .....	43
Bhlhe40 binds directly to the <i>Il10</i> locus in T <sub>H</sub> 1 cells and myeloid cells .....	47
IL-10 deficiency protects <i>Bhlhe40</i> <sup>-/-</sup> mice from <i>Mtb</i> infection .....	48
Discussion.....	50
Experimental Procedures .....	55

<b>Chapter 3: the role of Irg1 in control of <i>Mycobacterium tuberculosis</i> infection</b> .....	69
Abstract .....	70
Results.....	73
Irg1 enables resistance to a subset of pathogenic mycobacteria. ....	73
Irg1 modulates lung inflammatory responses after <i>Mtb</i> infection. ....	77
Neutrophil depletion extends the survival of <i>Irg1</i> <sup>-/-</sup> mice during <i>Mtb</i> infection. ....	79
Expression of Irg1 in LysM <sup>+</sup> and CD11c <sup>+</sup> cells enables survival of <i>Mtb</i> infection. ....	83
Susceptibility of <i>Irg1</i> <sup>-/-</sup> mice is dependent on <i>Mtb</i> expression of PDIM and ESX-1, but not ICL1 .....	85
Irg1 is not required for induction of ROS and NOS2 or control of <i>Mtb</i> in macrophages.....	88
Irg1 regulates inflammatory responses in myeloid cells during <i>Mtb</i> infection.....	91
Irg1 is the sole source of itaconate in the lung during <i>Mtb</i> infection.....	95
Discussion.....	96
Experimental Procedures .....	99
<b>Chapter 4: Conclusions</b> .....	110
Introduction.....	111
Discussion and Future Directions .....	111
Bhlhe40 expression patterns.....	111
Bhlhe40 and IL-10-dependent control of <i>Mtb</i> infection .....	113
IL-10-independent roles for Bhlhe40 in <i>Mtb</i> infection .....	117
Irg1 and restriction of neutrophil-mediated immunopathology .....	119
Myeloid cell-specific requirements for Irg1.....	120
Impact of Irg1 on adaptive immunity.....	121
Direct antibacterial roles for Irg1 in <i>Mtb</i> infection .....	122
Explanations for virulence of $\Delta icl1$ <i>Mtb</i> in <i>Irg1</i> <sup>-/-</sup> mice.....	124
Itaconate catabolism and vitamin B12 deficiency.....	125
Possible cross-talk between Bhlhe40 and Irg1 .....	126
Closing remarks .....	127
References.....	129

## List of Figures

### Chapter 2: The role of Bhlhe40 in control of *Mycobacterium tuberculosis* infection

Figure 1. Lower <i>BHLHE40</i> expression is specifically associated with active tuberculosis. ....	21
Figure 2. Bhlhe40 is required to control mycobacterial infection. ....	23
Figure 3. Bhlhe40 deficiency leads to severe lung inflammation. ....	24
Figure 4. Bhlhe40 deficiency leads to neutrophil-dominated inflammation. ....	27
Figure 5. Neutrophils and monocytes do not drive susceptibility in <i>Bhlhe40</i> <sup>-/-</sup> mice. ....	29
Figure 6. Bhlhe40 is expressed and required in hematopoietic cells. ....	30
Figure 7. Bhlhe40 enables control of <i>Mtb</i> in the context of T cell deficiency. ....	33
Figure 8. Bhlhe40 is required in CD11c <sup>+</sup> , Zbtb46 <sup>+</sup> , and T cells. ....	35
Figure 9. Bhlhe40 deficiency alters cytokine transcription after exposure to <i>Mtb</i> . ....	38
Figure 10. Bhlhe40 deficiency does not cause IL-10 overexpression in the absence of infection	41
Figure 11. Bhlhe40 deficiency causes overexpression of IL-10 during <i>Mtb</i> infection. ....	42
Figure 12. Bhlhe40 represses IL-10 in myeloid cells after <i>Mtb</i> stimulation. ....	44
Figure 13. Bhlhe40 directly binds the <i>Il10</i> locus in myeloid and lymphoid cells. ....	46
Figure 14. IL-10 deficiency protects <i>Bhlhe40</i> <sup>-/-</sup> mice from <i>Mtb</i> infection. ....	49
Figure 15. Model of Bhlhe40 function during <i>Mtb</i> infection. ....	54
Figure 16. Flow cytometry gating strategy used in Bhlhe40 experiments. ....	61

### Chapter 3: The role of Irg1 in control of *Mycobacterium tuberculosis* infection

Figure 17. Irg1 enables resistance to a subset of pathogenic mycobacteria. ....	74
Figure 18. GFP- <i>Mtb</i> is as virulent as WT <i>Mtb</i> . ....	75
Figure 19. Irg1 modulates cellular inflammation after <i>Mtb</i> infection. ....	76
Figure 20. Irg1 modulates inflammatory cytokine production after <i>Mtb</i> infection. ....	78
Figure 21. Neutrophil depletion enhances the survival of <i>Irg1</i> <sup>-/-</sup> mice. ....	80
Figure 22. Expression of Irg1 in myeloid cell subsets enables survival of <i>Mtb</i> infection. ....	82
Figure 23. Susceptibility of <i>Irg1</i> <sup>-/-</sup> mice is dependent on <i>Mtb</i> expression of PDIM and ESX-1, but not ICL1. ....	86
Figure 24. Irg1 is not required for induction of ROS, NOS2, or control of <i>Mtb</i> in BMDMs. ....	88
Figure 25. Irg1 alters transcription of inflammatory and metabolic genes in neutrophils during <i>Mtb</i> infection. ....	90

Figure 26. Irg1 alters the transcriptional signature of <i>Mtb</i> infected bone marrow-derived macrophages. ....	93
Figure 27. Irg1 is the sole source of lung itaconate during <i>Mtb</i> infection and intraperitoneal administration of dimethyl itaconate fails to rescue <i>Irg1</i> <sup>-/-</sup> susceptibility. ....	94
Figure 28. Model of Irg1 function during <i>Mtb</i> infection. ....	99
Figure 29. Flow cytometry gating strategy used in Irg1 experiments. ....	107

## List of Tables

### Chapter 2: the role of Bhlhe40 in *Mtb* infection

Table 1. Primers used for qRT-PCR in Bhlhe40 experiments.....	64
---	----

## List of Abbreviations

10BiT	IL-10 BAC-in transgene
BAC	Bacterial artificial chromosome
BCG	<i>Mycobacterium bovis</i> Bacillus Calmette-Guérin
Bhlhe40	Basic helix-loop-helix family, member e40
BMDM	Bone marrow-derived, M-CSF-cultured macrophage
CD	Cluster of differentiation
CFU	Colony-forming units
DC	Dendritic cell
dpi	days post-infection
EAE	Experimental autoimmune encephalomyelitis
fl/fl	Denotes that the preceding gene has an exon flanked by LoxP sites
GFP	Green fluorescent protein
GM-CSF	Granulocyte-macrophage colony stimulating factor
HDAC	Histone deacetylase
H&E	Haematoxylin and eosin
ICL	isocitrate lyase
IFN	Interferon
IGRA	Interferon- $\gamma$ release assay
IL	Interleukin
Irg1	Immune-regulated Gene 1
M-CSF	Macrophage colony stimulating factor

MFI	(Geometric) Mean fluorescence intensity
<i>Mtb</i>	<i>Mycobacterium tuberculosis</i>
NOS2	nitric oxide synthase 2 (also known as iNOS)
ROS	reactive oxygen species
TB-IRIS	tuberculosis-associated immune reconstitution inflammatory syndrome
TCA	Tricarboxylic acid
TNF- $\alpha$	Tumor necrosis factor $\alpha$
Tg	Transgenic
T <sub>H</sub>	T helper cell
WT	Wild type

## Acknowledgments

I have had the privilege to work with an incredible number of brilliant, hard-working, and friendly people over the course of my dissertation research. First and foremost is Christina Stallings, my PI and mentor. She has given me wonderful scientific training and more of her time, patience, and enthusiasm than I deserve. Brian Edelson has provided immunological guidance, exciting project ideas and reagents, and an unquenchable enthusiasm for science. Jacqueline Kimmey and Chih-Chung “Jerry” Lin personally taught me the scientific techniques that made my projects possible and offered advice and support when it was most needed. Michael Diamond, Maxim Artyomov, Sharmila Nair, and my thesis committee deserve credit for the guidance, reagents, and expertise that made my projects possible.

My friends and colleagues in the Stallings laboratory have been truly enjoyable to work and spend time with. Many thanks are due to Katherine Mann, Leslie Weiss, Ashley Garner, Kelly Flentie, and all my more recently joined lab mates for their help and enthusiasm. I would also like to acknowledge my friends here in Saint Louis and back in North Carolina who have provided me with much needed breaks from science and reminded me that there is a world outside of the BSL3. Special thanks are due to Jerome Prusa and Natalie Omattage for their friendship, scientific advice, and support.

I'll end by thanking the people it all started with: my family. Thank you Mom, Dad, Forrest, and Keegan for putting up with me, keeping me grounded and curious, and inspiring me to be a better, weirder person.

Jeremy Huynh

*Washington University in Saint Louis*

*August 2018*

Dedicated to my parents,  
Phuon and Deborah Huynh  
for encouraging me to challenge myself and for their unconditional love.

## **Abstract of the Dissertation**

Identification of Bhlhe40 and Irg1 as Essential Regulators of the Inflammatory Response to  
*Mycobacterium tuberculosis*

by

Jeremy P. Huynh

Doctor of Philosophy in Biology and Biomedical Sciences

Molecular Microbiology and Microbial Pathogenesis

Washington University in St. Louis, 2018

Professor Christina L. Stallings, Chair

Protective immune responses to *Mycobacterium tuberculosis* (*Mtb*) must induce bactericidal functions while minimizing damage to the lung. Such responses require precise control of pro- and anti-inflammatory factors to regulate the recruitment and function of protective immune cells but the mechanisms by which this control is exerted remain incompletely defined. Basic helix-loop-helix family, member e40 (Bhlhe40) is a transcription factor known to regulate production of pro- and anti-inflammatory cytokines that affect protective immunity to *Mtb*. Immune-responsive Gene 1 (Irg1) is an enzyme that generates itaconate, a metabolite with potential anti-inflammatory and antibacterial roles during *Mtb* infection. The impact of Bhlhe40 and Irg1 on protective immunity to *Mtb* was unknown prior to the studies detailed in this dissertation.

We utilized genetically deficient mice to assess the roles of Bhlhe40 and Irg1 expression on control of *in vivo* *Mtb* infection. We found that Bhlhe40 enables protective immune responses to *Mtb* by restricting expression of the anti-inflammatory cytokine IL-10 and is required in T

cells and CD11c<sup>+</sup> cells. Bhlhe40 does so by repressing *III0* transcription, likely by direct binding to the *III0* locus. Additionally, we discovered that Irg1 functions in LysM<sup>+</sup> and CD11c<sup>+</sup> cells to prevent neutrophil-mediated immunopathology. Irg1 expression restricts inflammatory responses in myeloid cells at a transcriptional level, likely through production of the metabolite itaconate. Thus, Bhlhe40 and Irg1 directly and indirectly tune the inflammatory response to *Mtb* at a transcriptional level. These findings advance our understanding of protective immunity to *Mtb* by revealing novel mechanisms used by specific immune cell types to promote bacterial killing and restrict pathologic inflammation.

# **Chapter 1**

## **Introduction**

## **Tuberculosis**

*Mycobacterium tuberculosis* (*Mtb*) is an acid-fast bacterium of the phylum *Actinobacteria* and the etiological agent of the disease tuberculosis. *Mtb* is an obligate human pathogen first isolated by Robert Koch in 1882 that has infected and co-evolved with humans for an estimated 70,000 years.<sup>1,2</sup> The burden that tuberculosis imposes on global public health is illustrated by a 2017 report by the World Health Organization estimating that 1.7 billion people are currently infected with *Mtb* and that tuberculosis has become the leading cause of death by a single infectious agent.<sup>3</sup> Infection is initiated when aerosolized *Mtb* bacilli are expelled from an infected host and inhaled by a new, susceptible host. Pulmonary tuberculosis is the most common form of the disease, but dissemination to extrapulmonary sites can occur.<sup>4</sup> Tuberculosis encompasses a dynamic spectrum of disease states that vary by the presence of disease symptoms and transmissibility. Despite this heterogeneity, patients are broadly classified as having either latent or active tuberculosis.<sup>4</sup> Approximately 90% of *Mtb* infections result in latent tuberculosis, a disease state in which the host immune system limits bacterial replication and minimizes lung pathology. Latent tuberculosis patients are generally asymptomatic and unable to transmit infection but maintain a life-long risk of progression to active tuberculosis. In active tuberculosis, which accounts for approximately 10% of cases, the immune response is unable to control bacterial replication and patients are able to transmit infection.<sup>5,6</sup> Active tuberculosis patients exhibit symptoms such as fever, fatigue, weight loss, persistent coughing, and coughing up blood.<sup>6</sup>

Most *Mtb* infections can be treated by a six month course of antibiotic therapy consisting of isoniazid, rifampicin, pyrazinamide, and ethambutol for two months, followed by isoniazid and rifampicin for four months. The long duration and potential toxicity of current antibiotic

treatment regimens often leads to problems with patient adherence. Incomplete patient adherence promotes the development of multiple drug resistant-tuberculosis (MDR-TB) strains resistant to rifampicin or isoniazid and extremely drug resistant-tuberculosis (XDR-TB), defined as MDR-TB with resistance to a second-line antibiotic.<sup>3</sup> MDR-TB cases currently comprise 4% of new cases and 19% of previously treated cases.<sup>3</sup> The emergence and spread of difficult to treat MDR-TB and potentially incurable XDR-TB strains highlights the need for therapeutics with novel mechanisms of action and shorter treatment durations. Therapies that target the host immune system to enhance bacterial control and minimize lung pathology have gained interest as an approach for treating drug resistant *Mtb* but their development requires a detailed understanding of how the immune system succeeds or fails in controlling *Mtb* infection.

Vaccines are another attractive approach for combating *Mtb* and also rely on knowledge of basic host-pathogen interaction. *Mycobacterium bovis* Bacillus Calmette-Guérin (BCG) is currently the only approved vaccine for prevention of tuberculosis. BCG was developed in the early 1900s by attenuation of a *Mycobacterium bovis* isolate through serial passage *in vitro* for 13 years.<sup>7</sup> Over 3 billion doses of BCG have been administered and it has proven effective at preventing severe forms of disseminated tuberculosis such as tuberculous meningitis and military tuberculosis in infants.<sup>8,9</sup> However, its efficacy in preventing pulmonary tuberculosis in adolescents and adults varies wildly and reports of protective efficacy range from 0-80%.<sup>10-12</sup> BCG vaccination has successfully reduced infant mortality, but a vaccine that prevents establishment of pulmonary infection in adults will be necessary to halt transmission and ultimately eradicate tuberculosis.

## **The immune response to *Mycobacterium tuberculosis***

Our current understanding of how the immune system controls *Mtb* infection is largely based on study of humans that develop severe forms of tuberculosis and animal disease models. These approaches enable identification of gene signatures and specific genes that are associated with or contribute to different disease outcomes. Once identified, protective genes can be mechanistically investigated in animal models to determine their function and the quality of the immune responses they promote, then further assessed for relevance in humans. Such studies have advanced understanding of the pathogenesis of tuberculosis and will inform the development of novel diagnostics, therapeutics, and vaccines to treat and prevent tuberculosis.

The genetically tractable mouse model of *Mtb* infection has proven to be an invaluable tool for dissecting how host genes and immunological processes affect disease outcome. The Cre-Flox conditional gene deletion system has proven especially useful in this regard.<sup>13</sup> In this system, LoxP DNA recognition sites flanking an exon of a gene of interest are inserted into the genome to generate a “flanked by LoxP” or “floxed” allele, denoted by “*Gene*<sup>fl/fl</sup>”.<sup>14</sup> When floxed mice are crossed to mice that express Cre recombinase under the control of cell-type specific promoters, Cre mediates deletion of the DNA sequence between the LoxP sites. This generates a mouse with conditional deletion of the gene of interest only in specified cell types and is a highly useful tool for identification of the key cell types that must express the gene as well as study of gene function in those cell types.

Experimental tuberculosis infection in mice is initiated by delivering 100-200 colony-forming units (CFUs) of aerosolized *Mtb* to the lungs of each mouse. After deposition in the lung bacilli are phagocytosed by lung resident alveolar macrophages. Alveolar macrophages fail to clear infection and produce inflammatory signals that recruit other innate immune cell types such

as neutrophils, monocytes, macrophages, and dendritic cells (DCs) to the site of infection. These recruited innate immune cell types also fail to clear infection and *Mtb* replicates logarithmically in them until the onset of adaptive immunity. Around 8-9 days post-infection (dpi) DCs migrating from the lung arrive in the mediastinal lymph node. Once in the lymph node DCs present *Mtb* antigens to naïve T cells and secrete IL-12, causing the naïve T cells to expand and differentiate into T helper (T<sub>H</sub>) 1-polarized effector cells. T cells are an essential component of protective immunity to *Mtb*, as demonstrated by the propensity of HIV/AIDS patients with latent tuberculosis to progress to active tuberculosis as their T cell counts decline.<sup>15,16</sup> Antigen-specific T cells reach the lung 18-20 dpi where they release cytokines, such as interferon (IFN)- $\gamma$ , that activate bactericidal effector mechanisms and limit pathologic inflammatory responses. *Mtb* burden in the lung peaks around 21 dpi, decreases slightly, then remains constant for the remainder of the lifetime of the mouse. The arrival of effector T cells in the lung enables the formation of structured innate and adaptive immune cell aggregates, referred to as “granulomas” in humans and “lesions” in mice that confine *Mtb* bacilli.<sup>17</sup> Human immune responses to *Mtb* are thought to progress in a similar fashion as those in mice, although differences in the amount of time before an antigen-specific immune response can be detected suggest that the timing of each event differs by species.<sup>18</sup> These immune responses are sufficient to limit infection to a latent, non-transmissible state in 90% of infected humans. Thus, a primary function of the immune system is to induce a durable, protective response that activates bactericidal mechanisms and limits the spread of *Mtb* while avoiding pathologic responses.

### *IFN- $\gamma$ -mediated protective responses to Mtb*

One important component of protective immunity to *Mtb* is IFN- $\gamma$ . IFN- $\gamma$  is a cytokine that activates cell-autonomous and non-autonomous mechanisms enabling control of *Mtb*. The importance of IFN- $\gamma$  for control of *Mtb* infection is demonstrated by the predisposition to severe tuberculosis in humans with in-born errors in genes essential for IFN- $\gamma$ -producing T<sub>H</sub>1 responses and genes in the IFN- $\gamma$  signaling pathway.<sup>19-22</sup> Protective cell-intrinsic effects of IFN- $\gamma$  signaling include increased fusion of *Mtb*-containing phagosomes with bactericidal low pH lysosomes via induction of LRG47 (also known as IRGM1),<sup>23</sup> restriction of neutrophil survival,<sup>24</sup> prevention of T<sub>H</sub>1 cell apoptosis by LRG47-mediated autophagy,<sup>25</sup> expression of antimicrobial peptides such as cathelicidin and  $\beta$ -defensin in human cells<sup>26</sup> or ubiquicidin-like peptides in mouse cells,<sup>27</sup> induction of reactive oxygen species (ROS),<sup>28</sup> divalent cation restriction or hyperaccumulation,<sup>29,30</sup> and tryptophan limitation via indoleamine-2,3-dioxygenase (IDO).<sup>31</sup> Although many studies have posited a critical role for IFN- $\gamma$ -driven canonical autophagy, this process is dispensable for *in vivo* control of *Mtb* infection.<sup>32</sup> IFN- $\gamma$  is typically considered a pro-inflammatory cytokine but it also prevents pathologic neutrophil-dominated inflammation by restricting neutrophil recruitment<sup>24</sup> and inducing nitric oxide production via nitric oxide synthase 2 (NOS2).<sup>33</sup> Mice deficient in IFN- $\gamma$  production or signaling rapidly succumb to *Mtb* infection.<sup>23,34,35</sup> T<sub>H</sub>1-polarized CD4<sup>+</sup> T cells are the primary source of IFN- $\gamma$  and production of IFN- $\gamma$  is necessary but not sufficient for the full extent of their protective capacity.<sup>24,36,37</sup> Natural killer cell production of IFN- $\gamma$  also contributes to resistance in the context of T cell deficiency.<sup>38</sup> Collectively, these studies demonstrate that IFN- $\gamma$  is necessary, but not sufficient, for host resistance to *Mtb* and mechanisms that support its production and function play important roles in protective immunity to *Mtb*.

IL-10 is an immunoregulatory cytokine that suppresses the production and effects of IFN- $\gamma$ .<sup>39,40</sup> Nearly all innate and adaptive immune cell types, with the exception of plasmacytoid DCs, can produce IL-10 during *Mtb* infection and it is detrimental for control of *Mtb* infection.<sup>41-44</sup> IL-10 antagonizes IFN- $\gamma$ -associated pathways by suppressing macrophage responsiveness to IFN- $\gamma$ ,<sup>39,45,46</sup> modulating T-helper (T<sub>H</sub>) 1 cell IFN- $\gamma$  production,<sup>40,42,43,47</sup> and restricting production of the hallmark T<sub>H</sub>1-inducing cytokine IL-12.<sup>47-51</sup> IL-10 can also inhibit DC migration to the lung-draining lymph node<sup>49</sup> and limit secretion of myeloid cell-derived proinflammatory cytokines.<sup>45,52,53</sup> Many observations have suggested an important role for IL-10 in human tuberculosis pathogenesis. Human single nucleotide polymorphisms in the *IL10* gene promoter have been linked to tuberculosis susceptibility in particular ethnic groups.<sup>54-60</sup> Patients with active tuberculosis express higher amounts of IL-10 in their lung pleural fluid,<sup>61</sup> bronchoalveolar lavage fluid,<sup>62</sup> sputum,<sup>63,64</sup> and serum<sup>65,66</sup> as compared to healthy controls or controls with non-mycobacterial lung disease. IL-10 has also been shown to decrease the amount of IFN- $\gamma$  produced by *Mtb*-stimulated peripheral blood mononuclear cells from active tuberculosis patients<sup>67,68</sup> or tuberculin skin test-positive individuals<sup>69</sup> and can block phagosome maturation in *Mtb* infected human monocyte-derived macrophages.<sup>41</sup> Surprisingly, studies on mice globally deficient in IL-10 production have either reported no role for IL-10<sup>70,71</sup> or that it causes a mild impairment of control during chronic *Mtb* infection.<sup>42-44,48</sup> This impairment has been attributed to IL-10 production by T cells and CD11c<sup>+</sup> cells.<sup>44</sup> *In vivo* over-expression of IL-10 by T cells or macrophages has also supported a negative role for IL-10 during chronic *Mtb* infection, although differences in mouse genetic background and the transgenic promoters used have resulted in an unclear picture.<sup>40,50</sup>

Given that IL-10 has the potential to negatively impact key protective immune responses to *Mtb* but global loss of IL-10 function does not result in excessive reduction of *Mtb* burden in mice, it is likely that cell-autonomous mechanisms that limit IL-10 induction pathways are important for control of *Mtb*. Mycobacteria directly stimulate IL-10 production from monocytes, macrophages, DCs, and neutrophils via signaling through pattern-recognition receptors such as toll-like receptor 2 (TLR2)<sup>72,73</sup> and the C-type lectin receptor DC-specific ICAM3-grabbing non-integrin (DC-SIGN).<sup>74</sup> In addition, different T<sub>H</sub> cell subsets and innate immune cell types produce IL-10 in response to distinct combinations of cytokines.<sup>75</sup> These signals lead to the binding of diverse transcription factors at promoter and enhancer elements within the *Il10* locus to activate transcription within myeloid and lymphoid cells.<sup>75-77</sup> Many transcription factors restricting IL-10 production have been identified, but none have been assessed for IL-10-dependent roles during *in vivo* *Mtb* infection. The transcription factors known to repress *Il10* in innate immune cells include B cell CLL/lymphoma 3 (Bcl3),<sup>78</sup> histone deacetylase 11 (HDAC11),<sup>79</sup> poly(ADP-ribose) polymerase 1 (PARP-1),<sup>80</sup> nuclear receptor subfamily 1 group D member 1 (NR1D1, Rev-erba),<sup>81</sup> programmed cell death protein 4 (PCDP4),<sup>82</sup> and interferon regulatory factor 5 (IRF5)<sup>83</sup> in macrophages as well as class II MHC transactivator (CIITA) in DCs.<sup>84</sup> NR1D1 is notable for its role in promoting *Mtb* control by human macrophages through repression of IL-10.<sup>81</sup> Repressors of *Il10* in adaptive immune cells include E26 transformation specific 1 (ETS-1)<sup>85</sup> and PU.1<sup>86</sup> in T cells as well as forkhead box D3 (Foxd3) in B cells.<sup>87</sup> The ability of IL-10 to suppress the actions of IFN- $\gamma$  suggests that it must be carefully regulated in order to allow the induction and maintenance of protective responses to *Mtb* but the mechanisms of its regulation during *Mtb* infection are poorly characterized.

### *Pathologic responses to Mtb*

In addition to establishing protective responses the immune system must also avoid responses that fail to restrict *Mtb* replication or cause lung pathology. The importance of strictly controlling the immune response to *Mtb* is illustrated by tuberculosis-associated immune reconstitution inflammatory syndrome (TB-IRIS), a condition that occurs in 18% of HIV/*Mtb* co-infected patients as anti-retroviral therapy allows the immune system to recover from the effects of HIV infection. During TB-IRIS the recovering immune system mounts an excessive pro-inflammatory cytokine and cellular response to *Mtb* that causes immunopathology and worsens tuberculosis-associated symptoms.<sup>88</sup> Murine studies have generated complementary data showing that even cellular and cytokine responses normally associated with resistance to *Mtb* can be pathological if produced in excess.<sup>89,90</sup>

Studies in humans and mice have suggested that neutrophils are key mediators of inflammatory responses that poorly control *Mtb* and cause lung pathology. In active tuberculosis patients neutrophils are the predominantly infected cell type<sup>91</sup> and active tuberculosis patients can be identified by a neutrophil-driven transcriptional signature.<sup>92</sup> Tuberculosis patients with higher blood neutrophil counts also have increased disease severity<sup>93</sup> and higher case fatality rates.<sup>94</sup> Acutely susceptible mouse strains often display neutrophilic inflammation that can cause or result from failed immunity to *Mtb*.<sup>24,32,95,96</sup> Neutrophils are thought to mediate susceptibility to *Mtb* by releasing pro-inflammatory cytokines that can exacerbate non-protective inflammation as well as proteases and reactive oxygen species (ROS) that damage the lung.<sup>32,97,98</sup> The resulting pathology may be an important cause of granuloma breakdown and lung cavitation, processes that allow *Mtb* to re-enter the respiratory tract and transmit to a new host.<sup>4</sup> In addition to causing lung pathology, neutrophils also provide a nutrient-rich replicative niche for *Mtb*.<sup>33</sup>

Restraint of pro-inflammatory cytokine production and neutrophilic inflammation are important components of protective immunity to *Mtb*, but the mechanisms by which the immune system controls these processes remain poorly defined.

## **Bhlhe40**

Homologs of the gene now officially named Bhlhe40 (**b**asic **h**elix-**l**oop-**h**elix family member **e40**) were identified by several independent groups and have thus has been referred to by multiple names (Bhlhb2, Clast5, Dec1, Sharp2, Stra13) over the course of its study. For simplicity, this gene will henceforth be referred to as “Bhlhe40,” regardless of the homolog name used in the original study. Bhlhe40 is a 411 amino acid protein of the basic helix-loop-helix (BHLH)-Orange subfamily of transcription factors which are characterized by a basic patch that enables DNA binding, a helix-loop-helix domain that enables protein dimerization, and an Orange domain conferring functional specificities that vary by family member.<sup>99</sup> Bhlhe40 is expressed in a wide range of organs and cell types and can be induced by many different stimuli. Cell types that express Bhlhe40 include neurons,<sup>100</sup> chondrocytes,<sup>101</sup> epithelial cells,<sup>102–104</sup> innate immune cells,<sup>105–108</sup> and adaptive immune cells.<sup>109–111</sup> Stimuli inducing Bhlhe40 transcription include growth factors,<sup>100,104</sup> light,<sup>112</sup> starvation,<sup>102</sup> hypoxia,<sup>103,113</sup> anti-CD3 stimulation,<sup>109</sup> anti-CD28 stimulation,<sup>114</sup> hormones,<sup>101,115–117</sup> retinoic acid,<sup>101,102</sup> cytokines,<sup>105,108</sup> and B cell receptor cross-linking.<sup>118</sup> Roles for Bhlhe40 have been reported in a wide variety of cellular processes including cell cycle arrest,<sup>102,110,119</sup> apoptosis,<sup>120,121</sup> epithelial to mesenchymal transition,<sup>122</sup> cellular differentiation,<sup>101,123</sup> circadian rhythm,<sup>112</sup> stress response,<sup>102,103,113</sup> and immune system function. Bhlhe40 typically mediates these effects by transcriptional repression and several mechanisms of action have been reported. Direct binding to the class B E-box DNA motif

CACGTG allows Bhlhe40 to repress transcription, likely by occluding other transcription factors.<sup>112,124</sup> Bhlhe40 can also associate with other transcription factors and inhibit their ability to bind DNA and activate transcription<sup>102,112,125,126</sup> or recruit histone deacetylases to modify chromatin accessibility.<sup>102,127</sup> Many of the stimuli that induce Bhlhe40 expression are present in the *Mtb* infected lung, suggesting that it may be operative in lung resident and recruited cells during infection.

### *Bhlhe40 in the immune system*

Study of Bhlhe40 in the context of the immune system has been limited to lymphoid cell types and multiple studies have identified it as an important regulator of cytokine production, particularly in T cells and in the context of autoimmunity. Naïve *Bhlhe40*<sup>-/-</sup> mice appear phenotypically similar to wild-type (WT) mice.<sup>109</sup> Bhlhe40 expression has no effect on  $\alpha\beta$  T cell polarization but promotes expression of many pro-inflammatory cytokines such as IL-2, IL-4, IL-17, IFN- $\gamma$ , and GM-CSF while suppressing anti-inflammatory IL-10.<sup>109,114,128,129</sup> Bhlhe40 expression is also required for production of IFN- $\gamma$  by invariant natural killer T cells<sup>111</sup> and GM-CSF by  $\gamma\delta$  T cells.<sup>128</sup> Bhlhe40 may also promote systemic immune regulatory functions by associating with the transcription factor Runx1 to sustain IL-2R $\alpha$  (CD25) expression, thus enabling long-term maintenance of regulatory T cells.<sup>130</sup> Aged *Bhlhe40*<sup>-/-</sup> mice exhibit an accumulation of activated B cells that may be due to a role for Bhlhe40 in inhibiting B cell activation and proliferation by blocking cell cycle progression.<sup>110</sup> Notably, Bhlhe40-deficient mice are highly resistant to the induction of experimental autoimmune encephalomyelitis (EAE), a T cell-driven model of multiple sclerosis-like neuroinflammation.<sup>108,114,128,129</sup> Resistance to EAE in *Bhlhe40*<sup>-/-</sup> mice is attributed to their decreased *Csf2* (GM-CSF) and increased *Il10* (IL-

10) transcription in T cells and is dependent on signaling through the IL-10 receptor.<sup>114,128</sup>

Collectively, these studies demonstrate that Bhlhe40 regulates multiple T cell functions important for control of *Mtb* infection, such as production of IL-10 and IFN- $\gamma$ . Despite its potential impact on *Mtb* infection, no prior studies had examined the role of Bhlhe40 in the context of an infectious disease.

## **Irg1**

**I**mmune-**r**esponsive **G**ene **1** (Irg1, also known as *cis*-aconitate decarboxylase 1 [Acod1]) is an enzyme that links cellular metabolism to immune system functionality. It is distinct from the similarly named Immunity-Related GTPase (IRG) proteins that play a prominent role in *Toxoplasma gondii* infection. Innate immune cells such as macrophages, microglia, and neutrophils strongly express Irg1 upon activation,<sup>131–133</sup> whereupon it localizes to the mitochondria.<sup>134,135</sup> Irg1 is also inducible in non-hematopoietic cell types such as uterine epithelial cells in response to progesterone signaling<sup>136</sup> and neurons.<sup>137</sup> Many types of pro-inflammatory stimuli such as lipopolysaccharide (LPS)<sup>131,138</sup> and CpG methylated DNA,<sup>134</sup> as well as viral,<sup>137,139</sup> parasitic,<sup>132,134</sup> and bacterial infection<sup>135,140</sup> are able to induce Irg1 expression. Notably, such bacterial species include both pathogenic and non-pathogenic mycobacteria.<sup>141,142</sup> Induction by these stimuli is likely mediated by inflammatory cytokines such as IFN- $\alpha$ , IFN- $\beta$ , IFN- $\gamma$ , TNF- $\alpha$ , IL-1 $\beta$ , and IL-17.<sup>134,135</sup> Upon its expression, Irg1 catalyzes the decarboxylation of *cis*-aconitate, a metabolic intermediate of the tricarboxylic acid (TCA) cycle, thus producing the metabolite itaconic acid. This enzymatic activity is mediated by its five *cis*-aconitate decarboxylase domains (CADs), all of which are fully conserved in mouse and human Irg1.<sup>143</sup> Itaconic acid is often referred to as itaconate, its neutral salt. Dimethyl itaconate (DI), an

itaconate derivative with increased membrane permeability, has been used to study the biological functions of itaconate.<sup>138</sup> Thus far, Irg1 is only known source of itaconate in mammalian cells and no itaconate-independent functions for Irg1 have been described. Reports of Irg1 induction during mycobacterial infection and the presence of Irg1-inducing cytokines in *Mtb* infected lungs strongly suggest that Irg1 is expressed during *Mtb* infection.

### *Antibacterial roles for Irg1*

Irg1 has gained attention for the potential of its metabolite product, itaconate, to function as an endogenous antibacterial effector molecule by inhibiting isocitrate lyase (ICL).<sup>144</sup> ICLs function in two important metabolic pathways, the glyoxylate shunt and the methylcitrate cycle.<sup>145,146</sup> The glyoxylate shunt enables certain bacteria and fungi to utilize fatty acids as alternative carbon sources and persist under what would otherwise be nutrient-limiting conditions by modifying their tricarboxylic acid (TCA) cycle.<sup>147</sup> The TCA cycle generates the essential cellular energy source adenosine triphosphate (ATP), but its intermediates can also be diverted into biosynthetic pathways. The glyoxylate shunt is an anaplerotic pathway that bypasses two decarboxylation reactions of the TCA cycle, allowing *Mtb* to use even-chain fatty acid substrates, such as host-derived lipids, to replenish TCA cycle intermediates that are diverted to biomass production.<sup>147</sup> ICLs in *Mtb* also possess methylisocitrate lyase activity that allows them to function in the methylcitrate cycle.<sup>148</sup> The methylcitrate cycle enables regeneration of the TCA cycle intermediates oxaloacetate and malonate while also preventing build-up of toxic propionyl-CoA and methylmalonyl-CoA that result from  $\beta$ -oxidation of odd-chain fatty acids such as cholesterol.<sup>146</sup> Loss of methylcitrate cycle function can lead to defects in

*Mtb* TCA cycle activity, pH homeostasis, and membrane potential homeostasis but it may not be essential for *in vivo* survival of *Mtb*.<sup>146,148</sup>

The glyoxylate shunt is an important metabolic pathway for persistence in pathogenic *Mycobacteria*, *Salmonella*, and *Yersinia* species.<sup>145,149</sup> The commonly studied *Mtb* Erdman strain has two isocitrate lyases, ICL1 and ICL2, encoded by the genes *icl1* and *icl2* (also known as *aceA*). ICL1-deficient ( $\Delta icl1$ ) *Mtb* exhibits a persistence defect during chronic *in vivo* infection of mice but ICL2-deficient ( $\Delta icl2$ ) *Mtb* exhibits no defects, suggesting that while ICL1 and ICL2 have some level of functional redundancy ICL1 plays a slightly more important role.<sup>145,150</sup> In contrast,  $\Delta icl1/\Delta icl2$  *Mtb* is dramatically attenuated *in vivo* and is cleared from the lung by two weeks post-infection.<sup>145</sup> An antibacterial role for itaconate was supported by the findings that it inhibits purified *Mtb* ICL proteins *in vitro*<sup>151</sup> and that itaconate concentrations two- to three-fold higher than those observed in activated macrophages had bacteriostatic effects on *Mtb* growth in liquid culture under conditions requiring the glyoxylate shunt.<sup>143</sup> Irg1 has also been reported to promote the generation of potentially bactericidal mitochondrial reactive oxygen species (ROS) during *Salmonella* infection of zebrafish.<sup>152</sup> However, Irg1 had no effect on ROS production in murine *Legionella* infection,<sup>135</sup> suggesting that this capability may be pathogen- or species-dependent. These reports suggested that Irg1 might restrict *Mtb* growth by promoting ROS production or inhibiting the glyoxylate shunt through itaconate production.

#### *Irg1 as a modulator of inflammation*

Recent studies have linked Irg1-mediated itaconate production to modulation of immune cell metabolism and inflammatory responses, with the majority of studies finding that it has a net anti-inflammatory effect. In bone marrow-derived macrophages (BMDMs), itaconate suppressed

a subset of pro-inflammatory cytokines including IFN- $\beta$ , IL-1 $\beta$ , IL-6, IL-12, and IL-18 through several different mechanisms.<sup>138,153,154</sup> Inhibition of succinate dehydrogenase by itaconate reduces production of IL-1 $\beta$  and IL-18,<sup>138,155</sup> while suppression of IL-6 and IL-12 is mediated by Atf3-induction that results in a translation-level block of I $\kappa$ B $\zeta$ , a transcription factor promoting *Il6* and *Il12b* expression.<sup>153</sup> Itaconate and its derivatives were also found to limit IL-1 $\beta$  and IFN- $\beta$  production by promoting post-translational modification-mediated degradation of KEAP1, a repressor of the anti-inflammatory transcription factor Nrf2.<sup>156</sup> Irg1 has also been proposed to suppress IL-1 $\beta$  and IL-6 production through induction of the anti-inflammatory transcription factor TNFAIP3 (also known as A20).<sup>154,157</sup> These anti-inflammatory effects on cytokine production are associated with improved outcomes in sepsis and psoriasis models in which pathology is mediated by excessive inflammation.<sup>153,156</sup>

Irg1 has been linked to the generation of ROS but reports vary as to whether it promotes or inhibits ROS production and the resulting effect on inflammation. ROS can mediate pro- or anti-inflammatory effects and the amount produced may be the determining factor.<sup>158,159</sup> Decreased ROS levels have been associated with itaconate-mediated inhibition of succinate dehydrogenase activity and protection from ischemic reperfusion injury.<sup>138</sup> During respiratory syncytial virus infection Irg1 is reported to increase ROS levels, leading to increased inflammation and lung injury.<sup>160</sup>

Macrophage-produced itaconate can also be secreted into the extracellular environment, suggesting that it may mediate immunomodulatory effects *in trans* on other cell types in the inflammatory environment.<sup>138,161,162</sup> The capacity of Irg1 and itaconate to modulate cell-autonomous and nonautonomous effects on inflammation suggested that it could have an

important role in the context of *Mtb* infection wherein immune responses must be precisely calibrated to balance bacterial clearance and prevention of tissue pathology.<sup>24,32</sup>

## **Chapter 2**

### **The role of Bhlhe40 in control of *Mycobacterium tuberculosis* infection**

**Portions of this chapter are excerpted from  
Huynh and Lin et al. *J. Exp. Med.* 215 (7), 1823-1838 (2018).**

## Abstract

The cytokine IL-10 antagonizes pathways that control *Mycobacterium tuberculosis* (*Mtb*) infection. Nevertheless, the impact of IL-10 during *Mtb* infection has been difficult to decipher because loss-of-function studies in animal models have yielded only mild phenotypes. We have discovered that the transcription factor basic helix-loop-helix family member e40 (Bhlhe40) is required to repress *Il10* expression during *Mtb* infection. Loss of Bhlhe40 in mice results in higher *Il10* expression, higher bacterial burden, and early susceptibility similar to that observed in mice lacking IFN- $\gamma$ . Deletion of *Il10* in *Bhlhe40*<sup>-/-</sup> mice reverses these phenotypes. Bhlhe40 deletion in T cells or CD11c<sup>+</sup> cells is sufficient to cause susceptibility to *Mtb*. Bhlhe40 represents the first transcription factor found to be essential during *Mtb* infection to specifically regulate *Il10* expression, revealing the importance of strict control of IL-10 production by innate and adaptive immune cells during infection. Our findings uncover a previously elusive but significant role for IL-10 in *Mtb* pathogenesis.

## Introduction

Host immune responses mediate both bacterial control and pathology during *Mycobacterium tuberculosis* (*Mtb*) infection. IFN- $\gamma$  signaling through the transcription factor STAT1 is essential for the control of mycobacterial infections in humans and mice.<sup>22,23,34,35</sup> IL-10 is an immunoregulatory cytokine produced by a wide variety of innate and adaptive immune cell types<sup>44,75</sup> that antagonizes IFN- $\gamma$ -associated pathways by suppressing macrophage responsiveness to IFN- $\gamma$ ,<sup>39</sup> modulating T-helper (T<sub>H</sub>) 1 cell IFN- $\gamma$  production,<sup>40,42,43</sup> and restricting production of the hallmark T<sub>H</sub>1-inducing cytokine IL-12.<sup>48-50</sup> IL-10 can also inhibit

dendritic cell (DC) migration<sup>49</sup> and limit secretion of myeloid cell-derived proinflammatory cytokines.<sup>52</sup> Global loss-of-function studies have demonstrated a detrimental role for *Il10* expression in the control of chronic *Mtb* infection in mice, although the magnitude of this effect appears dependent on genetic background and is generally mild.<sup>42,43,48</sup> More recently, conditional deletion of *Il10* in T cells or CD11c<sup>+</sup> cells showed that IL-10 production by these two cell types exacerbates *Mtb* infection.<sup>44</sup> Overexpression studies in mice have also supported a negative role for IL-10 in controlling mycobacterial infection, although differences in genetic background, transgenic (Tg) promoters, and mycobacterial species used have resulted in an unclear picture.<sup>40,50,163,164</sup>

Given the potential for IL-10 to negatively impact protective immune responses, cell-autonomous mechanisms likely exist to regulate IL-10 expression. However, the factors required for this regulation remain poorly understood. *Mtb* directly stimulates IL-10 production from monocytes, macrophages, DCs, and neutrophils via pattern-recognition receptor signaling.<sup>165</sup> In addition, different T<sub>H</sub> cell subsets produce IL-10 in response to distinct combinations of cytokines.<sup>75</sup> These signals lead to the binding of diverse transcription factors at various promoter and enhancer elements within the *Il10* locus to activate transcription within myeloid and lymphoid cells.<sup>75-77</sup> Less is known about transcriptional pathways that limit production of IL-10.<sup>166</sup>

The transcription factor basic helix-loop-helix family member e40 (Bhlhe40) has been shown to regulate production of cytokines, including IL-10, by T cells in the experimental autoimmune encephalomyelitis model, a T cell-driven model of neuroinflammation.<sup>108,114,128</sup> Prior to this study Bhlhe40 was uncharacterized in an infectious disease context. We utilized mice with genetic deletions of *Bhlhe40* to characterize its importance and function during *in vivo*

*Mtb* infection. Here we report that *Bhlhe40* serves an essential role in resistance to *Mtb* infection by repressing *Il10* expression in both T cells and myeloid cells.

## Results

### *Lower BHLHE40 expression is associated with active tuberculosis*

When we analyzed publicly available whole-blood gene expression datasets,<sup>92,167,168</sup> we found that *BHLHE40* transcripts were present at a significantly lower abundance in patients with active tuberculosis as compared with healthy controls, those with latent tuberculosis infection, or those with lung cancer, pneumonia, or sarcoidosis (**Fig. 1A**). This expression pattern contrasted with that of *STAT1*, whose expression was significantly increased in active tuberculosis patients (**Fig. 1B**) as previously noted.<sup>92,168</sup>

### *Bhlhe40 is required to control mycobacterial infection*

Our finding that *BHLHE40* expression is decreased in patients with active tuberculosis infection led us to investigate a role for this transcription factor during *Mtb* infection in mice. We infected WT, *Bhlhe40*<sup>+/-</sup>, and *Bhlhe40*<sup>-/-</sup> mice on the C57BL/6J background with the *Mtb* Erdman strain and monitored morbidity and mortality. WT and *Bhlhe40*<sup>+/-</sup> mice displayed no signs of morbidity and survived beyond 100 days post-infection (dpi). *Bhlhe40*<sup>-/-</sup> mice began losing weight around 21 dpi and succumbed to infection between 32 and 40 dpi with a median survival time of 33 dpi (**Fig. 2A, B**). This severe susceptibility phenotype is similar to that of mice lacking *STAT1*<sup>23</sup> and is more severe than that of mice lacking NF- $\kappa$ B p50,<sup>169</sup> both of which are central transcriptional regulators of the immune system. By 21 dpi, *Mtb* colony-forming units (CFUs) in *Bhlhe40*<sup>-/-</sup> mice were 23-fold higher in the lung and 5-fold higher in the spleen as

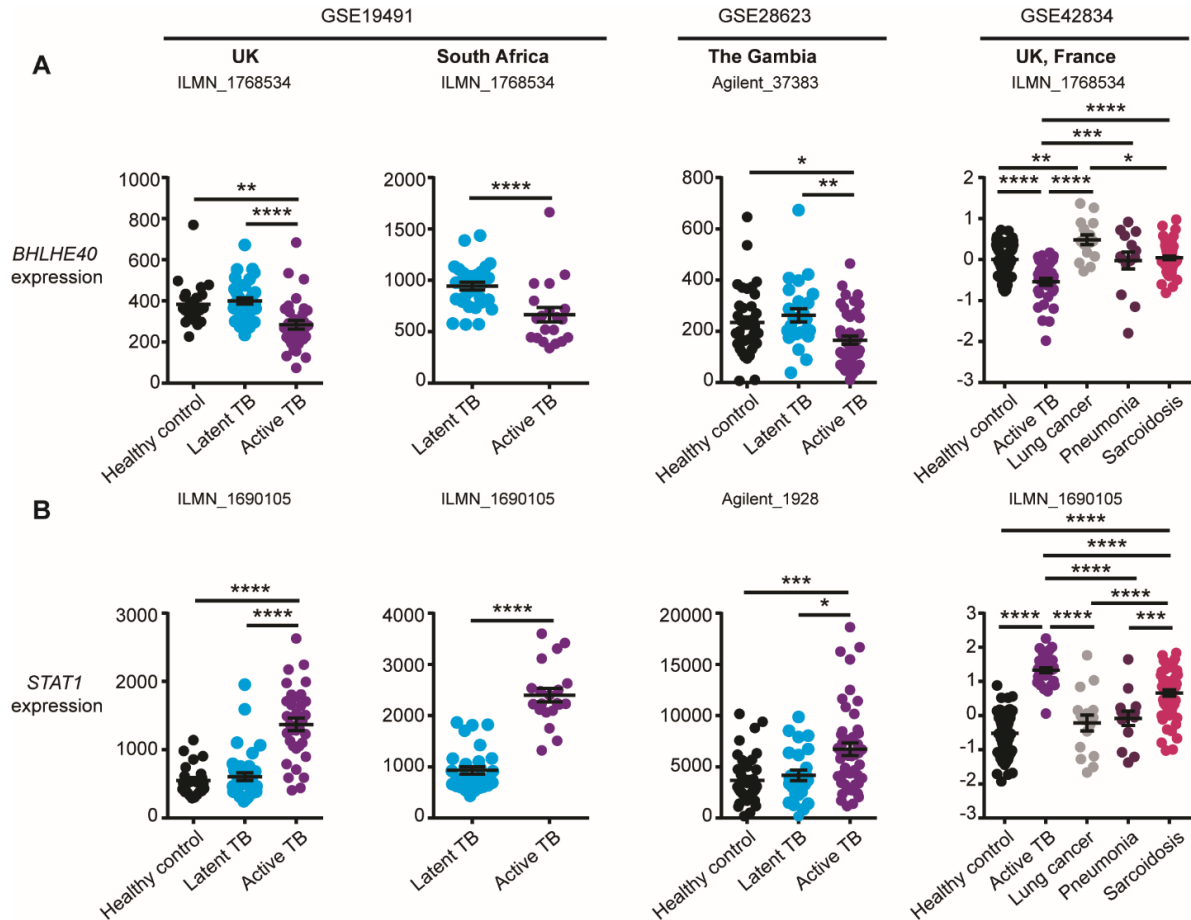


**Figure 1. Lower *BHLHE40* expression is specifically associated with active tuberculosis.**

Expression of (A) *BHLHE40* and (B) *STAT1* in human whole blood from healthy controls or patients with latent tuberculosis (TB), active TB, or other lung diseases. Data are derived from the analysis of the indicated publicly available GEO microarray datasets using the indicated probe sets. Each point represents data from one human. The mean  $\pm$  SEM is graphed. Statistical differences were determined by two-tailed unpaired Student's t test or unpaired one-way ANOVA for normally distributed groups and unpaired Kruskal-Wallis test or two-tailed unpaired Mann-Whitney test for non-normally distributed groups. \*,  $P < 0.05$ ; \*\*,  $P < 0.01$ ; \*\*\*,  $P < 0.001$ ; \*\*\*\*,  $P < 0.0001$ . Previously published in Huynh and Lin et al., 2018.

compared with WT mice (Fig. 2C, D). The differences in *Mtb* CFUs in both organs became even more pronounced at 28 dpi, demonstrating an ongoing defect in the ability of *Bhlhe40*<sup>-/-</sup> mice to control *Mtb* replication. We next tested the requirement for two important *Mtb* virulence factors, the ESX-1 secretion system and the membrane lipid phthiocerol dimycoserolate (PDIM), to cause susceptibility in *Bhlhe40*<sup>-/-</sup> mice. *Bhlhe40*-deficient mice infected with isogenic *Mtb*

strains lacking ESX-1 ( $\Delta$ ESX-1) or PDIM ( $\Delta$ PDIM) exhibited no susceptibility over 80 days of infection (**Fig. 2E**). At 81 dpi, lung CFU counts for PDIM-deficient *Mtb* were below the limit of detection in *Bhlhe40*<sup>-/-</sup> mice while ESX-1 deficient *Mtb* counts trended higher in *Bhlhe40*<sup>-/-</sup> lungs compared to WT *Mtb* (**Fig. 2F**). These experiments lack the statistical power to draw strong conclusions but suggest that expression of ESX-1 and PDIM by *Mtb* is required for the acute susceptibility of *Bhlhe40*<sup>-/-</sup> mice. *Bhlhe40*<sup>-/-</sup> mice may also have a defect in control of  $\Delta$ ESX-1 *Mtb*, though not to the same extent as WT *Mtb*.

We next tested whether *Bhlhe40*<sup>-/-</sup> mice were susceptible to a related mycobacterial species, *Mycobacterium bovis* Bacillus Calmette-Guérin (BCG) (**Fig. 2G**). No survival defect was observed prior to nine weeks post-infection but BCG lung titers were significantly higher in the lungs of *Bhlhe40*<sup>-/-</sup> mice. This demonstrated that *Bhlhe40*<sup>-/-</sup> mice have a reduced capacity to control lung infection by multiple mycobacterial species, although their susceptibility is species- and virulence-factor dependent. Upon infection with the intracellular bacterial pathogen *Listeria monocytogenes*, *Bhlhe40*<sup>-/-</sup> mice showed no increased susceptibility (**Fig. 2H**) and mounted a robust response to secondary *L. monocytogenes* challenge (**Fig. 2I**), indicating that their impaired immune response may be specific to mycobacterial infection.

### ***Bhlhe40* deficiency leads to severe lung inflammation**

Shortly before succumbing to infection, it was evident by gross examination that *Bhlhe40*<sup>-/-</sup> lungs had developed larger lesions than WT lungs (**Fig. 3A**). Histological analysis confirmed that although there were no differences in pulmonary inflammation before infection, the lungs of *Bhlhe40*<sup>-/-</sup> mice had developed larger neutrophil- and acid-fast bacilli-rich lesions with more widespread inflammation than WT lungs by 21 dpi (**Fig. 3B, C**).

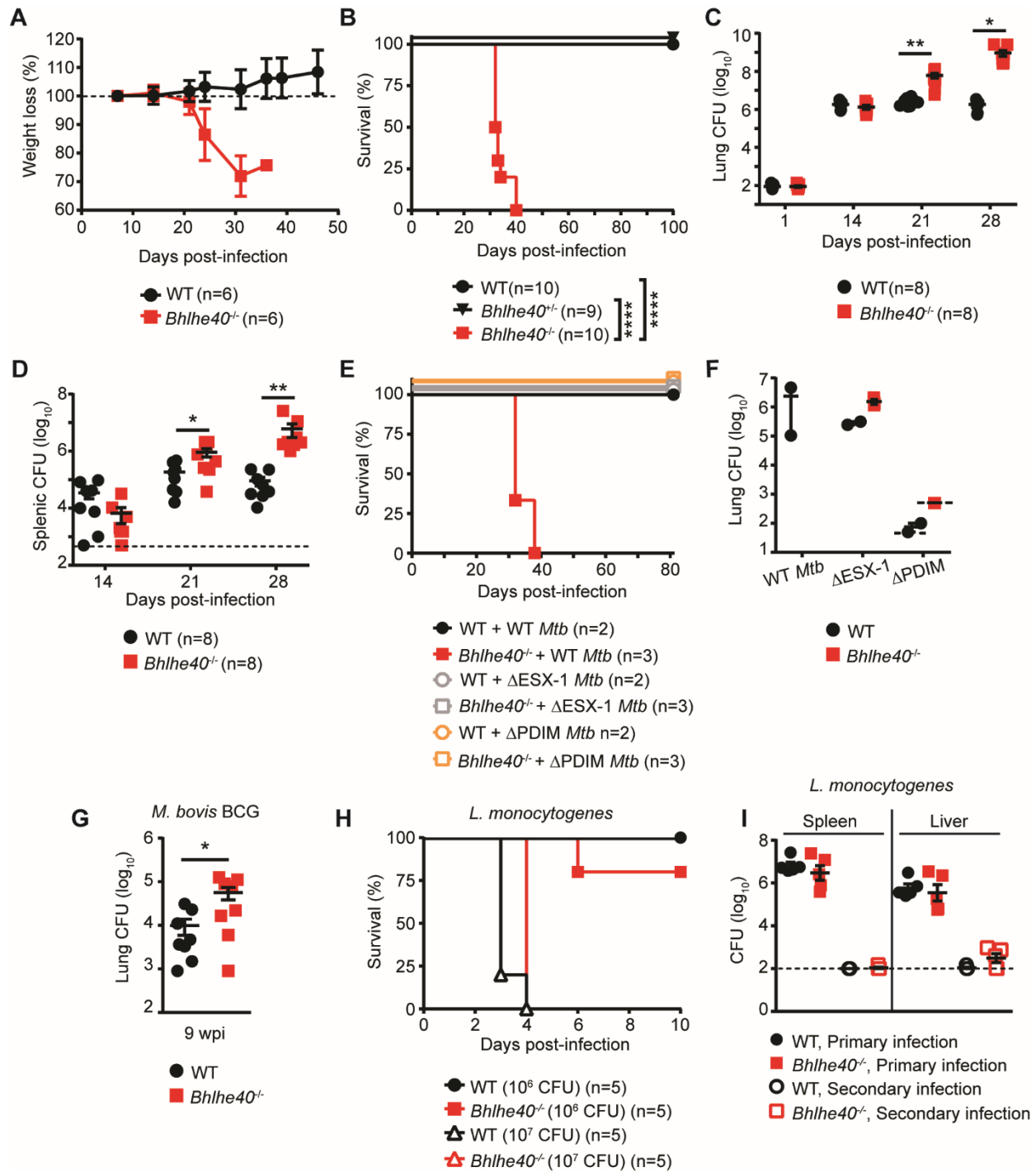


**Figure 2. *Bhlhe40* is required to control mycobacterial infection.**

(A-D) Mice were infected with WT *Mtb* and monitored for changes in (A) body weight, (B) survival, (C) lung *Mtb* burden, and (D) spleen *Mtb* burden. (E-F) Mice were infected with WT, ΔESX-1, and ΔPDIM *Mtb* then monitored for (E) survival and (F) lung *Mtb* burden at 81 dpi. *Bhlhe40*<sup>-/-</sup> mice infected with WT *Mtb* did not survive to 81 dpi and thus could not be assessed at this time point. (G) Mice were infected intranasally with *M. bovis* BCG and monitored for

lung BCG burden at 62 and 65 dpi. Data from 62 and 65 dpi is graphed and analyzed together. (H) Mice were intravenously infected with  $10^6$  or  $10^7$  CFU of *L. monocytogenes* and monitored for survival. (I) Mice were intravenously infected with  $10^6$  CFU and *L. monocytogenes* burden in the spleen and liver was assessed at 3 days after primary or secondary infection. Dotted lines indicate limits of detection ([B] 500, [B] 50 and 500, and [I] 100 CFU). The mean  $\pm$  SEM is graphed. Statistical differences were determined by log-rank Mantel-Cox test (B, E, H), two-tailed unpaired Student's t test for normally distributed groups, and two-tailed unpaired Mann-Whitney test for non-normally distributed groups (C, D, G, I). \*,  $P < 0.05$ ; \*\*,  $P < 0.01$ ; \*\*\*,  $P < 0.001$ ; \*\*\*\*,  $P < 0.0001$ . Data are from one (E, F, G, I) or two independent experiments (A-D, G). Panels (A-D, H-I) were previously published in Huynh and Lin et al., 2018.

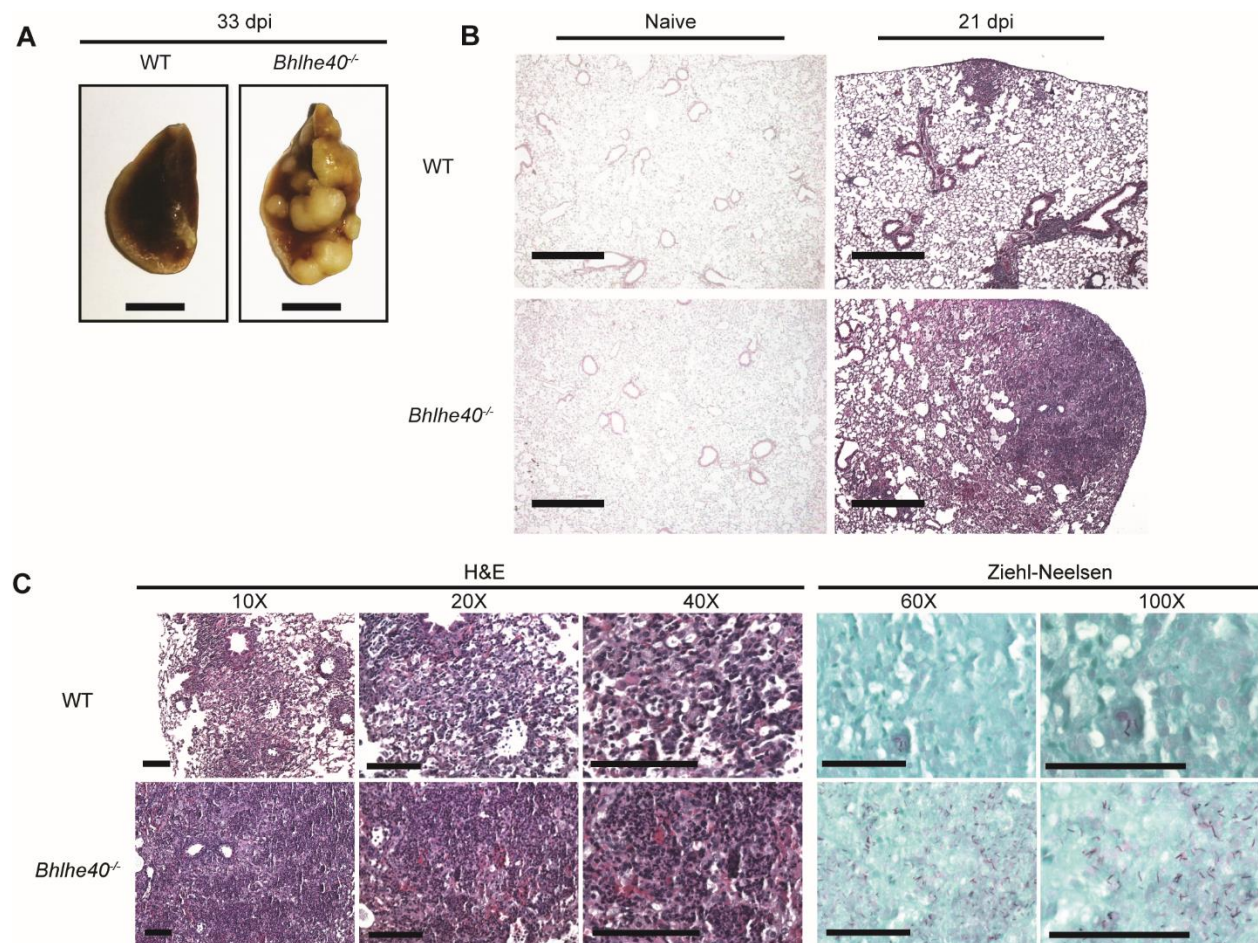


### Figure 3. *Bhlhe40* deficiency leads to severe lung inflammation.

(A-C) Mice were left uninfected or were infected with *Mtb*. (A) Gross lung pathology was assessed at 33 dpi. Lung histopathology in (B) naïve mice or (B, C) at 21 dpi was assessed by H&E staining. Images shown are at 4X magnification. (C) Acid-fast bacteria in lung samples were visualized by Ziehl-Neelsen stain at 21 dpi. Scale bars indicate 5 mm (A), 500  $\mu$ m (B), 100  $\mu$ m (C, H&E), or 50  $\mu$ m (C, Ziehl-Neelsen). Images are representative of two independent experiments with three biological replicates per experiment. Previously published in Huynh and Lin et al., 2018.

We analyzed these histological differences further by performing flow cytometry on the immune cell populations present in the lungs of mice before and after *Mtb* infection. By 21 dpi, neutrophils were the predominant CD45<sup>+</sup> cell type in the lungs of *Bhlhe40*<sup>-/-</sup> mice, and the absolute number of neutrophils in *Bhlhe40*<sup>-/-</sup> lungs was three times greater than in WT lungs (**Fig. 4A, D**). The number and frequency of neutrophils in the lungs of *Bhlhe40*<sup>-/-</sup> mice further increased as the infection progressed (**Fig. 4C, D**). The number of CD11b<sup>+</sup>Ly6C<sup>high</sup> monocyte-derived DCs (moDCs) was 12-fold lower and CD8<sup>+</sup> T cell counts trended downward in *Bhlhe40*<sup>-/-</sup> mice at 21 dpi, suggesting that *Bhlhe40* may regulate the development, recruitment, or survival of these populations (**Fig. 4A**). There were no significant differences in the populations sizes of other myeloid or lymphoid cell types analyzed at 21 dpi (**Fig. 4A**), nor were there any differences in the frequency of *Mtb* antigen-specific T cells in lungs or mediastinal lymph nodes (**Fig. 4B**).

The timing of the increased inflammation correlated with our initial observation of higher *Mtb* burden in the lungs of *Bhlhe40*<sup>-/-</sup> mice, leading us to investigate whether the accumulating myeloid cells were infected with *Mtb*. We infected WT and *Bhlhe40*<sup>-/-</sup> mice with a strain of *Mtb* Erdman that stably expresses GFP and monitored the number and frequency of *Mtb*-infected cells at 21 dpi. Neutrophils, CD11b<sup>+</sup> macrophages, inflammatory monocytes, moDCs, and CD11b<sup>+</sup> DCs were all infected at a higher frequency in *Bhlhe40*<sup>-/-</sup> lungs compared with WT lungs (**Fig. 4E**). Absolute numbers of infected neutrophils, inflammatory monocytes, and CD11b<sup>+</sup> DCs were also significantly higher in *Bhlhe40*<sup>-/-</sup> lungs (**Fig. 4F**), suggesting that *Mtb* residing within these cell types accounts for the difference in pulmonary *Mtb* burden in *Bhlhe40*<sup>-/-</sup> lungs at 21 dpi. Infected *Bhlhe40*<sup>-/-</sup> neutrophils, inflammatory monocytes, moDCs, and CD11b<sup>+</sup> DCs also exhibited an increase in mean fluorescence intensity (MFI) for GFP

compared with infected WT neutrophils, suggesting that they harbored more *Mtb* on a per-cell basis (**Fig. 4H**).

***Neutrophil and monocyte inflammation do not drive susceptibility in *Bhlhe40*<sup>-/-</sup> mice.***

To test whether the influx of neutrophils contributed to the susceptibility of *Bhlhe40*<sup>-/-</sup> mice, we used an anti-Ly6G monoclonal antibody to specifically deplete neutrophils between 10 and 30 dpi.<sup>32</sup> Neutrophil-depleted *Bhlhe40*<sup>-/-</sup> mice did not exhibit any improvements in morbidity, survival time, or control of *Mtb* replication (**Fig. 5A-C**). We further tested a role for neutrophils in susceptibility by infecting *Bhlhe40*<sup>-/-</sup> mice lacking granulocyte colony stimulating factor receptor (G-CSFR, *Csf3r*) (**Fig. 5D**). *Csf3r*<sup>-/-</sup> mice are reported to have basal neutropenia<sup>170</sup> although we did not confirm neutropenia in this setting. *Csf3r*<sup>-/-</sup>*Bhlhe40*<sup>-/-</sup> mice exhibited a statistically significant extension of survival time compared to *Csf3r*<sup>+/-</sup>*Bhlhe40*<sup>-/-</sup> mice, and the difference in survival time between *Bhlhe40*<sup>-/-</sup> and *Csf3r*<sup>-/-</sup>*Bhlhe40*<sup>-/-</sup> mice approached significance ( $p = 0.052$ ), suggesting that loss of G-CSFR signaling is partially protective in the context of *Bhlhe40*-deficiency. *Csf3r*<sup>-/-</sup> mice were susceptible in chronic *Mtb* infection, demonstrating that G-CSFR-signaling is host-protective in WT mice (**Fig. 5D**). We next tested a role for monocytes in susceptibility by infecting *Bhlhe40*<sup>-/-</sup> mice lacking C-C motif chemokine receptor 2 (CCR2, *Ccr2*) (**Fig. 5E**). CCR2 is essential for survival of high dose *Mtb* infection and *Ccr2*<sup>-/-</sup> mice exhibit defects in inflammatory monocyte recruitment,<sup>171</sup> although we did not confirm reduced monocyte recruitment in this setting. CCR2-deficiency had no impact on the susceptibility of *Bhlhe40*<sup>-/-</sup> mice. These results show that although neutrophils and monocytes are prominent replicative niches for *Mtb* and neutrophils may have a detrimental role, these cell types are not the sole cause of susceptibility to *Mtb* infection in *Bhlhe40*<sup>-/-</sup> mice.

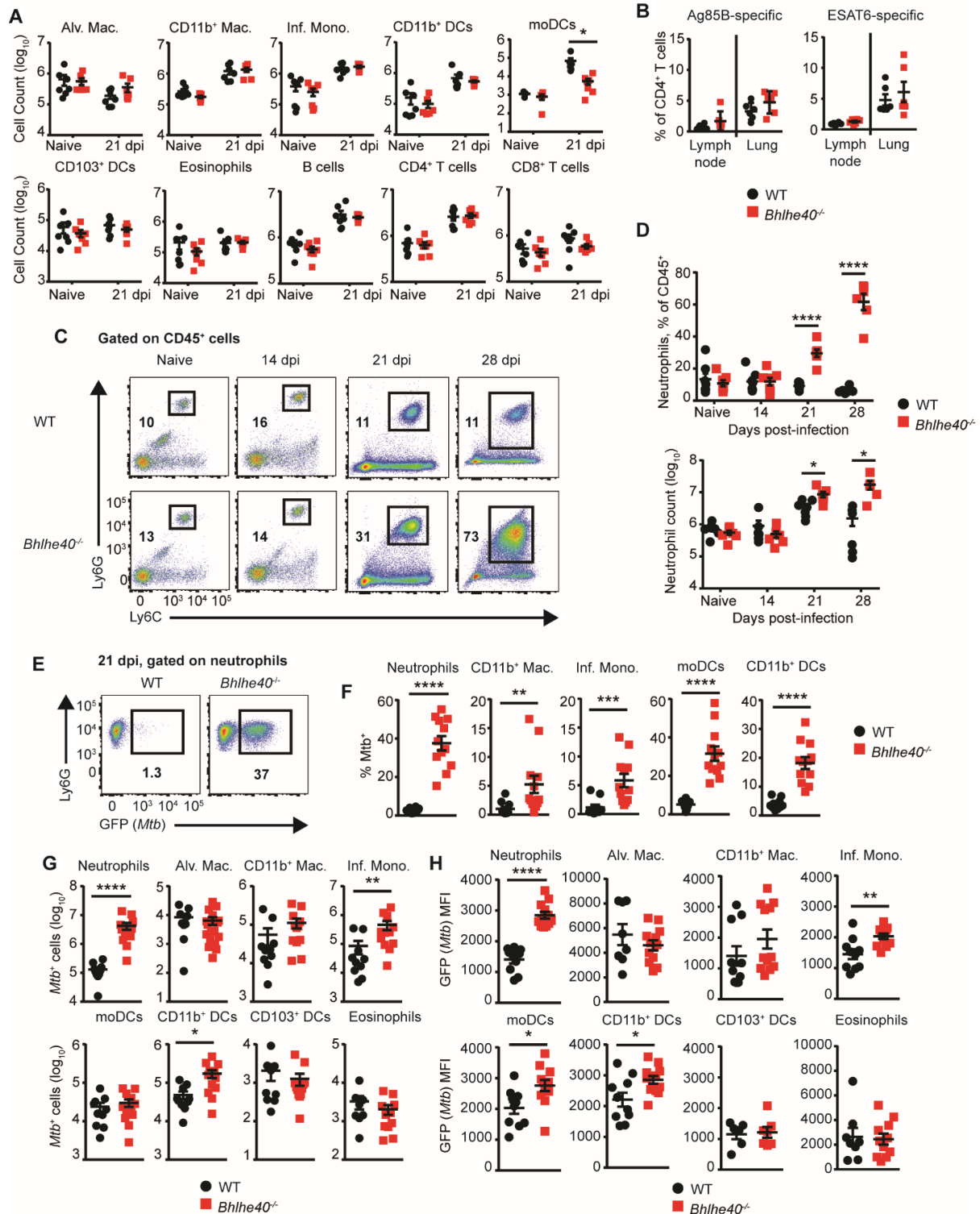


**Figure 4. *Bhlhe40* deficiency leads to neutrophil-dominated inflammation.**

(A-G) Mice were infected with *Mtb*. (A) Absolute cell counts for pulmonary immune cells before infection and at 21 dpi. MoDC counts in four naive WT and three naive *Bhlhe40*<sup>-/-</sup>

samples were below the limit of detection (~100 cells). **(B)** Frequency of *Mtb* antigen-specific CD4<sup>+</sup> T cells at 21 dpi. **(C)** Representative flow cytometry plots for neutrophils as a percentage of the total CD45<sup>+</sup> population. **(D)** Absolute count and percentage of the total CD45<sup>+</sup> population for lung neutrophils. **(E)** Representative flow cytometry plots for GFP<sup>+</sup> (*Mtb*<sup>+</sup>) neutrophils at 21 dpi. **(F)** Frequency of GFP<sup>+</sup> (*Mtb*<sup>+</sup>) cells in myeloid lung populations at 21 dpi. **(G)** Absolute count for GFP<sup>+</sup> (*Mtb*<sup>+</sup>) lung myeloid cells at 21 dpi. Four WT alveolar macrophage, four WT and five *Bhlhe40*<sup>-/-</sup> CD103<sup>+</sup> DC, and two WT and one *Bhlhe40*<sup>-/-</sup> eosinophil samples were below the limit of detection (~850 cells). **(H)** MFI for FITC in GFP<sup>+</sup> (*Mtb*<sup>+</sup>) lung cell populations at 21 dpi. Mac., macrophage; Inf. Mono., inflammatory monocyte. The mean ± SEM is graphed. Statistical differences were determined by two-tailed unpaired Student's t test for normally distributed groups or two-tailed unpaired Mann-Whitney test for nonnormally distributed groups as appropriate. \*, P < 0.05; \*\*, P < 0.01; \*\*\*, P < 0.001; \*\*\*\*, P < 0.0001. Data are from or representative of two (**A-D**) or five (**E-H**) independent experiments. Previously published in Huynh and Lin et al., 2018.

### ***Bhlhe40 is required within hematopoietic cells***

*Bhlhe40* is expressed in specific immune cell populations and in nonhematopoietic cell types.<sup>172</sup> To dissect which cells required *Bhlhe40* expression during *Mtb* infection, we infected reciprocal bone marrow chimeric mice with *Mtb* and monitored survival (**Fig. 6A**). As expected, all but one WT→WT chimeric mouse survived past 100 dpi, and *Bhlhe40*<sup>-/-</sup>→*Bhlhe40*<sup>-/-</sup> chimeras succumbed 27-35 dpi (median survival time of 33 days). WT→*Bhlhe40*<sup>-/-</sup> chimeras also survived past 100 dpi, whereas *Bhlhe40*<sup>-/-</sup>→WT chimeras died between 29-37 dpi (median survival time of 32 days), similar to *Bhlhe40*<sup>-/-</sup>→*Bhlhe40*<sup>-/-</sup> chimeras. These data demonstrate a specific role for *Bhlhe40* in radiosensitive hematopoietic cells during *Mtb* infection.

To determine which hematopoietic cells express *Bhlhe40* during *Mtb* infection, we used *Bhlhe40*-GFP reporter mice (*Bhlhe40*<sup>GFP</sup>).<sup>108,173</sup> We monitored GFP expression as a proxy for *Bhlhe40* expression in the lungs of naive and *Mtb* infected *Bhlhe40*<sup>GFP</sup> mice. Sizeable fractions of neutrophils, alveolar macrophages, CD11b<sup>+</sup> DCs, CD103<sup>+</sup> DCs, and eosinophils expressed GFP both before infection and at 21 dpi (**Fig. 6B-D**), with smaller fractions of CD11b<sup>+</sup> macrophages, moDCs, B cells, and CD8<sup>+</sup> T cells also showing this pattern of expression. Similar

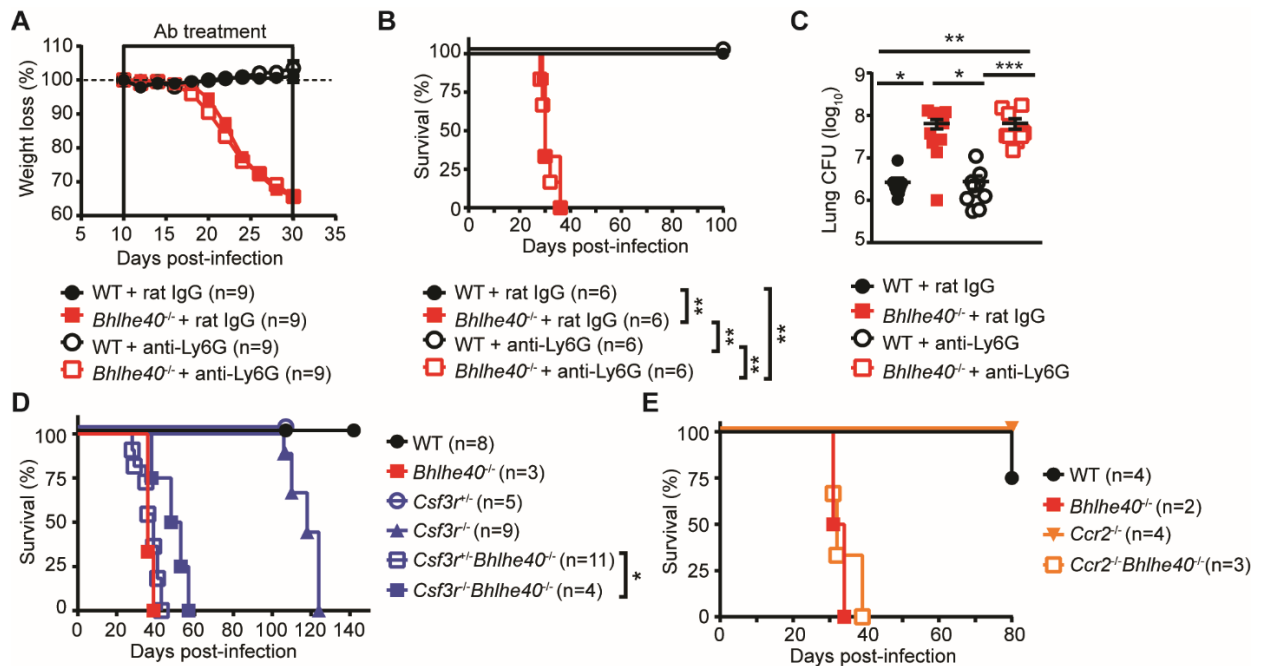


**Figure 5. Neutrophils and monocytes do not drive susceptibility in *Bhlhe40*<sup>-/-</sup> mice.**

(A-C) Mice were infected with *Mtb* and treated with rat IgG or anti-Ly6G mAb from 10-30 dpi. Mice were monitored for changes in (A) body weight, (B) survival, and (C) lung *Mtb* burden at 21 dpi. (D, E) Mice were infected with *Mtb* and monitored for survival. The mean ± SEM is graphed. Statistical differences were determined by log-rank Mantel-Cox test (B, D, E) or unpaired Kruskal-Wallis test with Dunn's multiple comparison test (B). \*, P < 0.05; \*\*, P < 0.01; \*\*\*, P < 0.001; \*\*\*\*, P < 0.0001. Data are from one (E) or two (A-D) independent experiments. Panels (A-C) were previously published in Huynh and Lin et al., 2018.

trends were observed at 14 dpi (data not shown). Therefore, these cell types constitutively express *Bhlhe40*, and this expression pattern does not change during *Mtb* infection. In contrast, CD4<sup>+</sup> T cells in naive mice expressed very little *Bhlhe40* but at 21 dpi, *Bhlhe40* levels increased in this cell type (Fig. 6B-D). These data show that *Bhlhe40* is expressed in both myeloid and lymphoid cells during *Mtb* infection.

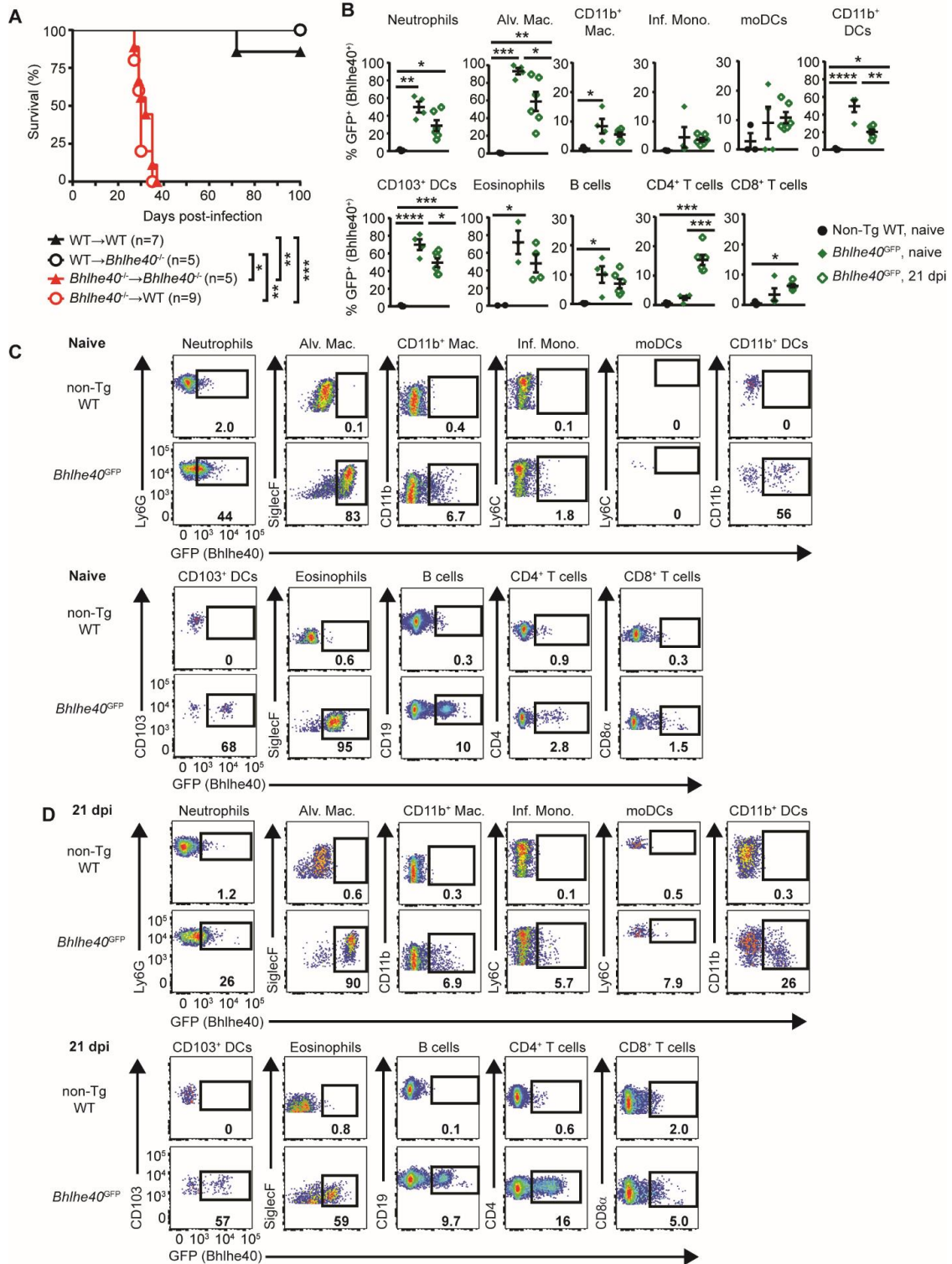


**Figure 6. *Bhlhe40* is expressed and required in hematopoietic cells.**

(A) WT or *Bhlhe40*<sup>-/-</sup> mice were lethally irradiated, reconstituted with WT or *Bhlhe40*<sup>-/-</sup> bone marrow, and monitored for survival after *Mtb* infection. (B) Frequency of GFP<sup>+</sup> (*Bhlhe40*<sup>+</sup>) cells

for lung cell populations in non-transgenic (Tg) and *Bhlhe40*<sup>GFP</sup> mice before infection and at 21 dpi. (C, D) Representative flow cytometry plots for GFP (*Bhlhe40*) in immune cells from the lungs of non-Tg WT and Tg *Bhlhe40*<sup>GFP</sup> mice before infection (C) or at 21 dpi (D). Bold numbers are the percentages of cells that fall within the gate. Mac., macrophage; Inf. Mono., inflammatory monocyte; Alv. Mac., alveolar macrophage. Data are from or representative of two (A) or three (B-D) independent experiments. The mean  $\pm$  SEM is graphed. Statistical differences were determined by log-rank Mantel-Cox test (A) and one-way unpaired ANOVA with Tukey's post-test for normally distributed groups or unpaired Kruskal-Wallis test with Dunn's multiple comparison test for non-normally distributed groups (B). \*, P < 0.05; \*\*, P < 0.01; \*\*\*, P < 0.001; \*\*\*\*, P < 0.0001. Previously published in Huynh and Lin et al., 2018.

### ***Bhlhe40 enables control of Mtb in the context of T cell deficiency***

*Bhlhe40* expression is required in CD4<sup>+</sup> T cells to regulate cytokine production in the experimental autoimmune encephalomyelitis (EAE) model of autoimmunity.<sup>114,128</sup> However, *Bhlhe40*<sup>-/-</sup> mice succumbed to *Mtb* infection between 32 and 40 dpi, which is earlier than *Rag1*<sup>-/-</sup> mice that lack mature B and T cell and succumb to *Mtb* infection between 46 and 50 dpi.<sup>24</sup> The timing of the death of *Mtb* infected *Bhlhe40*<sup>-/-</sup> mice suggests that there is a defect in the innate immune response to *Mtb*, as it preceded the point at which adaptive immunity is required, or the presence of pathological T cells is leading to earlier death than would occur in the absence of T cells, as previously observed in *Pdcd1*<sup>-/-</sup> mice.<sup>89</sup>

To measure the contribution of *Bhlhe40* to host resistance in the absence of B and T cells, we used anti-CD4 and anti-CD8 monoclonal antibodies to deplete CD4<sup>+</sup> and CD8<sup>+</sup> T cells in WT and *Bhlhe40*<sup>-/-</sup> mice, infected with *Mtb*, and measured *Mtb* burden at 22 dpi (**Fig. 7A**). CFU counts in T cell-depleted WT and *Bhlhe40*<sup>-/-</sup> mice were not significantly different from undepleted mice of the same genotype. However, when we assessed the numbers of lung CD4<sup>+</sup> and CD8<sup>+</sup> T cells we found that although depletion led to significant reductions, most mice retained a sizable number of T cells at 22 dpi (**Fig. 7B**). This suggested that the absence of observable differences in *Mtb* burden after depletion might be due to effects from residual T

cells. To avoid the potentially confounding effects of residual T cells we utilized *Rag1*<sup>-/-</sup> mice that lack mature adaptive immune cells. We compared the survival of *Mtb* infected WT, *Bhlhe40*<sup>-/-</sup>, *Rag1*<sup>-/-</sup>, and *Rag1*<sup>-/-</sup>*Bhlhe40*<sup>-/-</sup> mice (**Fig. 7C**). *Rag1*<sup>-/-</sup>*Bhlhe40*<sup>-/-</sup> mice (median survival time of 33 days) were significantly more susceptible than *Rag1*<sup>-/-</sup> mice (median survival time of 43 days) to *Mtb* infection and succumbed to infection at the same time as *Bhlhe40*<sup>-/-</sup> mice. These data demonstrate that Bhlhe40 is required during the innate immune response in the absence of T cells to prolong survival during *Mtb* infection and suggest that our T cell depletion experiments were confounded by the presence of residual T cells. *Mtb* CFUs were 4-fold higher in *Rag1*<sup>-/-</sup>*Bhlhe40*<sup>-/-</sup> mice compared with *Rag1*<sup>-/-</sup> mice at 21 dpi (**Fig. 7D**), and the frequency of neutrophils in the lungs of *Rag1*<sup>-/-</sup>*Bhlhe40*<sup>-/-</sup> mice was also significantly elevated (**Fig. 7E**). The frequency of infected neutrophils, CD11b<sup>+</sup> macrophages, and moDCs was significantly higher in *Rag1*<sup>-/-</sup>*Bhlhe40*<sup>-/-</sup> mice at 21 dpi (**Fig. 7F**). We also observed significantly higher MFIs for GFP in *Rag1*<sup>-/-</sup>*Bhlhe40*<sup>-/-</sup> neutrophils, CD11b<sup>+</sup> macrophages, inflammatory monocytes, and CD11b<sup>+</sup> DCs, suggesting that these cell types harbored more *Mtb* on a per-cell basis compared with *Rag1*<sup>-/-</sup> cells (**Fig. 7G**). Therefore, loss of Bhlhe40 in innate immune cells compromises their ability to control inflammation and *Mtb* replication independent of adaptive immunity.

### ***Bhlhe40 is required in CD11c<sup>+</sup>, Zbtb46<sup>+</sup>, and T cells***

To determine more precisely which cells require Bhlhe40 expression to control *Mtb* infection, we infected mice that conditionally delete Bhlhe40 in specific cell types. After *Mtb* infection, *Bhlhe40*<sup>fl/fl</sup>-*Lysm-Cre* and *Bhlhe40*<sup>fl/fl</sup>-*Mrp8-Cre* mice survived past 100 dpi (**Fig. 8A**) and showed no signs of morbidity over the first 45 days of infection (**Fig. 8B**), indicating that loss of Bhlhe40 in LysM<sup>+</sup> or Mrp8<sup>+</sup> cells was not sufficient to generate susceptibility to

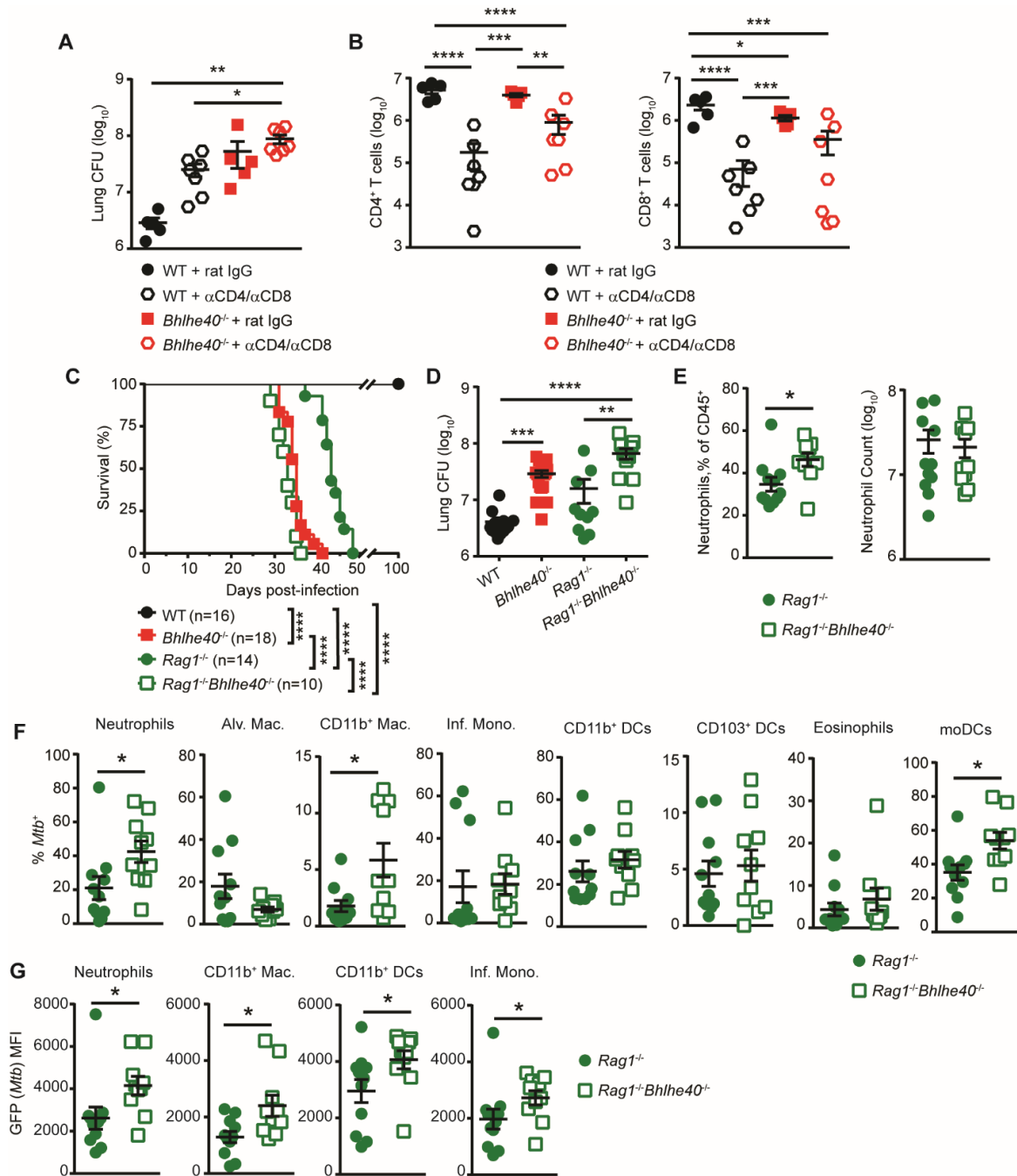


**Figure 7. *Bhlhe40* enables control of *Mtb* in the context of T cell deficiency.**

(A, B) Mice were treated with anti-CD4/anti-CD8 monoclonal antibodies, infected with *Mtb*, and assessed for (A) lung CFUs or (B) lung CD4<sup>+</sup> and CD8<sup>+</sup> T cells at 22 dpi. (C-G) Mice were infected with *Mtb* and monitored for (C) survival or analyzed at 21 dpi for (D) lung CFUs, (E) neutrophilic inflammation, (F) frequency of GFP<sup>+</sup> (*Mtb*<sup>+</sup>) cells, and (G) MFI for GFP in GFP<sup>+</sup> (*Mtb*<sup>+</sup>) cells. Mac., macrophage; Inf. Mono., inflammatory monocyte; Alv. Mac., alveolar macrophage. Data are from two (A, B) or five (C-G) independent experiments. The mean  $\pm$  SEM is graphed. Statistical differences were determined by log-rank Mantel-Cox test (C), two-tailed unpaired Student's t test or one-way unpaired ANOVA with Tukey's post-test for normally

distributed groups and two-tailed unpaired Mann-Whitney test or unpaired Kruskal-Wallis test with Dunn's multiple comparison test for non-normally distributed groups, as appropriate (**A,B, D-G**). \*,  $P < 0.05$ ; \*\*,  $P < 0.01$ ; \*\*\*,  $P < 0.001$ ; \*\*\*\*,  $P < 0.0001$ . Panels (**C-G**) were previously published in Huynh and Lin et al., 2018.

infection. In contrast, *Bhlhe40<sup>fl/fl</sup>-Cd11c-Cre* and *Bhlhe40<sup>fl/fl</sup>-Cd4-Cre* mice succumbed to infection at 34-62 dpi (median survival time of 56 days) and 31-73 dpi (median survival time of 52 days), respectively (**Fig. 8A**). Therefore, Bhlhe40 expression in both T cells and CD11c<sup>+</sup> cells is required to control *Mtb* infection. Given that the *Lysm* (also known as *Lyz2*) promoter can drive conditional deletion in alveolar macrophages but deletes poorly in myeloid DCs, whereas the *Cd11c* (also known as *Itgax*) promoter deletes equally well in both alveolar macrophages and DCs,<sup>174</sup> one interpretation is that loss of Bhlhe40 in alveolar macrophages is not sufficient to cause susceptibility and that loss of Bhlhe40 in DCs contributes to the susceptibility observed in *Bhlhe40<sup>fl/fl</sup>-Cd11c-Cre* mice. The *Cd11c* promoter has also been reported to drive conditional deletion in a subpopulation of T cells<sup>174</sup> that could be contributing to susceptibility. In order to examine a role for Bhlhe40 specifically in conventional DCs we infected a *Bhlhe40<sup>fl/fl</sup>-Zbtb46-Cre* mouse and found that it succumbed at 116 dpi (**Fig. 8A**). Although only one mouse was tested, its susceptibility demonstrates that loss of Bhlhe40 in conventional DCs is sufficient for susceptibility.

The longer survival times of *Bhlhe40<sup>fl/fl</sup>-Cd11c-Cre* and *Bhlhe40<sup>fl/fl</sup>-Cd4-Cre* mice compared to *Bhlhe40<sup>-/-</sup>* mice indicated that loss of Bhlhe40 in CD11c<sup>+</sup> and T cells separately did not account for the entirety of the defect observed in mice with global Bhlhe40-deficiency. To test whether simultaneous loss of Bhlhe40 in CD11c<sup>+</sup> and T cells accounted for the severe defect in *Bhlhe40<sup>-/-</sup>* mice we infected *Bhlhe40<sup>fl/fl</sup>-Cd4-Cre/Cd11c-Cre* mice and tracked survival (**Fig. 8A**). *Bhlhe40<sup>fl/fl</sup>-Cd4-Cre/Cd11c-Cre* were significantly more susceptible than *Bhlhe40<sup>fl/fl</sup>-*

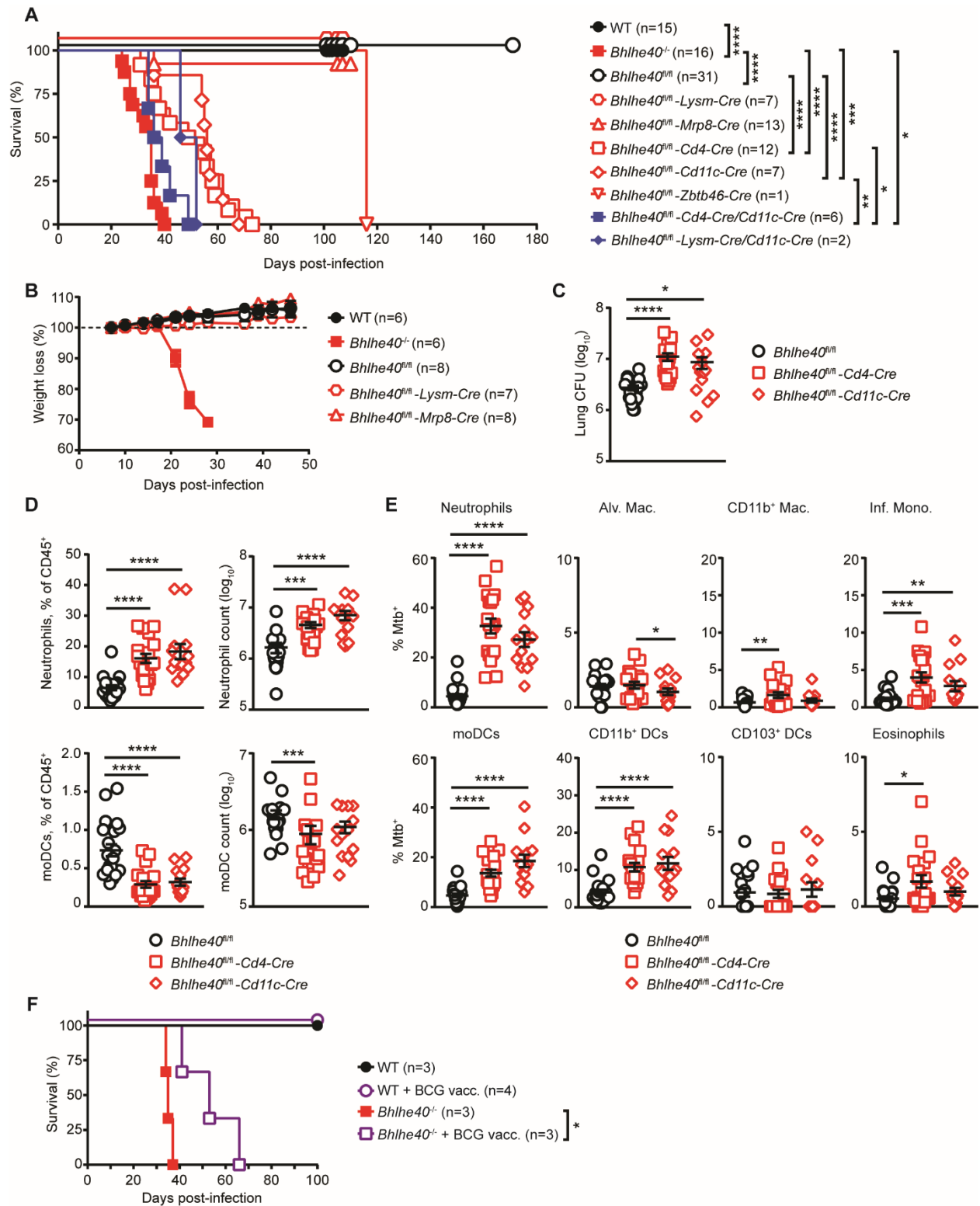


**Figure 8. *Bhlhe40* is required in CD11c<sup>+</sup>, Zbtb46<sup>+</sup>, and T cells.**

(A-E) Mice were infected with *Mtb* and monitored for (A) survival and (B) weight loss or (C) lung *Mtb* burden, (D) lung neutrophil and moDC absolute counts and frequency in the total

CD45<sup>+</sup> population, and (E) frequency of GFP<sup>+</sup> (*Mtb*<sup>+</sup>) lung cells at 21 dpi. Mac., macrophage; Inf. Mono., inflammatory monocyte; Alv. Mac., alveolar macrophage. (F) Mice were vaccinated with *M. bovis* BCG, rested for 30 days, then infected with *Mtb* and monitored for survival. The mean ± SEM is shown. Statistical differences were determined by log-rank Mantel-Cox test (A, F) or one-way unpaired ANOVA with Tukey's post-test for normally distributed groups and unpaired Kruskal-Wallis test with Dunn's multiple comparison test for non-normally distributed groups. \*, P < 0.05; \*\*, P < 0.01; \*\*\*, P < 0.001; \*\*\*\*, P < 0.0001. Data are from one to four (A), two (B), seven (C-E), or one (F) independent experiments. Parts of panel (A) and all of panels (B-D) were previously published in Huynh and Lin et al., 2018.

*Cd11c-Cre* and *Bhlhe40<sup>fl/fl</sup>-Cd4-Cre* mice, but not as susceptible as *Bhlhe40<sup>-/-</sup>* mice. These results confirm that loss of Bhlhe40 in CD11c<sup>+</sup> and T cells accounts for the majority of susceptibility observed in *Bhlhe40<sup>-/-</sup>* mice but other cell types make minor contributions to resistance.

To assess the role of myeloid cell expression of Bhlhe40 in a T cell-sufficient context we monitored the survival of *Bhlhe40<sup>fl/fl</sup>-Lysm-Cre/Cd11c-Cre* mice (Fig. 8A). Only two mice were tested, but their survival times displayed a trend towards increased susceptibility as compared to *Bhlhe40<sup>fl/fl</sup>-Cd11c-Cre* mice, suggesting that Bhlhe40 expression in LysM<sup>+</sup> cells plays a protective but minor role in resistance to *Mtb*.

We next analyzed susceptible *Bhlhe40<sup>fl/fl</sup>-Cd11c-Cre* and *Bhlhe40<sup>fl/fl</sup>-Cd4-Cre* mice to determine how loss of Bhlhe40 in CD11c<sup>+</sup> or T cells contributed to phenotypes observed in *Bhlhe40<sup>-/-</sup>* mice. By 21 dpi, pulmonary *Mtb* burden in *Bhlhe40<sup>fl/fl</sup>-Cd11c-Cre* and *Bhlhe40<sup>fl/fl</sup>-Cd4-Cre* mice was 3- and 4-fold higher than *Bhlhe40<sup>fl/fl</sup>* controls, respectively (Fig. 8C). *Bhlhe40<sup>fl/fl</sup>-Cd11c-Cre* and *Bhlhe40<sup>fl/fl</sup>-Cd4-Cre* mice also exhibited an increase in the frequency and absolute number of lung neutrophils (Fig. 8D). The frequency of moDCs was significantly lower in *Bhlhe40<sup>fl/fl</sup>-Cd4-Cre* and *Bhlhe40<sup>fl/fl</sup>-Cd11c-Cre* lungs, but the absolute number of moDCs was decreased in *Bhlhe40<sup>fl/fl</sup>-Cd4-Cre* lungs only, suggesting that loss of Bhlhe40 in T cells leads to the decreased number of moDCs observed in *Bhlhe40<sup>-/-</sup>* mice (Fig. 8D).

Neutrophils, inflammatory monocytes, moDCs, and CD11b<sup>+</sup> DCs were infected at a higher frequency in both *Bhlhe40*<sup>fl/fl</sup>-*Cd4-Cre* and *Bhlhe40*<sup>fl/fl</sup>-*Cd11c-Cre* mice (**Fig. 8E**). Collectively, the survival, *Mtb* burden, neutrophilic inflammation, and frequency of cellular infection phenotypes evident in mice with conditional deletions of *Bhlhe40* indicate that expression of *Bhlhe40* in CD11c<sup>+</sup> and T cells provides essential and synergistic functions that enable resistance to *Mtb* infection.

Our identification of an essential role for *Bhlhe40* in T cells led us to assess the functionality of vaccination-elicited adaptive immune responses in *Bhlhe40*<sup>-/-</sup> mice. Mice were vaccinated with *M. bovis* BCG and then monitored for survival after *Mtb* infection (**Fig. 8F**). Vaccination significantly extended the survival time of *Bhlhe40*<sup>-/-</sup> mice, although they remained susceptible to *Mtb*. These data suggested that a pre-existing adaptive immune response in *Bhlhe40*<sup>-/-</sup> mice can confer a degree of resistance, although it is ultimately insufficient to overcome defects that arise during *Mtb* infection.

### ***Bhlhe40* deficiency alters cytokine transcription after exposure to *Mtb***

*Bhlhe40* has previously been found to regulate cytokine production by CD4<sup>+</sup> T cells in the EAE model.<sup>114,128</sup> If *Bhlhe40* functions analogously during *Mtb* infection, *Bhlhe40*<sup>-/-</sup> cells could exert a dominant effect on WT cells through the production of secreted cytokines. We tested this by generating mixed bone marrow chimeric mice. Congenically marked WT (CD45.1/.2) recipients were lethally irradiated and reconstituted with a 1:1 mixture of WT (CD45.1/.1) and *Bhlhe40*<sup>-/-</sup> (CD45.2/.2) bone marrow cells. Control mice included mixed chimeras generated with WT (CD45.1/.1) and WT (CD45.2/.2) bone marrow cells as well as nonchimeric WT (CD45.2/.2) and *Bhlhe40*<sup>-/-</sup> (CD45.2/.2) mice. In mixed chimeras, *Bhlhe40*<sup>-/-</sup>

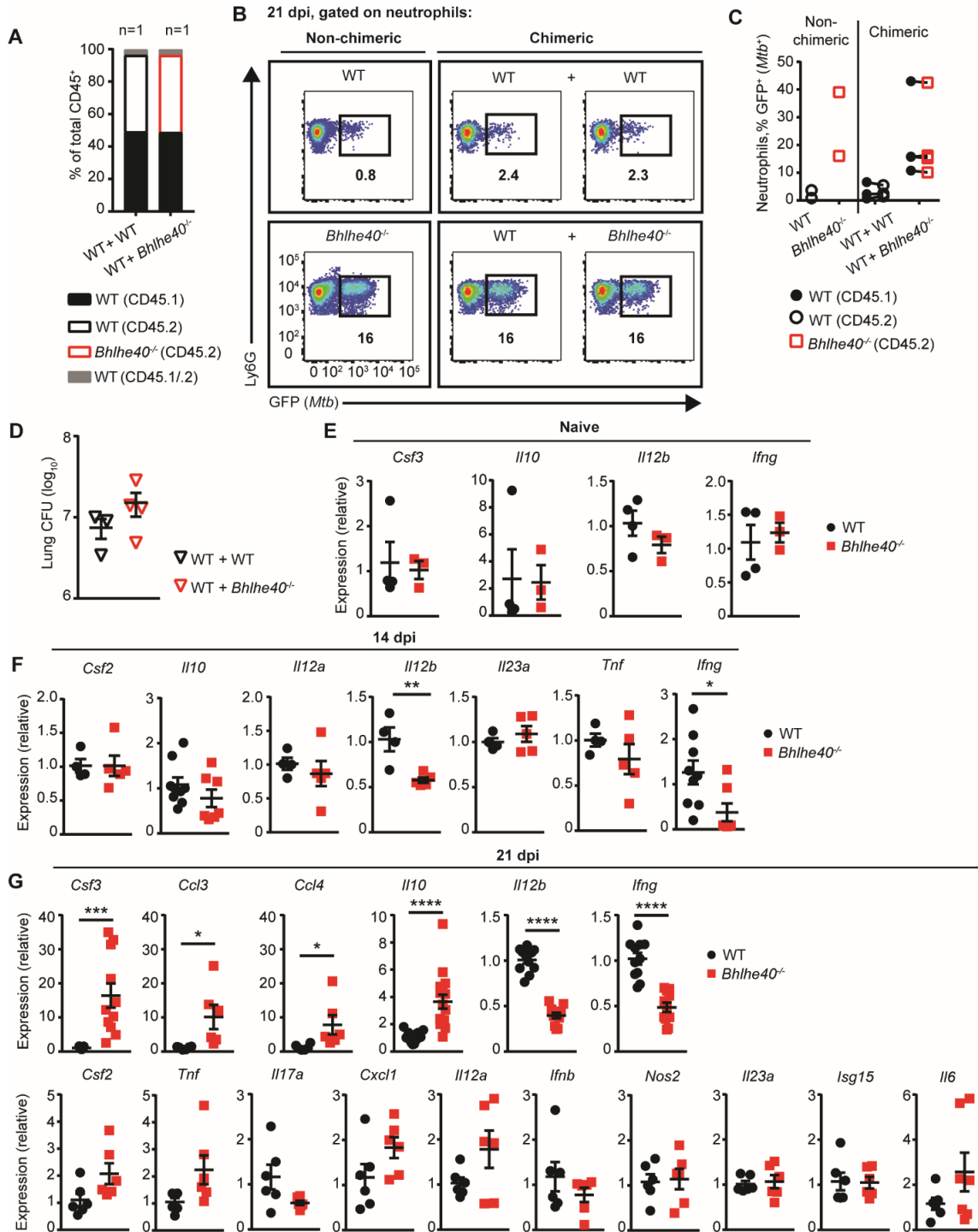


**Figure 9. *Bhlhe40* deficiency alters cytokine transcription after exposure to *Mtb*.**

(A) Mixed bone marrow chimera mice were generated and the frequency of CD45.1<sup>+</sup>, CD45.2<sup>+</sup>, and CD45.1<sup>+</sup>CD45.2<sup>+</sup> lung cells was assessed before infection. (B-D) Mixed bone marrow chimera mice were infected with *Mtb*. (B, C) The frequency of infected lung neutrophils and (D) lung *Mtb* burden was assessed in nonchimeric and mixed bone marrow chimeric mice infected with GFP-*Mtb* at 21 dpi. (E-G) Cytokine transcript levels in total lung samples were assessed by

qRT-PCR (**E**) prior to infection, (**F**) at 14 dpi, and (**G**) at 21 dpi. The mean  $\pm$  SEM is graphed. Statistical differences were determined by two-tailed unpaired Student's t test for normally distributed groups or two-tailed unpaired Mann-Whitney test for nonnormally distributed groups. \*,  $P < 0.05$ ; \*\*,  $P < 0.01$ ; \*\*\*,  $P < 0.001$ ; \*\*\*\*,  $P < 0.0001$ . Data are from one (**A**) or two (**B-G**) independent experiments. Panels (**A-D, G**) were previously published in Huynh and Lin et al., 2018.

bone marrow cells were capable of normal reconstitution of the hematopoietic compartment within the lung (**Fig. 9A**). Chimeric mice were infected with GFP-expressing *Mtb* and analyzed at 21 dpi. WT + WT chimeras controlled *Mtb* infection with a low frequency of neutrophil infection (**Fig. 9B, C**). Neutrophils of both genotypes displayed a high frequency of *Mtb* infection (**Fig. 9B, C**), which correlated with a trend toward higher CFUs in the lungs of mixed WT + *Bhlhe40*<sup>-/-</sup> chimeras (**Fig. 9D**). These results demonstrate that *Bhlhe40*<sup>-/-</sup> cells, even when present as only half of all hematopoietic cells, exert a dominant influence *in trans* on the ability of WT cells to control neutrophil accumulation and *Mtb* infection. These data indicate that Bhlhe40 likely regulates secreted factors such as cytokines or chemokines, which can impact other cells. Therefore, we analyzed cytokine and chemokine levels in total lung samples from WT and *Bhlhe40*<sup>-/-</sup> mice by quantitative RT-PCR. In the lungs of naive WT and *Bhlhe40*<sup>-/-</sup> mice, there were no differences in the levels of *Csf3* (G-CSF), *Il10* (IL-10), *Il12b* (IL-12/23p40), or *Ifng* (IFN- $\gamma$ ) transcript (**Fig. 9E**), indicating that loss of Bhlhe40 does not impact expression of these genes in naive mice. At 14 dpi, transcripts for *Il12b* and *Ifng* were significantly decreased in the lungs of *Bhlhe40*<sup>-/-</sup> mice (**Fig. 9F**). At 21 dpi, transcripts for the neutrophil-associated cytokines *Csf3*, *Ccl3* (MIP-1 $\alpha$ ), and *Ccl4* (MIP-1 $\beta$ ) were up-regulated in *Bhlhe40*<sup>-/-</sup> lungs (**Fig. 9G**) as expected given the neutrophil-dominated inflammation observed. We also found that at 21 dpi, *Il10* transcript levels were 3-fold higher in *Bhlhe40*<sup>-/-</sup> lungs, while *Il12b* and *Ifng* transcript levels were 3- and 2-fold lower in *Bhlhe40*<sup>-/-</sup> lungs, respectively, compared with WT

lungs (**Fig. 9G**). This finding was of particular interest because *Bhlhe40* represses *Il10* transcription in CD4<sup>+</sup> T cells in the EAE model<sup>128</sup> and IL-10 has been shown to inhibit IL-12/23p40 and IFN- $\gamma$  expression during *Mtb* infection.<sup>40,43,48,50</sup>

### ***Bhlhe40* suppresses IL-10 production during in vivo *Mtb* infection**

The increased *Il10* transcript levels in conjunction with decreased *Il12b* and *Ifng* transcript levels in *Bhlhe40*<sup>-/-</sup> lungs at 21 dpi indicated that *Bhlhe40* could be regulating *Il10* expression. To identify the cell types responsible for the increased *Il10* expression in *Bhlhe40*<sup>-/-</sup> lungs, we used *Il10* bacterial artificial chromosome (BAC)-in transgene (10BiT) IL-10 reporter mice,<sup>175</sup> where *Il10*-expressing cells display Thy1.1 on their surface. We observed a similar distribution of *Il10*-expressing cells in 10BiT<sup>+</sup> WT mice as reported in a recent study that used these reporter mice to characterize sources of IL-10 before and after *Mtb* infection.<sup>44</sup> We crossed 10BiT and *Bhlhe40*<sup>-/-</sup> mice to generate a *Bhlhe40*<sup>-/-</sup> 10BiT<sup>+</sup> strain, and then we analyzed Thy1.1 expression as a proxy for *Il10* expression. We observed low levels of Thy1.1 expression in naive 10BiT<sup>+</sup> WT and 10BiT<sup>+</sup> *Bhlhe40*<sup>-/-</sup> mice (**Fig. 10**). At 21 dpi, the frequency of Thy1.1<sup>+</sup> neutrophils, inflammatory monocytes, moDCs, CD11b<sup>+</sup> DCs, B cells, CD4<sup>+</sup> T cells, and CD8<sup>+</sup> T cells was significantly higher in *Bhlhe40*<sup>-/-</sup> mice (**Fig. 11A, C**), but no differences were observed when comparing the absolute number of Thy1.1<sup>+</sup> cells (**Fig. 11B**). In addition, when we compared MFIs for Thy1.1 on Thy1.1<sup>+</sup> cells, we found that not only were a higher percentage of *Bhlhe40*<sup>-/-</sup> moDCs and B cells expressing Thy1.1, but these cell types also expressed more Thy1.1 on a per-cell basis during *Mtb* infection (**Fig. 11D**). Significantly higher Thy1.1 MFI was also observed on *Bhlhe40*<sup>-/-</sup> Thy1.1<sup>+</sup> alveolar macrophages and CD11b<sup>+</sup> macrophages (**Fig. 11D**). The increased frequency of Thy1.1 positivity observed in *Bhlhe40*<sup>-/-</sup> CD4<sup>+</sup> T cells was

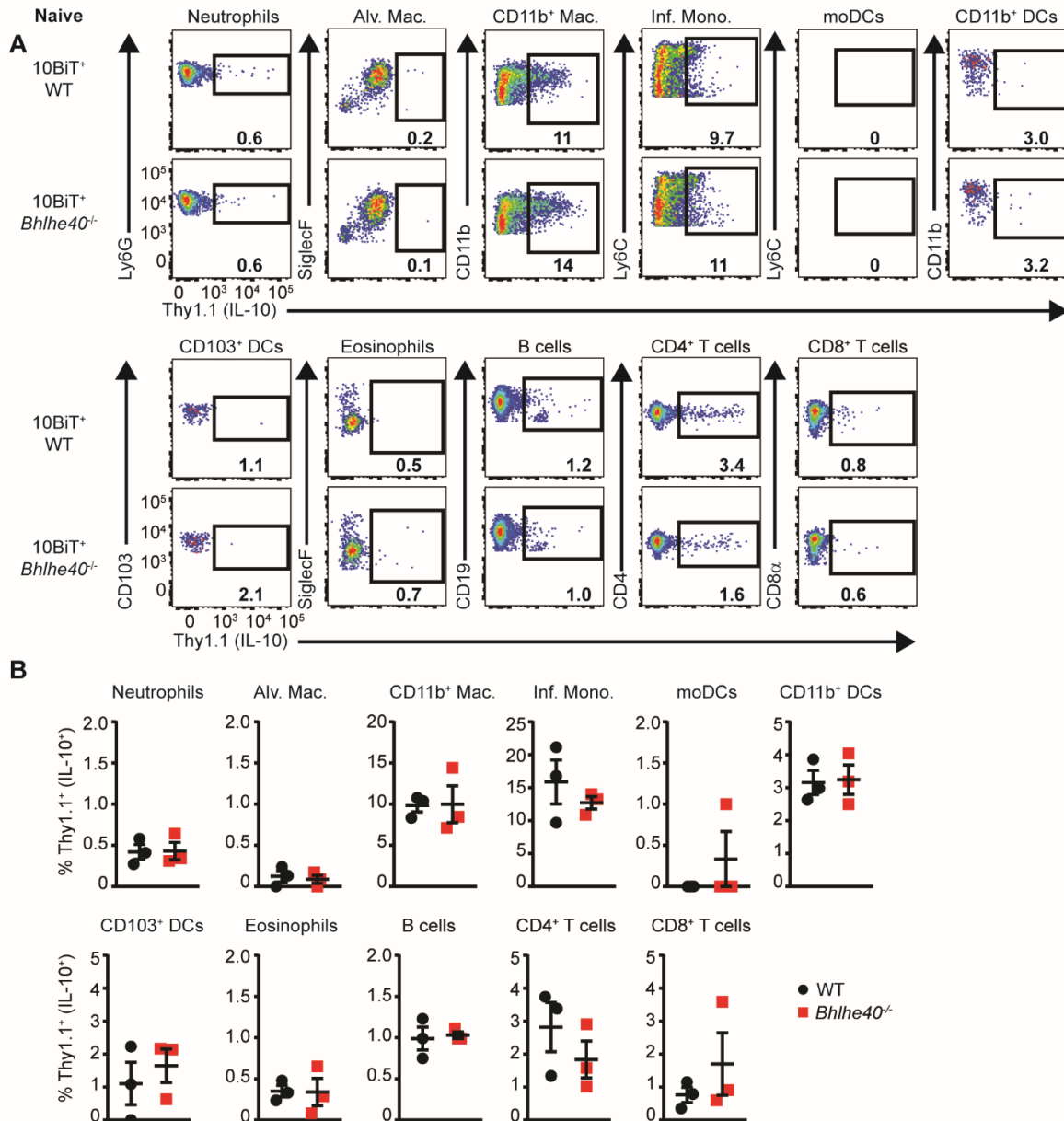


**Figure 10. *Bhlhe40* deficiency does not cause IL-10 overexpression in the absence of infection.**

(A-B) Uninfected 10BiT<sup>+</sup> mice were analyzed for the frequency of Thy1.1<sup>+</sup> (IL-10<sup>+</sup>) lung immune cells. The frequency of Thy1.1<sup>+</sup> (IL-10<sup>+</sup>) lung immune cells was assessed in uninfected mice. Mac., macrophage; Inf. Mono., inflammatory monocyte; Alv. Mac., alveolar macrophage. The mean  $\pm$  SEM is graphed. Statistical differences were determined by two-tailed unpaired Student's t test for normally distributed groups or two-tailed unpaired Mann-Whitney test for non-normally distributed groups. \*,  $P < 0.05$ ; \*\*,  $P < 0.01$ ; \*\*\*,  $P < 0.001$ ; \*\*\*\*,  $P < 0.0001$ . Data are from one experiment (A, B).

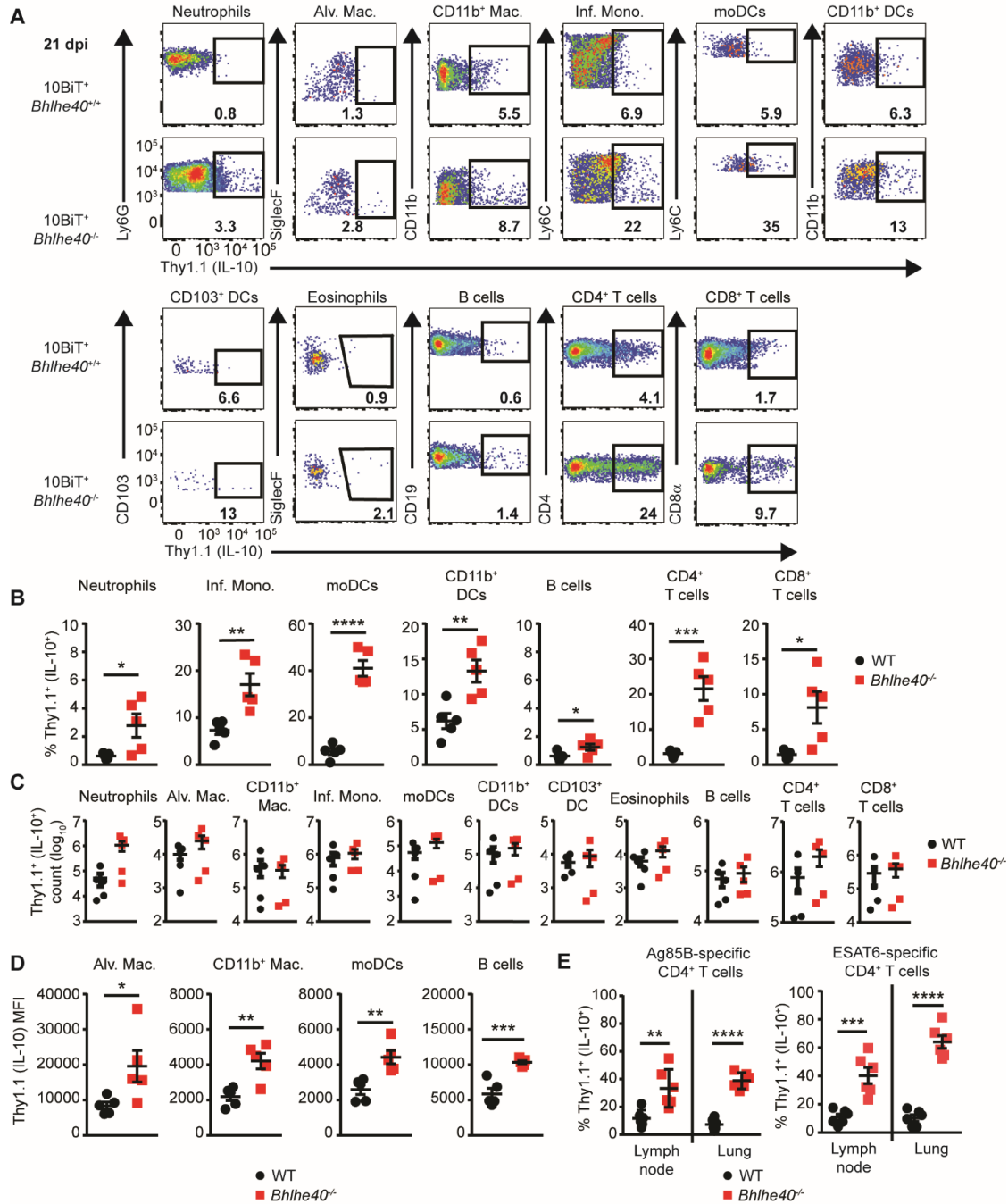


**Figure 11. *Bhlhe40* deficiency causes overexpression of IL-10 during *Mtb* infection.**

(A-E) Mice were infected with *Mtb* and assessed for (A, B) frequency and (C) absolute number of Thy1.1<sup>+</sup> (IL-10<sup>+</sup>) lung immune cells at 21 dpi. (D) MFI for FITC (Thy1.1 [IL-10]) on Thy1.1<sup>+</sup> lung cells at 21 dpi. Mac., macrophage; Inf. Mono., inflammatory monocyte; Alv. Mac., alveolar macrophage. Thy1.1<sup>+</sup> (E) Ag85B- or ESAT6-specific CD4<sup>+</sup> T cells as a percentage of the total Ag85B- or ESAT6-specific CD4<sup>+</sup> T cell population in the lung or mediastinal lymph node at 21 dpi. The mean ± SEM is graphed. Statistical differences were determined by two-tailed unpaired Student's t test for normally distributed groups or two-tailed unpaired Mann-

Whitney test for non-normally distributed groups. \*,  $P < 0.05$ ; \*\*,  $P < 0.01$ ; \*\*\*,  $P < 0.001$ ; \*\*\*\*,  $P < 0.0001$ . Data are from two independent experiments (A-E). Panels (A-E) were previously published in Huynh and Lin et al., 2018.

even more pronounced in *Bhlhe40*<sup>-/-</sup> *Mtb*-specific CD4<sup>+</sup> T cells in the mediastinal lymph node and lung, indicating that *Mtb*-specific CD4<sup>+</sup> T cells take on an immunosuppressive phenotype in the absence of Bhlhe40 (Fig. 11E). These data demonstrated that the frequency and per-cell expression of *Il10* was increased in multiple *Bhlhe40*<sup>-/-</sup> myeloid and lymphoid populations.

### ***Bhlhe40 suppresses IL-10 expression in myeloid cells in vitro***

We next sought to identify an *in vitro* myeloid cell culture system that recapitulates the effects of Bhlhe40 deficiency on IL-10 production in response to *Mtb*. We cultured WT bone marrow cells with GM-CSF or macrophage colony stimulating factor (M-CSF) and determined by Western blot analysis that only cells cultured with GM-CSF, which comprise a mixture of granulocytes, macrophage-like cells, and DC-like cells,<sup>176,177</sup> express Bhlhe40 (**Fig. 12A**). Analysis of GM-CSF- and M-CSF-cultured cells from *Bhlhe40*<sup>GFP</sup> reporter mouse bone marrow confirmed that only GM-CSF-cultured bone marrow-derived cells expressed GFP (**Fig. 12B**). This expression of Bhlhe40 in granulocytes, macrophage-like cells, and DC-like cells cultured with GM-CSF may relate to the expression of Bhlhe40 by these cell types in the lung (**Fig. 6**),<sup>108,178</sup> where GM-CSF is abundant and plays an important part in the development and function of lung myeloid cells.<sup>179</sup>

We next assessed IL-10 expression from WT and *Bhlhe40*<sup>-/-</sup> cells cultured with GM-CSF. In the absence of stimulation with heat-killed *Mtb*, minimal IL-10 protein was detected in culture supernatants (**Fig. 12C**). In contrast, *Bhlhe40*<sup>-/-</sup> GM-CSF-cultured bone marrow-derived

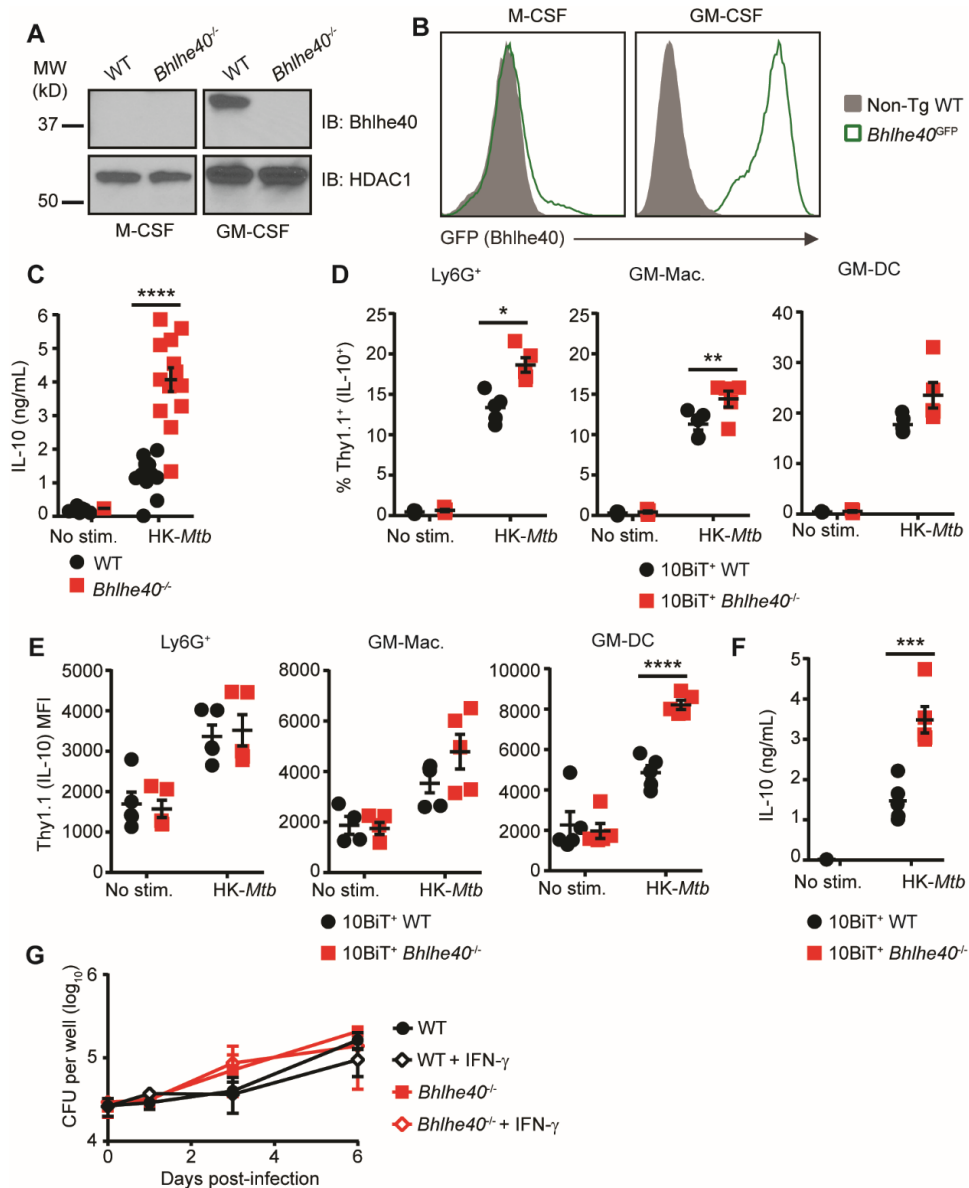


**Figure 12. *Bhlhe40* represses IL-10 in myeloid cells after *Mtb* stimulation.**

(A-B) Bone marrow cells were differentiated in the presence of M-CSF or GM-CSF and analyzed for expression of *Bhlhe40* by (A) immunoblot (IB) with HDAC1 as a loading control or (B) GFP as a reporter for *Bhlhe40* expression. MW, molecular weight. (C) GM-CSF-cultured bone marrow-derived cells were left unstimulated or were stimulated with heat-killed (HK) *Mtb* for 24 hrs, and culture supernatants were analyzed for IL-10 production by ELISA. IL-10 expression in six unstimulated WT and 12 unstimulated *Bhlhe40*<sup>-/-</sup> samples was below the limit of detection (~0.1 ng/ml). (D-F) 10BiT<sup>+</sup> WT and *Bhlhe40*<sup>-/-</sup> bone marrow cells were differentiated in the presence of GM-CSF and stimulated with heat-killed *Mtb* antigen for 24 hrs. Thy1.1 was assessed on three subpopulations of cells within the GM-CSF cultures. These included Ly6G<sup>+</sup> cells, GM-macrophages (GM-Macs; identified as CD11c<sup>+</sup>CD11b<sup>high</sup>MHC-II<sup>mid</sup>), and GM-DCs (identified as CD11c<sup>+</sup>CD11b<sup>mid</sup>MHC-II<sup>high</sup>). (D) Frequency of Thy1.1<sup>+</sup> (IL-10<sup>+</sup>) cells after 24 hrs of stimulation. (E) MFI for Thy1.1 on Thy1.1<sup>+</sup> cells after 24 hrs of stimulation. (F) IL-10 production in 10BiT<sup>+</sup> WT and 10BiT<sup>+</sup> *Bhlhe40*<sup>-/-</sup> cells after 24 hrs of stimulation. (G) Bacterial load (CFU) over 6 days post-infection.

(F) Culture supernatants were analyzed for IL-10 production by ELISA. IL-10 expression in four unstimulated 10BiT<sup>+</sup> WT and five unstimulated 10BiT<sup>+</sup> *Bhlhe40*<sup>-/-</sup> samples was below the limit of detection (~0.1 ng/ml). (G) GM-CSF-cultured bone marrow-derived cells were infected with *Mtb*, in some cases treated with IFN- $\gamma$ , and CFUs were measured. The mean  $\pm$  SEM is graphed. Statistical differences were determined by two-tailed unpaired Student's t test for normally distributed groups or two-tailed unpaired Mann-Whitney test for non-normally distributed groups. \*, P < 0.05; \*\*, P < 0.01; \*\*\*, P < 0.001; \*\*\*\*, P < 0.0001. Data are from or representative of two (A, B, D-F), five (C), or one (G) independent experiments. Panels (A-G) were previously published in Huynh and Lin et al., 2018.

cells stimulated with heat-killed *Mtb* for 24 hours produced significantly more IL-10 than WT cells (Fig. 12C). We also stimulated 10BiT<sup>+</sup> WT and *Bhlhe40*<sup>-/-</sup> GM-CSF-cultured cells with heat-killed *Mtb*, assessed Thy1.1 expression by flow cytometry, and measured IL-10 in culture supernatants by ELISA. *Mtb* stimulation increased the frequency of Thy1.1<sup>+</sup> cells in both WT and *Bhlhe40*<sup>-/-</sup> cultures relative to unstimulated cultures, and this increase was greater in *Bhlhe40*<sup>-/-</sup> cells compared with WT cells (Fig. 12D). *Mtb* stimulation also increased the amount of Thy1.1 expression on a per-cell basis, where *Bhlhe40*<sup>-/-</sup> CD11c<sup>+</sup>CD11b<sup>+</sup>MHC-II<sup>high</sup> (GM-DC) cells exhibited a 1.7-fold higher MFI than WT GM-DCs (Fig. 12E). ELISAs confirmed that 10BiT<sup>+</sup> *Bhlhe40*<sup>-/-</sup> cells secreted more IL-10 than 10BiT<sup>+</sup> WT cells after stimulation with heat-killed *Mtb* (Fig. 12F). These experiments confirm that loss of *Bhlhe40* in GM-CSF-cultured cells results in higher levels of IL-10 production. Loss of *Bhlhe40* did not significantly affect the ability of GM-CSF-cultured cells to control *Mtb* replication in the presence or absence of IFN- $\gamma$  (Fig. 12G), suggesting that *Bhlhe40* is dispensable for the ability of these cell types to control *Mtb* replication *in vitro*.

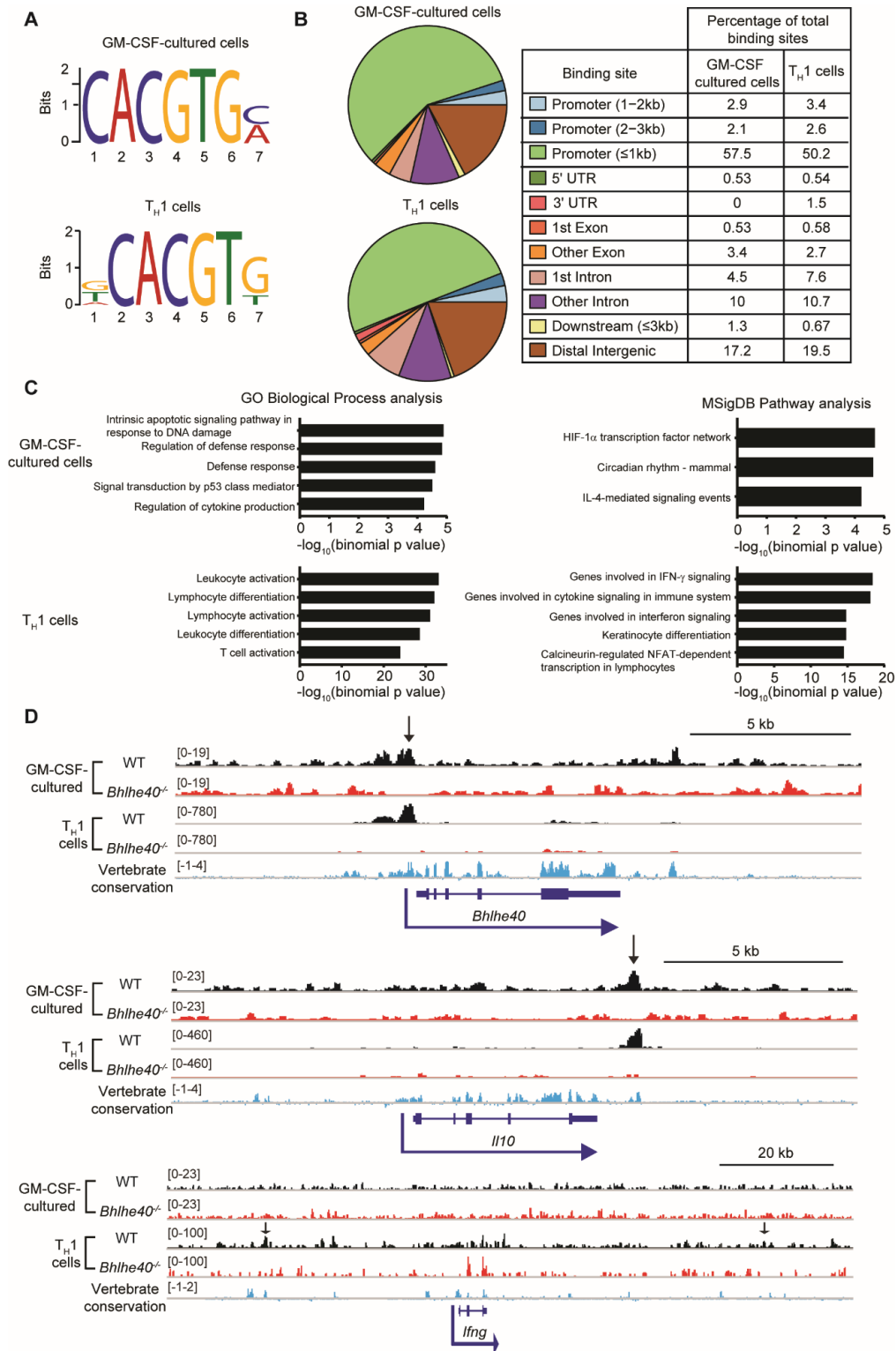


**Figure 13. *Bhlhe40* directly binds the *Il10* locus in myeloid and lymphoid cells.**

(A-D) Bone marrow cells were differentiated in the presence of GM-CSF and stimulated with heat-killed *Mtb* for 4 hrs. CD4<sup>+</sup> T cells were isolated from the spleen of naïve mice and *T<sub>H</sub>1*

polarized *in vitro* for 4 days. DNA was immunoprecipitated using anti-Bhlhe40 antibody and sequenced. (A) Sequence motifs present within DNA bound by Bhlhe40 were analyzed by MEME-ChIP. (B) Bhlhe40 binding sites were annotated using ChIP-seeker v3.5. (C) Functions of *cis*-regulatory regions were predicted for Bhlhe40 binding site data using GREAT. The top five most highly enriched gene sets with minimum region-based fold enrichment of 2 and binomial and hypergeometric false discovery rates of  $\leq 0.05$  in the Gene Ontology (GO) Biological Process and MSigDB Pathway gene sets are displayed for each dataset (in GM-CSF-cultured cells, only three MSigDB Pathway gene sets met these criteria). NFAT, nuclear factor of activated T cells. (D) ChIP-seq binding tracks for Bhlhe40 at the *Bhlhe40*, *Il10*, and *Ifng* loci in WT and *Bhlhe40*<sup>-/-</sup> myeloid and lymphoid cells. Vertebrate conservation of each genomic region is displayed in blue, and peaks identified by MACS are indicated by arrows. Bracketed numbers indicate the trace height range. Data are from a single experiment. Panels (A-D) were previously published in Huynh and Lin et al., 2018.

### ***Bhlhe40 binds directly to the Il10 locus in T<sub>H</sub>1 cells and myeloid cells***

We performed chromatin immunoprecipitation sequencing (ChIP-seq) experiments in *in vitro*-polarized T<sub>H</sub>1 cells and GM-CSF-cultured bone marrow-derived cells to interrogate whether Bhlhe40 directly binds to the *Il10* locus in these cells as well as to identify other genes that may be directly regulated by Bhlhe40. We performed these studies with WT and *Bhlhe40*<sup>-/-</sup> cells, where *Bhlhe40*<sup>-/-</sup> cells served as controls for nonspecific binding by the anti-Bhlhe40 antibody. Bhlhe40 bound 379 sites in WT GM-CSF-cultured cells and 5,532 sites in WT T<sub>H</sub>1-polarized T cells. Of these sites, 273 were found in both datasets. Bhlhe40 can directly bind to regulatory DNA elements as a homodimer through recognition of E-box sites, with a preference for the sequence CACGTG.<sup>180</sup> Motif finding identified the expected E-box (CACGTG) as the most frequent motif present within the peaks identified in both cell types (**Fig. 13A**). Analysis of binding sites revealed that Bhlhe40 predominantly bound promoters within 1 kb of the transcriptional start site, introns, and distal intergenic regions (**Fig. 13B**). Pathway analysis of predicted Bhlhe40-regulated genes revealed an enrichment in immune activation and cytokine response pathways in both datasets (**Fig. 13C**). Bhlhe40 is known to bind a conserved

autoregulatory site in the *Bhlhe40* promoter,<sup>102</sup> and this binding site was identified as a peak in both datasets (**Fig. 13D**). Importantly, our ChIP-seq experiment identified a *Bhlhe40* binding site at +6 kb relative to the transcriptional start site of *Il10* in both datasets, coinciding with an evolutionarily conserved region that is close to a +6.45 kb site previously identified as an enhancer element in T<sub>H2</sub> cells (**Fig. 13D**).<sup>181</sup> These data suggest that *Bhlhe40* directly represses *Il10* transcription in myeloid and lymphoid cells through direct binding of a downstream *cis*-regulatory element. ChIP-seq analysis did not reveal binding of *Bhlhe40* to the *Il12b* locus in either dataset. *Bhlhe40* did not bind the *Ifng* locus in GM-CSF-cultured cells but bound two sites distal (-33.5 kb and +53.2 kb) to the *Ifng* transcriptional start site in T<sub>H1</sub> cells (**Fig. 13D**). These findings suggest that the transcriptional down-regulation of *Il12b* in *Bhlhe40*<sup>-/-</sup> total lung samples (**Fig. 9F, G**) is indirect and likely a result of increased IL-10 signaling, whereas the decreased levels of *Ifng* may result from either increased IL-10 signaling or T cell-intrinsic loss of direct regulation by *Bhlhe40*.

### ***IL-10 deficiency protects Bhlhe40*<sup>-/-</sup> mice from *Mtb* infection**

To investigate the role of IL-10 production in the susceptibility of *Bhlhe40*<sup>-/-</sup> mice, we generated *Il10*<sup>-/-</sup>*Bhlhe40*<sup>-/-</sup> mice and compared their survival to WT, *Bhlhe40*<sup>-/-</sup>, and *Il10*<sup>-/-</sup> mice after *Mtb* infection. The absence of IL-10 signaling resulted in near-complete rescue of the acute susceptibility phenotype caused by *Bhlhe40* deficiency as shown by the significant increase in the median survival time of *Il10*<sup>-/-</sup>*Bhlhe40*<sup>-/-</sup> mice (122 days) compared with *Bhlhe40*<sup>-/-</sup> mice (31 days) (**Fig. 14A**). The increased survival of *Il10*<sup>-/-</sup>*Bhlhe40*<sup>-/-</sup> mice was accompanied by decreased *Mtb* titer in *Il10*<sup>-/-</sup>*Bhlhe40*<sup>-/-</sup> lungs (8-fold) and spleens (5-fold)

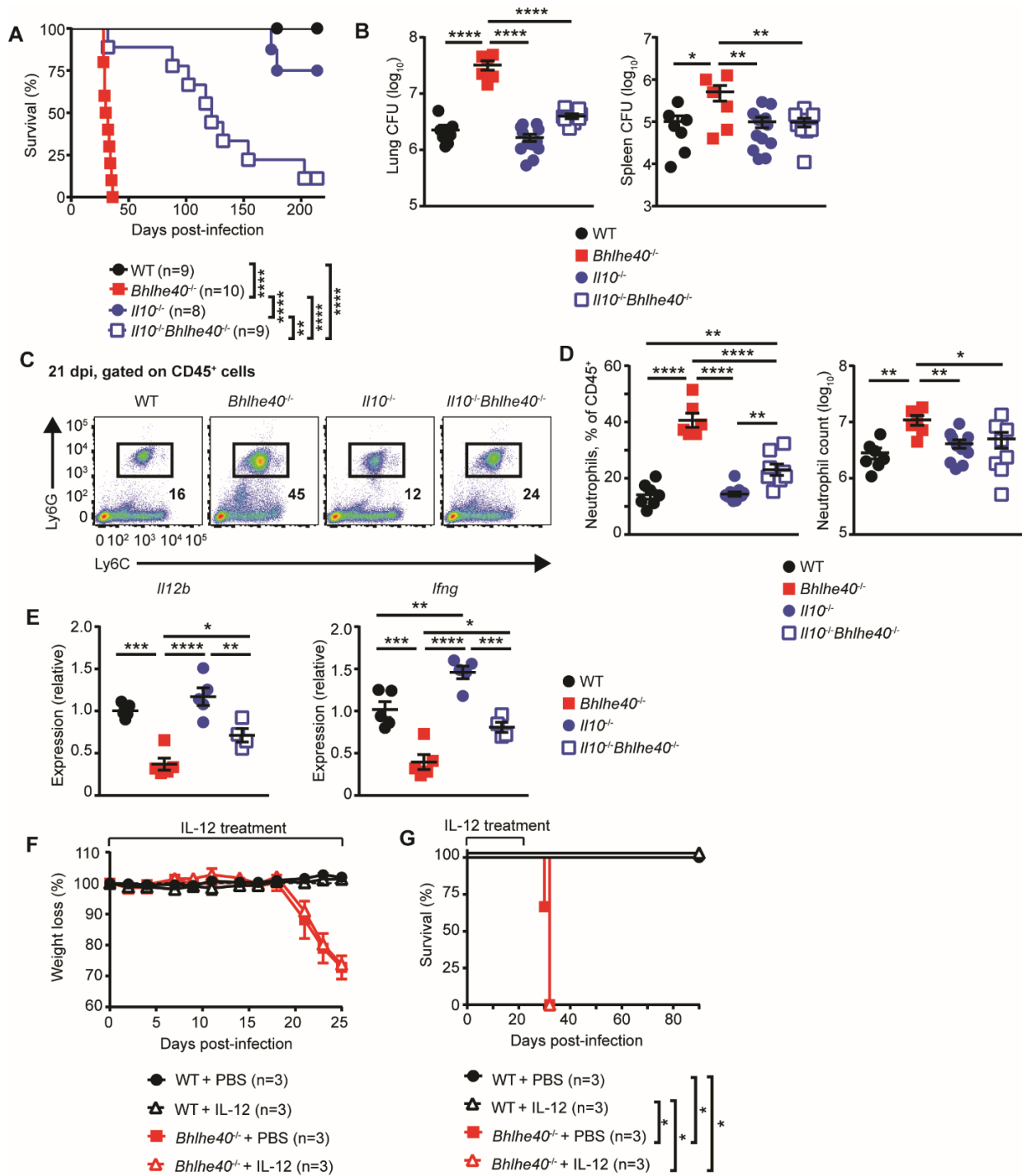


**Figure 14. IL-10 deficiency protects *Bhlhe40*<sup>-/-</sup> mice from *Mtb* infection.**

(A-F) Mice were infected with *Mtb* and monitored for (A) survival and (B) lung and spleen CFU, (C, D) frequency and absolute number of lung neutrophils, and (E) cytokine transcript levels in total lung samples at 21 dpi. (F, G) Mice were infected with *Mtb* and treated with IL-12 three times per week for the first 4 weeks of infection. (F) Weight loss and (G) survival were monitored. The mean  $\pm$  SEM is graphed. Statistical differences were determined by log-rank Mantel-Cox test (A, B) and one-way unpaired ANOVA with Tukey's post-test for normally

distributed groups or unpaired Kruskal-Wallis test with Dunn's multiple comparison test for non-normally distributed groups (**B, D, E**). \*,  $P < 0.05$ ; \*\*,  $P < 0.01$ ; \*\*\*,  $P < 0.001$ ; \*\*\*\*,  $P < 0.0001$ . Data are from or representative of two (**A, E**), four (**B, C, D**), or one (**F, G**) independent experiments. Parts of panels (**A, B**) and all of panels (**C-E**) were previously published in Huynh and Lin et al., 2018.

compared with *Bhlhe40*<sup>-/-</sup> mice at 21 dpi (**Fig. 14B**). These data demonstrate that the inability of *Bhlhe40*<sup>-/-</sup> mice to control acute phase *Mtb* replication is likely caused in large part by higher IL-10 levels. When compared with *Bhlhe40*<sup>-/-</sup> lungs, *Il10*<sup>-/-</sup>*Bhlhe40*<sup>-/-</sup> lungs contained a significantly lower frequency and total number of neutrophils (Fig. 14C, D). However, the frequency of neutrophils in *Il10*<sup>-/-</sup>*Bhlhe40*<sup>-/-</sup> lungs remained higher than in WT or *Il10*<sup>-/-</sup> lungs (Fig. 14C, D). *Il10*<sup>-/-</sup>*Bhlhe40*<sup>-/-</sup> lungs also contained 2-fold more *Il12b* and *Ifng* transcripts than *Bhlhe40*<sup>-/-</sup> lungs at 21 dpi, demonstrating that IL-10 signaling was at least partially responsible for the decreased expression of these genes in *Bhlhe40*<sup>-/-</sup> lungs (Fig. 14E). The association of higher *Il12b* transcript levels and increased resistance in *Il10*<sup>-/-</sup>*Bhlhe40*<sup>-/-</sup> mice suggested that an early defect in IL-12 production might contribute to the susceptibility of *Bhlhe40*<sup>-/-</sup> mice. We tested this with an IL-12 administration regimen previously shown to extend the susceptibility of *Il12b*<sup>-/-</sup> mice.<sup>182</sup> *Bhlhe40*<sup>-/-</sup> mice were treated with IL-12 during *Mtb* infection and weight loss (Fig. 14F) and survival (Fig. 14G) were monitored. IL-12 administration had no effect on weight loss or survival, suggesting that lower *Il12b* levels are not limiting protective immunity or that there are additional obstacles to protective immunity. These data establish *Bhlhe40* as an essential regulator of *Il10* expression in myeloid cells and lymphocytes during *Mtb* infection and reveal the importance of IL-10 regulation for innate and adaptive immune responses that control *Mtb* infection.

## Discussion

We have identified Bhlhe40 as a transcription factor that is essential for coordinating immune responses that protect the host from *Mtb* infection. Based on our research, we propose the following model (**Fig. 15**). During the acute phase of infection, CD11c<sup>+</sup> cells encounter *Mtb* antigens that trigger a putative transcriptional activator to induce *Il10* expression, the activity of which is restricted by the binding of Bhlhe40 to a *cis*-acting regulatory region +6 kb downstream of the *Il10* transcriptional start site. The identity of the activator that induces *Il10* transcription in the absence of Bhlhe40 during *Mtb* infection is currently unknown but may be one of the activators previously described.<sup>75</sup> In addition, Bhlhe40 is induced in T cells during *Mtb* infection, where it also represses *Il10* transcription. The repression of *Il10* expression by Bhlhe40 in these cell types allows for higher expression of *Il12b* and *Ifng*, both of which are essential for control of *Mtb* replication.<sup>34,35,183,184</sup>

These findings represent the first study of roles for Bhlhe40 in the immune response to an infection and within myeloid cells, although a report that T cell expression of Bhlhe40 is essential for control of *Toxoplasma gondii* infection was published concurrently.<sup>129</sup> Additionally, although other negative regulators of *Il10* transcription have been described,<sup>78–81,83,84</sup> Bhlhe40 is the first transcription factor that has been shown to be essential during *Mtb* infection specifically to regulate *Il10* expression. Our findings reveal the importance of controlling IL-10 generation by both innate and adaptive immune cells and shed light on how different levels of IL-10 could impact tuberculosis disease in humans. Survival experiments showed that about one quarter of *Bhlhe40<sup>fl/fl</sup>-Cd11c-Cre* and *Bhlhe40<sup>fl/fl</sup>-Cd4-Cre* mice recapitulated the very early susceptibility of *Bhlhe40<sup>-/-</sup>* mice (**Fig. 8A**), with the remainder of these Bhlhe40 conditionally deleted mice dying between 50 and 75 dpi. In the case of the *Bhlhe40<sup>fl/fl</sup>-Cd4-Cre* strain, the finding that 4 out

of 12 of these mice succumbed at 31-38 dpi (**Fig. 8A**), whereas *Rag1*<sup>-/-</sup> mice succumbed at ~45 dpi (**Fig. 7C**), indicates that *Bhlhe40*<sup>-/-</sup> T cells can be actively pathological and generate a worse outcome than the absence of T cells, likely through the production of a factor such as IL-10. However, the extension of survival observed in BCG-vaccinated *Bhlhe40*<sup>-/-</sup> mice (**Fig. 8F**) suggests that *Bhlhe40*<sup>-/-</sup> T cells may have some protective capacity in specific contexts. The delay in susceptibility of most of the *Bhlhe40*<sup>fl/fl</sup>-*Cd11c-Cre* and *Bhlhe40*<sup>fl/fl</sup>-*Cd4-Cre* mice as compared with *Bhlhe40*<sup>-/-</sup> mice could indicate that the susceptibility of *Bhlhe40*<sup>-/-</sup> mice is a result of the combination of loss of Bhlhe40 in both CD11c<sup>+</sup> and T cells, insufficient ability of the *Cd11c* and *Cd4* promoters to drive Bhlhe40 exon deletion in all Cre-expressing cells, or the ability of Bhlhe40 deficiency in a non-CD11c<sup>+</sup> or -CD4<sup>+</sup> cell type to enhance susceptibility. Although only one *Bhlhe40*<sup>fl/fl</sup>-*Zbtb46-Cre* mouse was tested, it proved to be susceptible during chronic infection, demonstrating the requirement for Bhlhe40 expression in DCs. The delayed susceptibility of *Bhlhe40*<sup>fl/fl</sup>-*Zbtb46-Cre* mice compared to *Bhlhe40*<sup>fl/fl</sup>-*Cd11c-Cre* mice may be due to incomplete deletion in all DCs, *Cd11c* promoter-driven deletion of *Bhlhe40* in non-DCs, or a protective role for Bhlhe40 in alveolar macrophages when other CD11c<sup>+</sup> cell lack Bhlhe40. IL-10 production by T cells and CD11c<sup>+</sup> cells during *Mtb* infection in mice was recently shown to contribute to host susceptibility,<sup>44</sup> further supporting the notion that regulation of *Il10* expression in these cell populations would be important during *Mtb* infection.

Our analyses of *Il10*<sup>-/-</sup>*Bhlhe40*<sup>-/-</sup> mice revealed that IL-10 deficiency conferred a near-complete rescue of multiple phenotypes associated with the acute susceptibility of *Bhlhe40*<sup>-/-</sup> mice (**Fig. 14**), indicating that the up-regulation of *Il10* transcription in the absence of Bhlhe40 is a major contributor to the acute susceptibility of these mice. Nonetheless, some phenotypes partially remained in the absence of *Il10*. For example, nearly all *Il10*<sup>-/-</sup>*Bhlhe40*<sup>-/-</sup> mice

succumbed by 200 dpi (**Fig. 14A**) and *Il10<sup>-/-</sup>Bhlhe40<sup>-/-</sup>* mice had a significantly higher frequency of lung neutrophils at 21 dpi compared with WT mice (**Fig. 14C, D**). The incomplete rescue of these phenotypes indicates that Bhlhe40 likely regulates the expression of other genes during *Mtb* infection that impact pathogenesis. Future studies will explore the other Bhlhe40-bound loci identified by ChIP-seq to identify additional Bhlhe40 targets that contribute to the control of *Mtb* infection.

Patients with active tuberculosis have increased levels of IL-10 in their serum<sup>65,66</sup> and lungs,<sup>61,63,64,185</sup> suggesting a link between increased IL-10 levels and tuberculosis disease.<sup>165</sup>

Although it is unclear whether the reduced expression of *BHLHE40* in the blood of patients with active tuberculosis (**Fig. 1A**) is a cause or effect of their disease or related to the higher IL-10 levels found in this form of tuberculosis, this correlation agrees with the increased susceptibility of mice lacking Bhlhe40 and suggests that our experiments could be relevant to human *Mtb* infection.

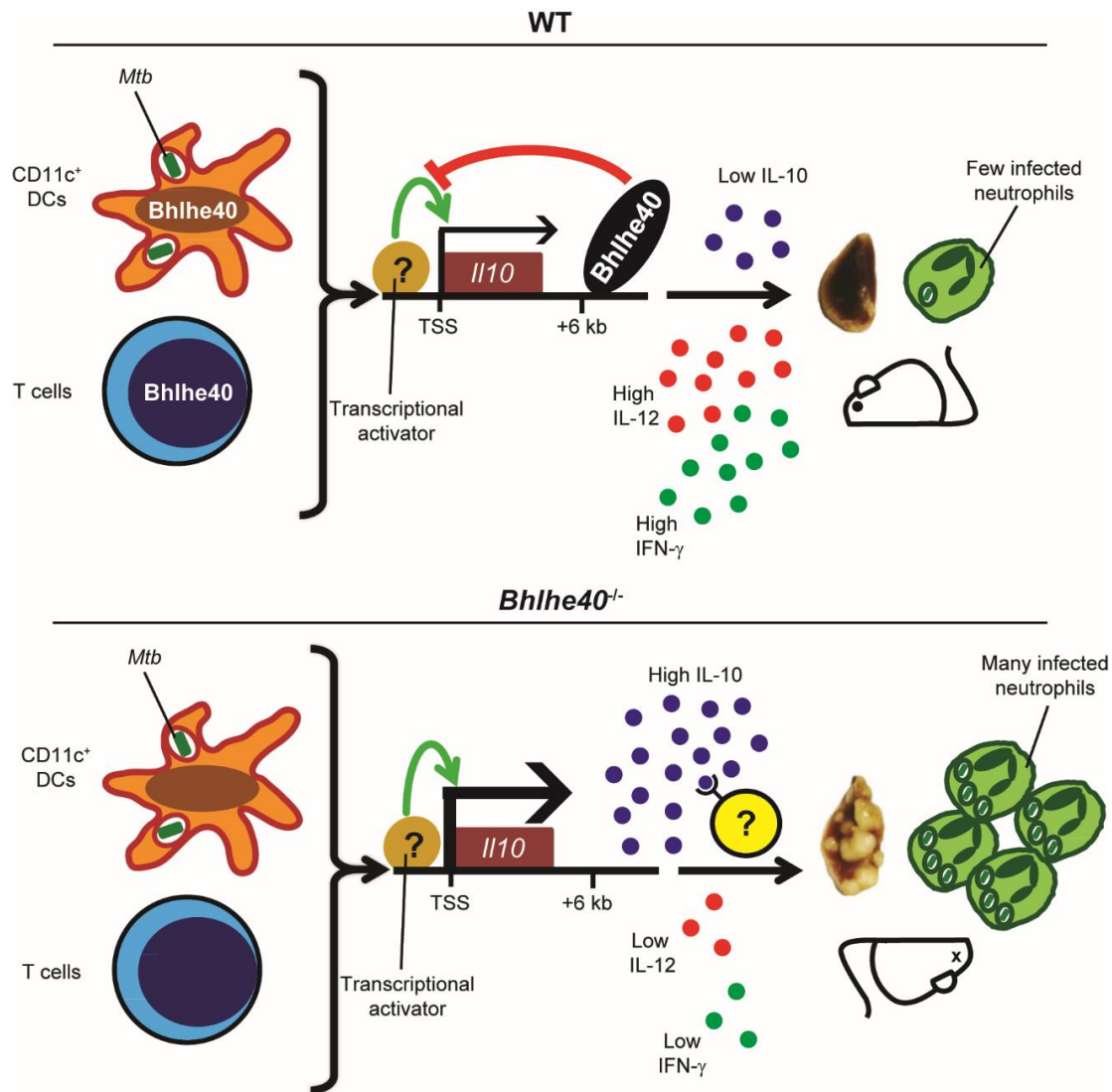


**Figure 15. Model of Bhlhe40 function during *Mtb* infection.**

During *Mtb* infection of WT cells, *I110* transcription is restricted by Bhlhe40 in CD11c<sup>+</sup> DCs and T cells through direct binding to an enhancer site +6 kb downstream of the *I110* transcriptional start site (TSS). The resulting amount of IL-10 expression is insufficient to compromise host resistance, leading to an immunological stalemate in which *Mtb* replication is controlled for the remainder of the lifetime of the host. In *Bhlhe40*<sup>-/-</sup> mice, the absence of Bhlhe40 in CD11c<sup>+</sup> DCs and T cells allows for high levels of *I110* expression. Excessive IL-10 signaling then acts on lung immune cells to suppress the production and protective effects of IL-12 and IFN- $\gamma$ , both of which are essential for control of *Mtb* pathogenesis. As a result, *Mtb* lung burdens are higher and neutrophil-dominated inflammation is uncontrolled in *Bhlhe40*<sup>-/-</sup> mice, ultimately resulting in susceptibility. Previously published in Huynh and Lin et al., 2018.

## Experimental Procedures

### *Bacterial strains and cultures*

*Mtb* strain Erdman and its derivatives were cultured at 37°C in 7H9 broth (Sigma-Aldrich) or on 7H11 agar (BD) medium supplemented with 10% oleic acid/albumin/dextrose/catalase (OADC), 0.5% glycerol, and 0.05% Tween-80 (broth only). *Mtb*-GFP was generated by transforming *Mtb* strain Erdman with a plasmid (pMV261-kan-GFP) that drives constitutive expression of GFP under the control of the *hsp60* promoter. Cultures were grown in the presence of kanamycin to ensure plasmid retention.  $\Delta$ PDIM *Mtb* was generated by transducing *Mtb* strain Erdman with a phage containing homology to nucleotides 3243062-3243567 and 3272196-3272718.  $\Delta$ ESX-1 *Mtb* was generated by transducing *Mtb* strain Erdman with a phage containing homology to nucleotides 4349945-4350677 and 4356534-4357206. Phage transduction was used to replace the endogenous *fadD26* and *ppsABCDE* ( $\Delta$ PDIM strain) and *pe35*, *ppe68*, *esxAB*, *espI*, and *eccD1* ( $\Delta$ ESX-1 strain) genes with a hygromycin resistance cassette. Mutants were selected by culture on hygromycin-containing 7H11 agar. Individual hygromycin-resistant colonies were expanded by inoculation into hygromycin-supplemented 7H9 media. Replacement of target genes with the hygromycin resistance cassette was confirmed by Southern blotting of genomic DNA from expanded cultures.

*M. bovis* BCG was a gift from S. Khader (Washington University in Saint Louis, Saint Louis, MO). Bacteria were not cultured and were used directly after thawing.

*L. monocytogenes* expressing chicken ovalbumin (LM-Ova) on the 10403S genetic background was a gift from H. Shen (University of Pennsylvania, Philadelphia, PA). Bacteria were grown to mid-logarithmic phase with shaking at 37°C in brain-heart infusion broth (HiMedia Laboratories) before washing and storage as glycerol stocks at -80°C.

### Mouse strains

All mice used were on a C57BL/6 background. C57BL/6 (Taconic), B6.SJL (CD45.1; Taconic), *Bhlhe40*<sup>GFP</sup> BAC Tg (N10 to C57BL/6),<sup>108</sup> *Bhlhe40*<sup>-/-</sup> (N10 to C57BL/6),<sup>109</sup> *Rag1*<sup>-/-</sup>, *Il10*<sup>-/-</sup>, and 10BiT IL-10 reporter mice<sup>175</sup> were maintained in a specific pathogen-free facility. *Bhlhe40*<sup>-/-</sup> mice were crossed to *Ccr2*<sup>-/-</sup>, *Csf3r*<sup>-/-</sup>, *Il10*<sup>-/-</sup>, *Rag1*<sup>-/-</sup>, or 10BiT mice for some experiments. *Bhlhe40*<sup>fl/fl</sup> mice were generated with two loxP sites flanking exon 4 of *Bhlhe40*. These mice originated as a KO-first promoter-driven mouse line from the Knockout Mouse Project (KOMP) and were purchased from The Jackson Laboratory (*Bhlhe40*<sup>tm1a(KOMP)Wtsi</sup>; 024395). These initial mice contained a *Bhlhe40* allele with a splice acceptor-LacZ reporter and a *Neo* cassette flanked by two Frt sites, which were removed by crossing them to B6N.129S4-*Gt(ROSA)26Sor*<sup>tm1(FLP1)Dym/J</sup> mice (016226; The Jackson Laboratory), leaving behind an allele of *Bhlhe40* with a loxP-flanked exon 4. Subsequent crosses yielded *Bhlhe40*<sup>fl/fl</sup> mice with no residual Rosa26-Flp transgene. *Bhlhe40*<sup>fl/fl</sup> mice were crossed with one of four mouse strains, *Mrp8-Cre* (B6.Cg-Tg(S100A8-cre,-EGFP)1Ilw/J; 021614), *Lysm-Cre* (B6N.129P2(B6)-*Lyz2*<sup>tm1(cre)lfo</sup>/J; 018956), *Cd11c-Cre* (B6. Cg-Tg(Itgax-cre)1-1Reiz/J; 008068), and *Cd4-Cre* (B6.Cg-Tg(Cd4- cre)1Cwi/Bflu/J; 022071), all from The Jackson Laboratory.

Age-matched littermate adult mice (9-23 weeks of age) of both sexes were used, and mouse experiments were randomized. No blinding was performed during animal experiments. All procedures involving animals were conducted following the National Institutes of Health guidelines for housing and care of laboratory animals, and they were performed in accordance with institutional regulations after protocol review and approval by the Institutional Animal Care and Use Committee of The Washington University in St. Louis School of Medicine (protocol 20160094, Immune System Development and Function, and protocol 20160118, Analysis of

Mycobacterial Pathogenesis). Washington University is registered as a research facility with the United States Department of Agriculture and is fully accredited by the American Association of Accreditation of Laboratory Animal Care. The Animal Welfare Assurance is on file with Office for Protection from Research Risks–National Institutes of Health. All animals used in these experiments were subjected to no or minimal discomfort. All mice were euthanized by CO<sub>2</sub> asphyxiation, which is approved by the American Veterinary Association Panel on Euthanasia.

#### *Generation of bone marrow chimeric mice*

Bone marrow chimeric mice were generated by lethal irradiation (1,000 rads) of WT or *Bhlhe40*<sup>-/-</sup> recipients and reconstitution with 1-2 x 10<sup>7</sup> bone marrow cells from WT or *Bhlhe40*<sup>-/-</sup> donors. Mixed bone marrow chimeric mice were generated by lethal irradiation (1,000 rads) of WT (CD45.1/.2) recipients and reconstitution with 1-2 x 10<sup>7</sup> bone marrow cells from WT (CD45.1/.1) and either WT (CD45.2/.2) or *Bhlhe40*<sup>-/-</sup> (CD45.2/.2) donors mixed at a 1:1 ratio before transfer. Mice received drinking water containing 1.3 mg sulfamethoxazole and 0.26 mg trimethoprim per ml for 2 weeks after reconstitution and were allowed to reconstitute for at least 8 weeks before infection with *Mtb*.

#### *Cell culture*

Bone marrow cells were isolated from femurs and tibias of mice and treated with ACK lysis buffer (0.15 M NH<sub>4</sub>Cl, 10 mM KHCO<sub>3</sub>, and 0.1 mM EDTA) to lyse red blood cells. To generate M-CSF bone marrow-derived macrophages, bone marrow cells were cultured in complete IMDM (10% heat-inactivated FBS + 2 mM l-glutamine + 1X penicillin/streptomycin + 55 μM β-mercaptoethanol + 1X MEM nonessential amino acids + 1 mM sodium pyruvate) in

Petri dishes with the addition of 20 ng/ml M-CSF (PeproTech). To generate GM-CSF-cultured bone marrow-derived DCs and macrophages, bone marrow cells were cultured in complete RPMI (10% heat-inactivated FBS + 2 mM l-glutamine + 1X penicillin/streptomycin + 55  $\mu$ M  $\beta$ -mercaptoethanol) in six-well plates with the addition of 20 ng/ml GM-CSF (PeproTech). Cells were incubated at 37°C in 8% CO<sub>2</sub> for 8-9 days. At the end of the cultures, cells were harvested, counted, and adjusted to the desired cell concentrations. For flow cytometry analysis and ELISA assays, cells were seeded at a concentration of 5 x 10<sup>5</sup> cells/well in 96-well plates and were stimulated with or without 50  $\mu$ g/ml heat-killed *Mtb* (H37Ra strain; Difco) for 18 (FACS) or 24 (ELISA) hrs. In some experiments, suspension cells were stimulated in the presence of 10  $\mu$ g/ml heat-killed *Mtb* (H37Ra strain; Difco) for 4 hrs for ChIP assays.

To generate *in vitro*-polarized T<sub>H</sub>1 cells, naive splenic CD4<sup>+</sup> T cells (Easysep mouse naive CD4<sup>+</sup> T cell isolation kit, typical purity ~90-96%; StemCell Technologies, Inc.) were cultured in IMDM with plate-bound anti-CD3 (2  $\mu$ g/ml; clone 145-2C11; BioLegend) and anti-CD28 antibodies (2  $\mu$ g/ml; clone 37.51; BioLegend) in the presence of IL-12 (10 ng/ml; BioLegend) and anti-IL-4 (20  $\mu$ g/ml; Leinco). Cultures were split on day 3 and used for ChIP-seq on day 4.

#### *Bone marrow-derived GM-CSF-cultured cell infections*

For *Mtb* infection, cells were seeded at a concentration of 2.5 x 10<sup>5</sup> cells/well in 96-well plates. *Mtb* was washed with PBS + 0.05% Tween-80, sonicated to disperse clumps, diluted in antibiotic-free cell culture media, and added to cells at a multiplicity of infection of 1. After 4 hrs of incubation, cells were pelleted and washed twice with PBS, fresh culture media was added, and cells were incubated at 37°C in 5% CO<sub>2</sub>. In some cases, cells were pre-treated with 50 ng

IFN- $\gamma$  (BioLegend)/ml for 12 hrs before infection. CFUs were enumerated by pelleting cells, removing supernatant, lysing with PBS + 0.5% Triton X-100, and plating serial dilutions on 7H11 agar. Colonies were counted after 3 weeks of incubation at 37°C in 5% CO<sub>2</sub>.

### *Mouse infections*

*Mtb* cultures in logarithmic growth phase (OD<sub>600 nm</sub> = 0.5-0.8) were washed with PBS + 0.05% Tween-80, sonicated to disperse clumps, and diluted in sterile water. Mice were exposed to  $1.6 \times 10^8$  *Mtb* CFUs, a dose chosen to deliver 100–200 CFUs of aerosolized *Mtb* per lung using an Inhalation Exposure System (Glas-Col). Within the first 24 hrs of each infection, lungs were harvested from at least two control mice, homogenized, and plated on 7H11 agar to determine the input CFU dose. The mean dose determined at this time point was assumed to be representative of the dose received by all other mice infected simultaneously. At each time point after infection, *Mtb* titers were determined by homogenizing the superior, middle, and inferior lobes of the lung or the entire spleen and plating serial dilutions on 7H11 agar. Colonies were counted after 3 weeks of incubation at 37°C in 5% CO<sub>2</sub>.

*M. bovis* BCG was thawed and diluted in PBS. Mice were sedated with ketamine (Henry Schein) and xylazine (Akorn) and intranasally infected with  $2 \times 10^5$  CFU. BCG titers were determined by homogenizing the superior, middle, and inferior lobes of the lung and plating serial dilutions on 7H11 agar. Colonies were counted after 3 weeks of incubation at 37°C in 5% CO<sub>2</sub>.

LM-Ova was diluted into pyrogen-free saline for i.v. injection into mice. For experiments involving secondary infection, some mice were initially infected with a sublethal dose of  $10^4$  LM-Ova i.v. and rested for 30 d before secondary challenge with  $10^6$  LM-Ova i.v. After 3 days,

spleens and livers were homogenized separately in PBS + 0.05% Triton X-100. Homogenates were plated on brain-heart infusion agar, and *L. monocytogenes* CFUs were determined after growth at 37°C overnight.

### *Flow cytometry*

Lungs were perfused with sterile PBS before harvest. Lungs and lymph nodes were digested at 37°C with 630 µg/ml collagenase D (Roche) and 75 U/ml DNase I (Sigma-Aldrich). All antibodies were used at a dilution of 1:200. Single-cell suspensions were preincubated with anti-CD16/CD32 Fc Block antibody (BD) in PBS + 2% heat-inactivated FBS for 10 min at RT before surface staining. The following anti-mouse antibodies were obtained from BioLegend: PE-Cy7 anti-CD4 (RM4-5), APC-Cy7 anti-CD8 $\alpha$  (53–6.7), APC anti-CD11b (M1/70), BV605 anti-CD11c (N418), BV605 anti-CD19 (6D5), APC anti-CD45.2 (104), FITC anti-CD90.1 (Thy-1.1; OX-7), PerCP-Cy5.5 anti-CD103 (2E7), Pacific blue (PB) or PerCP-Cy5.5 anti-Ly6C (HK1.4), PE anti-Ly6G (1A8), PB anti-TCR $\beta$  (H57-597), and APC anti-TCR $\gamma\delta$  (GL3). The following anti-mouse antibodies were purchased from BD: PB anti-CD3 $\epsilon$  (145-2C11), BV510 anti-CD45 (30F11), and PE anti-Siglec F (E50-2440). The following anti-mouse antibodies were obtained from Tonbo Biosciences: redFluor710 anti-CD44 (IM7), V450 or PerCP-Cy5.5 anti-CD45.1 (A20), PE-Cy7 anti-Ly6G (1A8), and redFluor710 anti-I-A/I-E (M5/114.15.2).

Cells were stained for 20 min at 4°C, washed, and fixed in 4% paraformaldehyde (Electron Microscopy Sciences) in PBS for 20 min at 4°C. Cell counts were determined by hemocytometer.

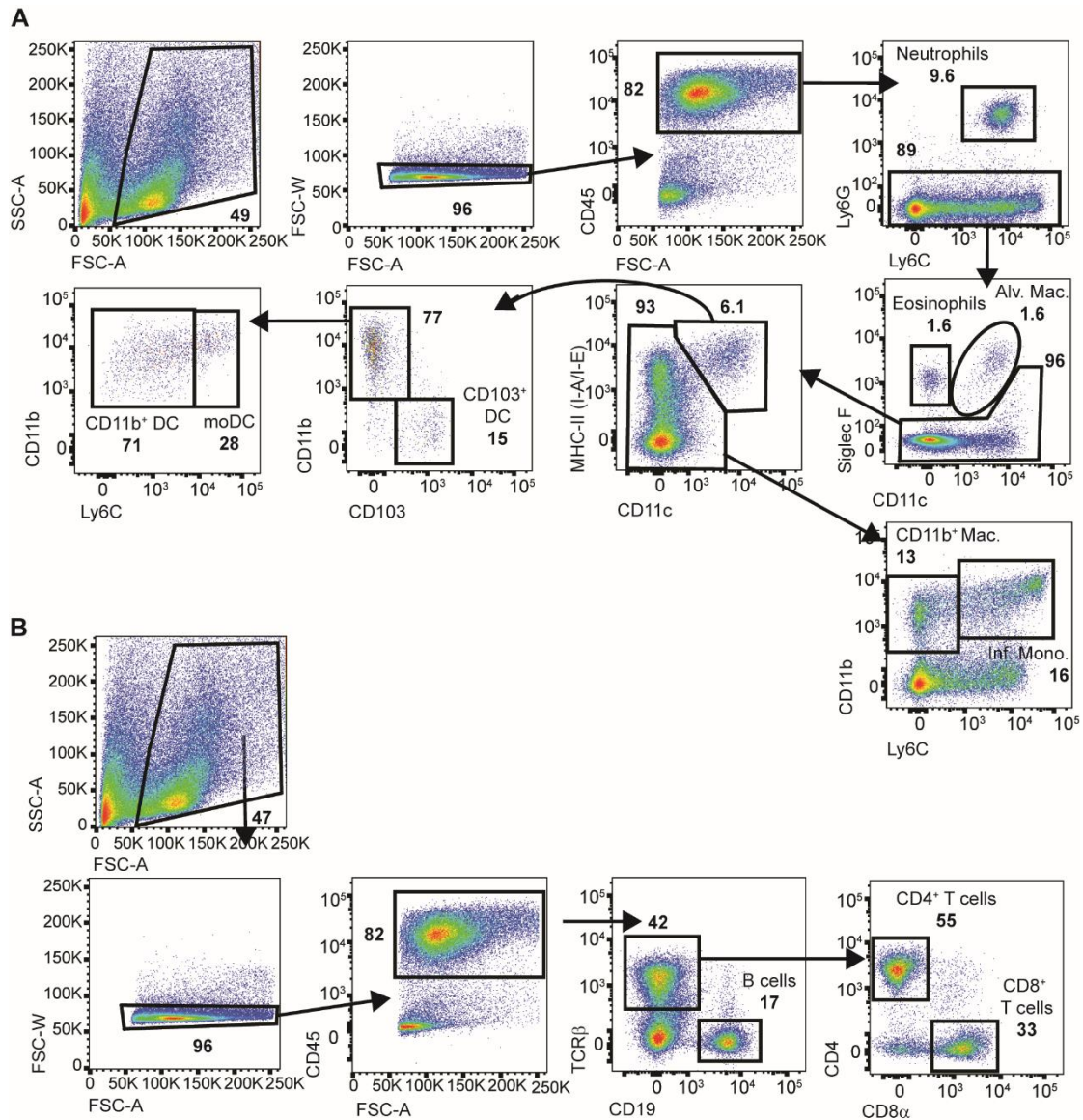


**Figure 16. Flow cytometry gating strategy used in Bhlhe40 experiments.**

(A) Gating strategy for innate immune cell types in the lung. (B) Gating strategy for adaptive immune cell types in the lung. Previously published in Huynh and Lin et al., 2018.

For identification of antigen-specific T cells, APC-conjugated tetramers of Ag85B<sub>280-294</sub> peptide (FQDAYNAAGGHNAVF) or ESAT6<sub>4-17</sub> peptide (QQWNFAGIEAAASA) bound to MHC-II<sup>I-A(b)</sup> (National Institutes of Health Tetramer Core) were added to digested cells at final dilutions of 1:25 or 1:100, depending on the age of the tetramer stock, and incubated at RT for 75

min. Cells were then surface stained as above. Antigen-specific cells were defined as CD45<sup>+</sup>/CD3ε<sup>+</sup>/CD4<sup>+</sup>/CD44<sup>+</sup>/tetramer<sup>+</sup>.

Flow cytometry data were acquired on an LSR Fortessa cytometer (BD) and analyzed using FlowJo software (TreeStar). Gating strategies are depicted in **Figure 16**. Gates for transgenic (*Bhlhe40*<sup>GFP</sup> and 10BiT) mice were set using non-transgenic mice to control for background staining.

#### *In vivo cell depletions*

For neutrophil depletion, mice were i.p. injected with 200 μg monoclonal anti-Ly6G antibody (clone 1A8; BioXCell or Leinco) or 200 μg polyclonal rat serum IgG (Sigma-Aldrich) diluted in sterile PBS (HyClone) every 48 hrs beginning at 10 dpi and ending at 30 dpi.

For T cell depletion, mice were i.p. injected with 250 μg anti-CD4 (clone GK1.5; Leinco) and 250 μg anti-CD8 (clone YTS-169; Leinco) monoclonal antibody diluted in sterile PBS beginning 2 days before infection then at 4, 11, and 18 dpi.

#### *IL-12 administration*

Mice were treated using the protocol published by Feng et al 2005.<sup>182</sup> Mice were i.p. injected with 0.25 μg recombinant IL-12p70 (Leinco) diluted in PBS. Treatment was initiated at 0 dpi and mice were injected three times per week (Monday, Wednesday, Friday) for 4 weeks.

### *BCG vaccination*

Mice were sedated with ketamine (Henry Schein) and xylazine (Akorn) then subcutaneously injected with  $2 \times 10^5$  CFUs of *M. bovis* BCG. Mice were infected with *Mtb* 30 days after vaccination.

### *Quantitative RT-PCR*

Lung samples were lysed by bead-beating in TRIzol reagent (Invitrogen), pelleted to remove beads, and stored at  $-80^{\circ}\text{C}$  until RNA extraction. RNA was purified from TRIzol using the Direct-zol RNA miniprep kit (Zymo Research) and immediately reverse transcribed with SuperScript III reverse transcription using Oligo-dT primers (Thermo Fisher Scientific). Quantitative RT-PCR was performed using iTAQ SYBR green (Bio-Rad Laboratories) on a C1000 thermal cycler with the CFX96 real-time system (Bio-Rad Laboratories). Transcript levels were analyzed using the  $2^{-\Delta\Delta\text{Ct}}$  method normalized to *Actb* ( $\beta$ -actin) as the reference gene. Primer sequences are listed in **Table 1**.

<b>Target</b>	<b>Orientation</b>	<b>Primer sequence (5'-3')</b>
<i>Actb</i>	Forward	ACCTTCTACAATGAGCTGCG
<i>Actb</i>	Reverse	CTGGATGGCTACGTACATGG
<i>Ccl3</i>	Forward	ACACTCTGCAACCAAGTCTTC
<i>Ccl3</i>	Reverse	AGGAAAATGACACCTGGCTG
<i>Ccl4</i>	Forward	CTGTTTCTCTTACACCTCCCG
<i>Ccl4</i>	Reverse	TGTCTGCCTCTTTTGGTCAG
<i>Csf2</i>	Forward	GCCATCAAAGAAGCCCTGAA
<i>Csf2</i>	Reverse	GCGGGTCTGCACACATGTTA
<i>Csf3</i>	Forward	GCAGGCTCTATCGGGTATTTC
<i>Csf3</i>	Reverse	CACCCCTAGGTTTTCCATCTG
<i>Ifnb</i>	Forward	CTCGAGCAGCTGAATGGAAAG
<i>Ifnb</i>	Reverse	CTTCTCCGTCATCTCCATAGGG
<i>Ifnγ</i>	Forward	CCTAGCTCTGAGACAATGAACG
<i>Ifnγ</i>	Reverse	TTCCACATCTATGCCACTTGAG
<i>Il6</i>	Forward	CAAAGCCAGAGTCCTTCAGAG
<i>Il6</i>	Reverse	GTCCTTAGCCACTCCTTCTG
<i>Il10</i>	Forward	AGCCTTATCGGAAATGATCCAGT
<i>Il10</i>	Reverse	GGCCTTGTAGACACCTTGGT
<i>Il12a</i>	Forward	ACAGATGACATGGTGAAGACG
<i>Il12a</i>	Reverse	TCGTTCTTGTGTAGTTCCAGTG
<i>Il12b</i>	Forward	ACTCCCCATTCTACTTCTCC
<i>Il12b</i>	Reverse	CATTCCCGCCTTTGCATTG
<i>Il17a</i>	Forward	TCCAGAATGTGAAGGTCAACC
<i>Il17a</i>	Reverse	TATCAGGGTCTTCATTGCGG
<i>Il23a</i>	Forward	CCCGTATCCAGTGTAAGATG
<i>Il23a</i>	Reverse	GGCTCCCCTTTGAAGATGTC
<i>Nos2</i>	Forward	TTGCTCATGACATCGACCAG
<i>Nos2</i>	Reverse	ACATCAAAGGTCTCACAGGC
<i>Tnf</i>	Forward	CTTCTGTCTACTGAACTTCGGG
<i>Tnf</i>	Reverse	CAGGCTTGTCACTCGAATTTTG

**Table 1. Primers used for qRT-PCR in Bhlhe40 experiments.**

### *Western blots*

Bone marrow-derived cells were counted and lysed at  $10^6/40 \mu\text{l}$  in Laemmli sample buffer (Bio-Rad Laboratories) containing 2.5%  $\beta$ -mercaptoethanol. Cell lysates were loaded and separated by 12% SDS-PAGE (Bio-Rad Laboratories) and transferred to Bio-Blot–polyvinylidene difluoride membranes (Costar). Blots were incubated with anti-Bhlhe40 (1:1,000; NB100-1800, Lot A; Novus Biologicals) or anti-HDAC1 (1:2,000; Abcam) primary antibodies at 4°C overnight with shaking. Blots were washed four to five times before incubation with anti–rabbit IgG-HRP (clone 5A6- 1D10 [light chain specific]; Jackson ImmunoResearch Laboratories, Inc.) at RT for 60 min with shaking. After five washes, Clarity Western ECL substrate (Bio-Rad Laboratories) was applied, and blots were placed on blue basic autoradiography film (Gene-Mate). Film was developed with a medical film processor (model SRX-101A; Konica Minolta).

### *Cytokine ELISAs*

IL-10 ELISA assays were performed on Nunc Maxisorp plates using IL-10 ELISPOT antibody pairs (BD). The enzyme reaction was developed with streptavidin-HRP (BioLegend) and 3,3',5,5'-tetramethylbenzidine substrate (BioLegend). Recombinant mouse IL-10 (BioLegend) was used to generate the standard curve.

### *Histology*

Lung samples were fixed in 10% buffered formalin (Thermo Fisher Scientific), embedded in paraffin, sectioned, and stained with H&E or Ziehl-Neelsen stain to identify acid-fast bacilli.

### *Chromatin immunoprecipitation Sequencing (ChIP-seq)*

Anti-Bhlhe40 ChIP was modified from the protocol published by Chou et al. 2016.<sup>186</sup> GM-CSF-cultured cells were harvested after 9 days and stimulated with 10 µg/ml heat-killed *Mtb* (strain H37Ra; Difco) for 4 hrs. *In vitro*-polarized T<sub>H</sub>1 cells were stimulated with PMA (50 ng/ml; Enzo Life Sciences) and ionomycin (1 µM; Enzo Life Sciences) for 1.5 hrs. Stimulated cells were fixed for 10 min at RT with 1% paraformaldehyde with shaking. Cross-linked chromatin was fragmented by sonication and then immunoprecipitated with polyclonal rabbit anti-Bhlhe40 antibody (NB100-1800, Lot A or Lot C1; Novus Biologicals). After immunoprecipitation, DNA was purified by the GenElute PCR cleanup kit (Sigma-Aldrich). Purified DNA was used for library construction followed by single-read sequencing on a HiSeq3000 system (Illumina) at the Genome Technology Access Center at Washington University in St. Louis. Read lengths were 101 bp and 50 bp in the case of GM-CSF-cultured bone marrow cells and T<sub>H</sub>1 cells, respectively. Fastq files were provided by the Genome Technology Access Center sequencing facility. Quality control of fastq files was performed using FastQC (0.11.3). Raw reads were mapped on the mm10 mouse reference genome using Bowtie (1.1.1). *Bhlhe40*<sup>-/-</sup> samples were used as input samples for peak calling on WT samples. Peak calling was performed using MACS v1.4<sup>187</sup> with the following flags: macs14-t WT-cKO-f BAM-g mm-n WTvsKO-p 0.00001. BEDtools (2.6; bedClip and bedGraphToBigWig) were used to visualize raw alignments. Normalized tracks were built using Deeptools (2.5.3). The UCSC Genome Browser was used for visualization. R package ChIPseeker (1.14.1) was used for peak annotation. Multiple EM for Motif Elicitation (MEME)-ChIP (4.12.0)<sup>188</sup> was used for motif enrichment analysis using all acquired peaks. Genomic Regions Enrichment of Annotations Tool

(GREAT; 3.0.0) was used to predict the function of *cis*-regulatory regions for Gene Ontology Biological Process and MSigDB Pathway gene sets.<sup>189</sup> Links for raw sequencing data are available at GSE113054. All primary processed data (including mapped reads) for ChIP-seq experiments are also available there.

#### *Analysis of human expression microarrays*

We used the GEO2R web tool ([www.ncbi.nlm.nih.gov/geo/geo2r](http://www.ncbi.nlm.nih.gov/geo/geo2r)) to query the expression of genes in three publicly available GEO datasets (GSE19491<sup>92</sup>, GSE28623<sup>167</sup>, and GSE42834<sup>168</sup>) that compared the whole-blood transcriptomes of humans with active tuberculosis to other humans with either no disease, latent tuberculosis, or in some cases, lung cancer, pneumonia, or sarcoidosis. The following probesets were used to examine the expression of *BHLHE40* (previously called *BHLHB2*): for GSE19491 and GSE42834, ILMN\_1768534; and for GSE28623, Agilent Technologies feature number 37383. The following probesets were used to examine the expression of *STAT1*: for GSE19491 and GSE42834, ILMN\_1690105, ILMN\_1691364, and ILMN\_1777325; and for GSE28623, Agilent Technologies feature numbers 1928, 4610, 4763, 15819, 24587, 29771, 37967, and 42344. For analysis of GSE19491, the training and test sets, both encompassing samples from the United Kingdom, were combined, and the validation set containing samples from South Africa was analyzed separately. GSE28623 contained samples from The Gambia. For analysis of GSE42834, the training, test, and validation sets encompassing samples from the United Kingdom and France were combined.

### *Data and statistics*

Samples represent biological (not technical) replicates of mice randomly sorted into each experimental group. No blinding was performed during animal experiments. Mice were excluded only when pathology unrelated to *Mtb* infection was present (i.e., weight loss caused by malocclusion or cage flooding). Statistical differences were calculated using Prism (7.0; GraphPad Software) using log-rank Mantel-Cox tests (survival), unpaired two-tailed Student's *t* tests (to compare two groups with normal distributions), unpaired two-tailed Mann-Whitney tests (to compare two groups with non-normal distributions), one-way ANOVA with Tukey's multiple comparisons tests (to compare more than two groups with normal distributions), or unpaired Kruskal-Wallis tests with Dunn's multiple comparisons tests (to compare more than two groups with non-normal distributions). Normality was determined using a D'Agostino-Pearson omnibus normality test. Sample sizes were sufficient to detect differences as small as 10% using the statistical methods described. When used, center values and error bars represent means  $\pm$  SEM.

## **Chapter 3**

### **The role of Irg1 in control of *Mycobacterium tuberculosis* infection**

**Portions of this chapter are excerpted from  
Nair and Huynh et al. *J. Exp. Med.* 215 (4), 1035-1045 (2018).**

## Abstract

Immune-Responsive Gene 1 (Irg1) is a mitochondrial enzyme that produces itaconate under inflammatory conditions principally in cells of myeloid lineage. Cell culture studies suggest that itaconate regulates inflammation through its inhibitory effects on cytokine and reactive oxygen species production. To evaluate the functions of Irg1 *in vivo*, we challenged wild-type (WT) and *Irg1*<sup>-/-</sup> mice with *Mycobacterium tuberculosis* (*Mtb*) and monitored disease progression. *Irg1*<sup>-/-</sup> but not WT mice succumbed rapidly to *Mtb*, and mortality was associated with increased infection, inflammation, and pathology. Infection of *Irg1*<sup>fl/fl</sup>-*Lysm-Cre*, *Irg1*<sup>fl/fl</sup>-*Mrp8-Cre*, and *Irg1*<sup>fl/fl</sup>-*Cd11c-Cre* conditional knockout mice along with neutrophil depletion experiments revealed a role for Irg1 in LysM<sup>+</sup> myeloid cells in preventing neutrophil-mediated immunopathology and disease. RNA-sequencing analyses suggest that Irg1 and its production of itaconate temper *Mtb*-induced inflammatory responses in myeloid cells at the transcriptional level. Thus, an Irg1 regulatory axis modulates inflammation to curtail *Mtb*-induced lung disease.

## Introduction

*Mycobacterium tuberculosis* (*Mtb*), the etiologic agent of tuberculosis (TB), causes up to 10.4 million new clinical infections and 1.3 million deaths annually.<sup>3</sup> Following inhalation of *Mtb*, the interplay between the immune response and the bacilli determines whether infection leads to active disease or latency. Although innate immune pathways that are triggered early can limit disease, myeloid cells also serve as a niche for *Mtb* replication.<sup>190</sup> Indeed, *Mtb* has adapted to its human host to persist in myeloid cells despite their ability to induce an antibacterial inflammatory immune response.

In the mouse model of tuberculosis, pulmonary infection is established after exposure to aerosolized bacteria. The acute phase of infection is marked by exponential growth of the bacteria in the lungs. In its persistence phase, *Mtb* undergoes a metabolic shift triggered by changes in nutrient availability, as substrates for glycolysis become limited.<sup>191</sup> The bacterial glyoxylate shunt pathway, which is absent in mammals, is an alternative anaplerotic pathway that facilitates the use of fatty acids derived from host lipids and cholesterol as a carbon source for biosynthetic pathways and generation of ATP. *Mtb* strains encode at least one and sometimes two isocitrate lyases, ICL1 (*icl1*) and ICL2 (*icl2* or *aceA*) that function within the glyoxylate shunt.<sup>151</sup> The *in vivo* attenuation exhibited by *Mtb* mutants lacking ICL expression has provided evidence for a role of the glyoxylate shunt in *Mtb* pathogenesis.<sup>145,150</sup>

The host Immune-Responsive Gene 1 (Irg1, also called Acod1) is a mitochondrial enzyme induced under inflammatory conditions that produces the metabolite itaconate by decarboxylating *cis*-aconitate, a tricarboxylic acid (TCA) cycle intermediate.<sup>143</sup> Since itaconate production in activated myeloid cells reportedly inhibits the activity of bacterial ICLs, it has gained interest as an endogenous antibacterial effector molecule.<sup>143,144</sup> This role was supported by a study showing that non-physiologically relevant (25 to 50 mM) concentrations of exogenously administered itaconate had bacteriostatic effects on *Mtb* growth during liquid culture under conditions requiring the glyoxylate shunt pathway.<sup>143</sup> Some bacteria such as *Yersinia pestis* and *Pseudomonas aeruginosa* have genes that can metabolize itaconate, thereby avoiding its antimicrobial activity and achieving persistence in the host.<sup>149</sup> Thus, one hypothesis is that Irg1 produced itaconate would act as a direct antimicrobial molecule during *Mtb* infection.

Beyond its possible antibacterial functions, itaconate also links immune cell metabolism and inflammatory responses. *Irg1* mRNA is highly expressed in macrophages in response to pro-

inflammatory stimuli that induce type I and type II interferon (IFN) signaling.<sup>134,135,138,143,192</sup>

Experiments in bone marrow-derived macrophages (BMDM) showed that itaconate suppressed the production of mitochondrial reactive oxygen species (ROS) as well as pro-inflammatory cytokines, including IL-1 $\beta$ , IL-6 and IL-12p70.<sup>138</sup> This capacity to modulate inflammation could be of particular importance during *Mtb* infection because excessive immune responses can prevent bacterial clearance and cause pathology.<sup>24,32</sup> Thus, Irg1 and its production of itaconate could modulate *Mtb* infection and pathogenesis indirectly through their signaling and regulatory functions.

We addressed the *in vivo* function of Irg1 in regulating immune responses and *Mtb* pathogenesis using mice with global and conditional deletions of *Irg1*. A complete absence of Irg1 during *Mtb* infection resulted in severe pulmonary disease and ultimately death, with greater numbers of infected myeloid cells and higher production of inflammatory cytokines and chemokines. Bone marrow chimera studies suggested that Irg1 expression in hematopoietic cells was necessary to control neutrophil recruitment, *Mtb* infection, and immune-mediated tissue injury. This data was supported by experiments in mice with conditional deletion of Irg1 in myeloid cells. Transcriptional profiling of *Mtb* infected WT and *Irg1*<sup>-/-</sup> BMDM and neutrophils *ex vivo* and *in vivo* revealed a principal role for Irg1 and itaconate in regulating the expression of genes associated with inflammation. Collectively, our studies define a key role for Irg1 in regulating immune cell metabolism in subsets of myeloid cells, which minimizes the pathological neutrophil-mediated immune response that contributes to pulmonary disease caused by *Mtb*.

## Results

### *Irg1 enables resistance to a subset of pathogenic mycobacteria.*

To determine the role of *Irg1* during *Mtb* infection, *Irg1*<sup>-/-</sup> C57BL/6N mice<sup>138</sup> were monitored for clinical and bacterial outcomes following aerosol inoculation with the *Mtb* Erdman strain. Whereas all WT and *Irg1*<sup>+/-</sup> mice survived past 80 days post-infection (dpi), approximately 75% of *Irg1*<sup>-/-</sup> mice succumbed to *Mtb* 30-40 dpi, a phenotype similar to animals lacking IFN- $\gamma$  signaling (**Fig. 17A**).<sup>24,34,35</sup> The timing of the susceptibility of *Irg1*<sup>-/-</sup> mice to *Mtb* infection is earlier than *Rag1*<sup>-/-</sup> mice that lack mature B and T cells and succumb between 46 and 50 dpi,<sup>24</sup> suggesting there is a defect in the innate immune response to *Mtb* that precedes the time point at which adaptive immunity is required. At 21 dpi, the lungs of *Irg1*<sup>-/-</sup> mice infected with *Mtb* had larger numbers and size of macroscopic lesions compared to infected WT mice (**Fig. 17B**). To determine whether *Irg1* controls *Mtb* infection, we monitored bacterial burdens in *Mtb* infected WT and *Irg1*<sup>-/-</sup> mice. Although bacterial levels were similar in the lung and spleen of both mouse strains at 10 dpi, by 14 and 21 dpi *Mtb* burden was 3- and 25-fold higher, respectively, in the lungs of *Irg1*<sup>-/-</sup> compared to WT mice (**Fig. 17C**). At 21 dpi, *Mtb* burden also was 8-fold higher in the spleens of *Irg1*<sup>-/-</sup> compared to WT mice (**Fig. 17C**).

Having found that *Irg1* played an essential role in restricting *Mtb* infection, we next asked whether it was important for control of two other pathogenic mycobacteria, *Mycobacterium abscessus* (strain L948) and *Mycobacterium avium* (strain TMC724). *Irg1*<sup>-/-</sup> mice infected intranasally with *M. abscessus* showed no signs of morbidity (**Fig. 17D**) but bacterial burden was nearly 100-fold higher in the lung as compared to WT at 10 dpi (**Fig. 17E**). After plating *M. abscessus* from the lungs of WT and *Irg1*<sup>-/-</sup> mice at 10 dpi we observed a significantly lower frequency of colonies with a rough morphotype in *Irg1*<sup>-/-</sup> mice (**Fig. 17F**). The *M. abscessus*

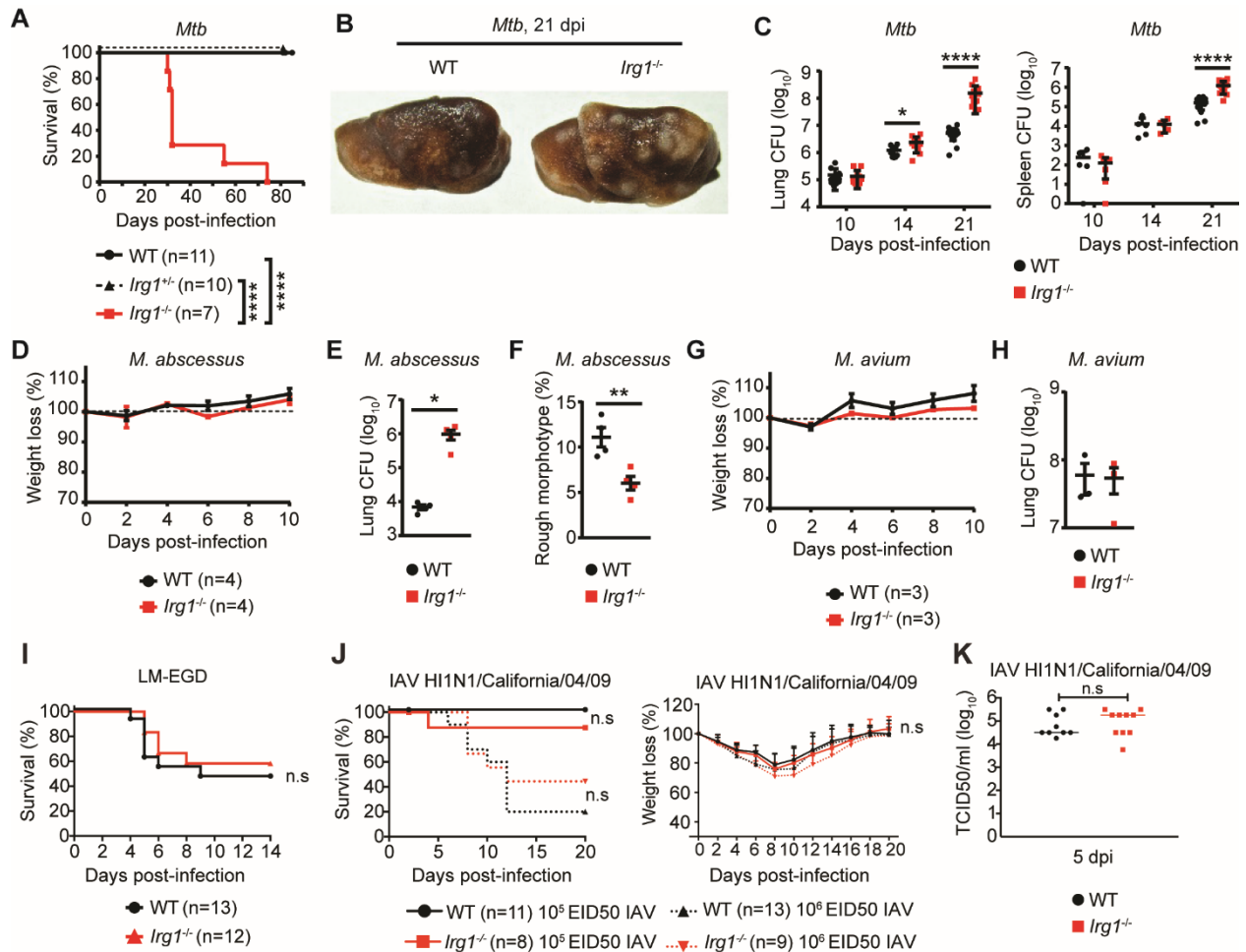


**Figure 17. Irg1 enables resistance to a subset of pathogenic mycobacteria.**

(A-C) Mice were infected with aerosolized *Mtb* and monitored for (A) survival, (B) gross lung pathology at 21 dpi, and (C) *Mtb* burden in lung and spleen at 10, 14, and 21 dpi. (D-F) Mice were intranasally infected with *M. abscessus* and monitored for (D) weight loss and (E) lung CFUs at 10 dpi. (F) The frequency of *M. abscessus* rough morphotype colonies in WT and *Irg1<sup>-/-</sup>* lungs at 10 dpi was assessed. (G-H) Mice were intranasally infected with *M. avium* and monitored for (G) weight loss and (H) lung CFUs at 10 dpi. (I) Mice were intravenously infected with *L. monocytogenes* (LM) and monitored for survival. (J-K) Mice were intranasally infected with IAV and monitored for (J) survival and weight loss, as well as (K) lung viral burden at 5 dpi. The median  $\pm$  SEM is graphed. Statistical differences were determined by log-rank Mantel-Cox test (A, I, J) and two-tailed unpaired Student's t test for normally distributed groups or two-tailed unpaired Mann-Whitney test for non-normally distributed groups (C, E, F, H, J, K). n.s., not significant, \*,  $P < 0.05$ ; \*\*,  $P < 0.01$ ; \*\*\*,  $P < 0.001$ ; \*\*\*\*,  $P < 0.0001$ . Data are from or representative of two (A-C, I-K) or one (D-H) independent experiments. Panels (A-C, I-K) were previously published in Nair and Huynh et al., 2018.

rough morphotype is associated with increased virulence and ability to persist *in vivo*<sup>193,194</sup> and its decreased frequency suggests that *M. abscessus* may be encountering a less restrictive host environment in the *Irg1*<sup>-/-</sup> lung that allows improved persistence of the less virulent smooth morphotype. Intranasal *M. avium* infection did not induce morbidity in *Irg1*<sup>-/-</sup> mice (**Fig. 17G**) and they were able to restrict infection to the same extent as WT mice (**Fig. 17H**). These results demonstrate that *Irg1* is important for control of a subset of pathogenic mycobacteria.

We also tested the effects of *Irg1* on two other pathogens, the intracellular bacterium, *Listeria monocytogenes* (strain EGD) and Influenza A virus (IAV strain A/California/04/2009 H1N1), a respiratory pathogen (**Fig. 17D-F**). Loss of *Irg1* expression in mice did not result in altered susceptibility to *L. monocytogenes* (**Fig. 17I**) or IAV infection (**Fig. 17E-F**). These results suggest that *Irg1* is not broadly protective in bacterial and viral infections but rather has a more specific role in restricting a subset of mycobacterial infections.

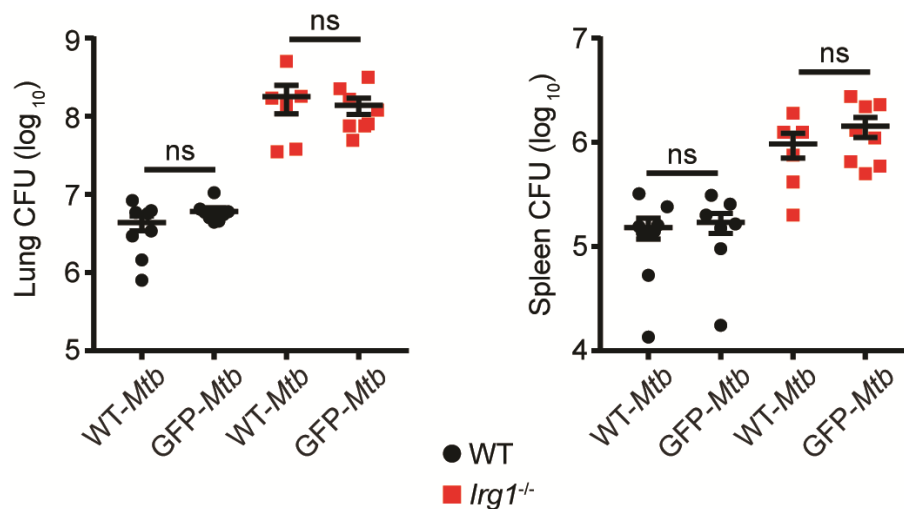


**Figure 18. GFP-*Mtb* is as virulent as WT *Mtb*.**

Mice were infected with WT or GFP-*Mtb* and bacterial burden was analyzed in the lung and spleen at 21 dpi. The mean  $\pm$  SEM is graphed. Statistical differences were determined by one-way ANOVA with Tukey's post-test. n.s., not significant. Data are from three independent experiments. Previously published in Nair and Huynh et al., 2018.

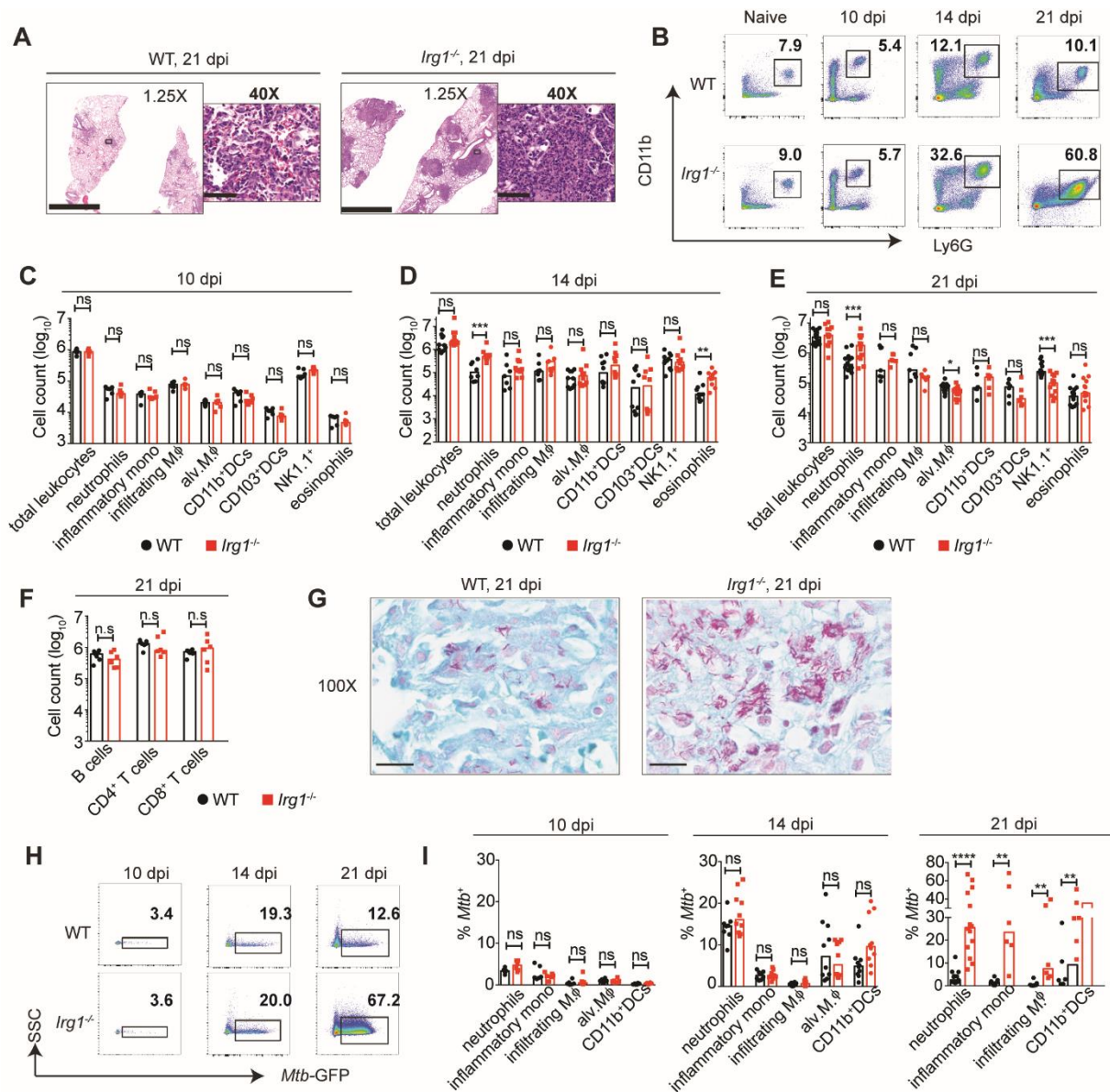


**Figure 19. *Irg1* modulates cellular inflammation after *Mtb* infection.**

(A-H) Mice were infected with *Mtb*. (A) Histopathology was visualized by H&E staining of lungs at 21 dpi. Bars: 2.5 mm (1.25x); 50  $\mu$ m (40x). (B) Representative flow cytometry plots for neutrophils as a percentage of total lung CD45<sup>+</sup> cells in lungs before *Mtb* infection and at 10, 14, and 21 dpi. Absolute number of innate immune cell populations in lungs at (C) 10 dpi, (D) 14 dpi, and (E) 21 dpi. (F) Absolute number of adaptive immune cell populations in lungs at 21 dpi. (G) Acid-fast bacilli in *Mtb*-infected lungs at 21 dpi. Bars, 10  $\mu$ m. (H) Representative flow cytometry plots for GFP<sup>+</sup> (*Mtb*<sup>+</sup>) neutrophils in lungs at 10, 14, and 21 dpi. SSC, side scatter. (I) Frequency of GFP<sup>+</sup> (*Mtb*<sup>+</sup>) cells in indicated cell types at 10, 14, and 21 dpi. The median  $\pm$  SEM is graphed. Statistical differences were determined by Mann-Whitney test. Ns, not significant; \*, P < 0.05; \*\*, P < 0.01; \*\*\*, P < 0.001; \*\*\*\*, P < 0.0001). M $\phi$ , macrophages. Data are from or representative of two (A, C, D, G, I) or three (B, E, F, H) independent experiments. Previously published in Nair and Huynh et al., 2018.

### ***Irg1* modulates lung inflammatory responses after *Mtb* infection.**

Since *Irg1* has been reported to regulate inflammatory responses<sup>138</sup> we next evaluated cellular inflammation in the lungs of WT and *Irg1*<sup>-/-</sup> mice infected with a strain of *Mtb* Erdman that stably expresses GFP and has the same virulence properties as WT *Mtb* (**Fig. 18**). Histological analysis at 21 dpi showed that lung lesions in *Irg1*<sup>-/-</sup> mice were larger and contained denser cellular infiltrates than those in WT mice (**Fig. 19A**). To define the composition of these infiltrates, we performed a kinetic analysis of immune cells in infected lungs by flow cytometry (gating strategy defined in **Fig. 29**). At 10 dpi, no differences in the number of neutrophils, inflammatory monocytes, infiltrating (CD11b<sup>+</sup>) macrophages, alveolar macrophages, CD11b<sup>+</sup> and CD103<sup>+</sup> DCs, NK and NKT cells, or eosinophils were detected in the lungs of WT and *Irg1*<sup>-/-</sup> mice (**Fig. 19B, C**). However, by 14 dpi infected lungs from *Irg1*<sup>-/-</sup> mice had 4-fold more neutrophils and 3-fold more eosinophils compared to WT mice, and this difference remained at 21 dpi for neutrophils (**Fig. 19B, D, E**). At 21 dpi, lungs from *Irg1*<sup>-/-</sup> mice also had 1.3-fold fewer alveolar macrophages and 3-fold fewer NK1.1<sup>+</sup> cells. Analysis of other innate immune cell populations in the lungs at 14 and 21 dpi revealed no significant differences in numbers of inflammatory monocytes, infiltrating macrophages, and DCs between WT and *Irg1*<sup>-/-</sup> mice. In addition, no differences in the numbers of CD4<sup>+</sup> T cells, CD8<sup>+</sup> T cells, and B cells were found between WT and *Irg1*<sup>-/-</sup> mice at 21 dpi (**Fig. 19F**).

As the timing of the increased myeloid cell inflammation correlated with the higher *Mtb* burden in the lungs of *Irg1*<sup>-/-</sup> mice, we evaluated whether the accumulating myeloid cells were infected with *Mtb*. Acid-fast staining of tissue sections at 21 dpi revealed that bacilli were predominantly found in lung lesions, with greater numbers of bacilli present in *Irg1*<sup>-/-</sup> mice (**Fig. 19G**). To analyze the extent of infection in each myeloid cell type, we monitored the presence of

*Mtb*-GFP in the various cell populations by flow cytometry. At 10 and 14 dpi myeloid cell types in WT and *Irg1*<sup>-/-</sup> lungs were infected at similar frequencies (**Fig. 19H, I**). However, by 21 dpi lungs from *Irg1*<sup>-/-</sup> mice had higher percentages of infected neutrophils (8-fold), inflammatory monocytes (19-fold), infiltrating macrophages (19-fold), and CD11b<sup>+</sup> DCs (3-fold) compared to WT mice. Collectively, this data suggests that *Irg1* regulates inflammatory responses during *Mtb* infection and controls the recruitment of multiple types of myeloid cells, many of which become targets for subsequent rounds of infection.

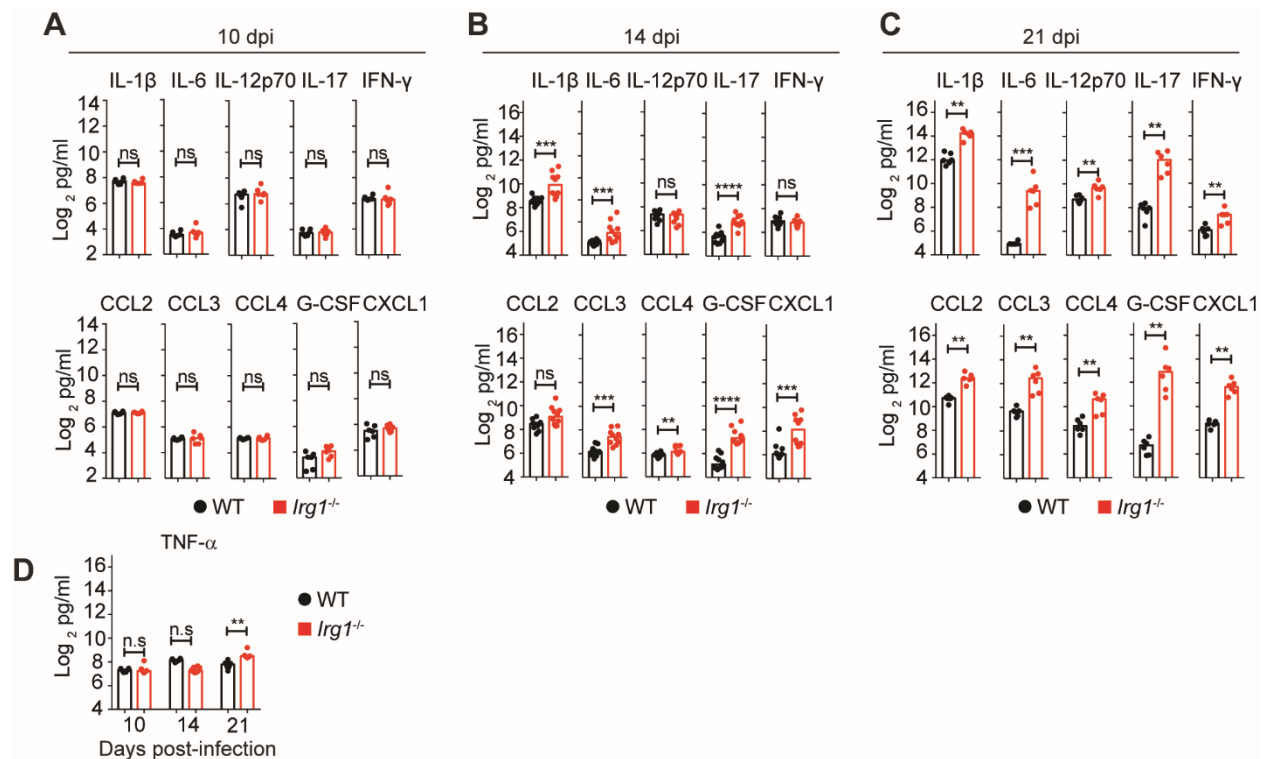


**Figure 20. *Irg1* modulates inflammatory cytokine production after *Mtb* infection.**

(A-C) Cytokine and chemokine levels in *Mtb* infected lungs at (A) 10 dpi, (B) 14 dpi, and (C) 21 dpi. (D) Lung TNF-α levels. The median ± SEM is graphed. Statistical differences were determined by Mann-Whitney test. ns, not significant; \*, P < 0.05; \*\*, P < 0.01; \*\*\*, P < 0.001; \*\*\*\*, P < 0.0001). Mφ, macrophages. Data are from or representative of two (A, B, D) or three (C) independent experiments. Previously published in Nair and Huynh et al., 2018.

Given the increased inflammatory cell recruitment in *Irg1*<sup>-/-</sup> mice, we measured the effect of *Irg1* on the accumulation of inflammatory mediators in the lung during *Mtb* infection. Equivalent levels of chemokines and pro-inflammatory cytokines were detected in lung homogenates of WT and *Irg1*<sup>-/-</sup> mice at 10 dpi (**Fig. 20A, D**), a time point at which we observed no difference in the numbers of lung immune cells. By 14 dpi, higher levels of several pro-inflammatory cytokines (IL-1 $\beta$ , IL-6, IL-17, G-CSF) and chemokines (CXCL1, CCL3, CCL4) were detected in the lungs of *Irg1*<sup>-/-</sup> mice compared to WT mice (**Fig. 20B**), although TNF- $\alpha$  levels remained unchanged (**Fig. 20D**). By 21 dpi, all eleven pro-inflammatory cytokines (IL-1 $\beta$ , IL-6, IL-12p70, IL-17, IFN- $\gamma$ , TNF- $\alpha$ , G-CSF) and chemokines (CCL2, CXCL1, CCL3, CCL4) measured were higher in the lungs of *Irg1*<sup>-/-</sup> mice compared to WT mice (**Fig. 20C, D**). Thus, enhanced accumulation of immune cells in the lungs of infected *Irg1*<sup>-/-</sup> mice at 14 and 21 dpi correlated with increased expression of pro-inflammatory cytokines and chemokines.

### ***Neutrophil depletion extends the survival of *Irg1*<sup>-/-</sup> mice during *Mtb* infection.***

Excessive neutrophil recruitment is associated with tissue damage and progression of *Mtb* disease.<sup>24,32</sup> We speculated that the susceptibility of *Irg1*<sup>-/-</sup> mice to *Mtb* infection was related to the increased accumulation of neutrophils in their lungs. To test this hypothesis, we administered a neutrophil depleting anti-Ly6G ( $\alpha$ Ly6G) or isotype control monoclonal antibody to WT and *Irg1*<sup>-/-</sup> mice every other day, beginning at 10 dpi and ending at 34 dpi. Flow cytometry analysis demonstrated that anti-Ly6G treatment of *Irg1*<sup>-/-</sup> mice led to a 7-fold reduction in the number of lung neutrophils compared to isotype control-treated mice at 21 dpi (**Fig. 21A, F**). Neutrophil depleted *Irg1*<sup>-/-</sup> mice exhibited less weight loss (**Fig. 21B**) and extended survival time (**Fig. 21C**)

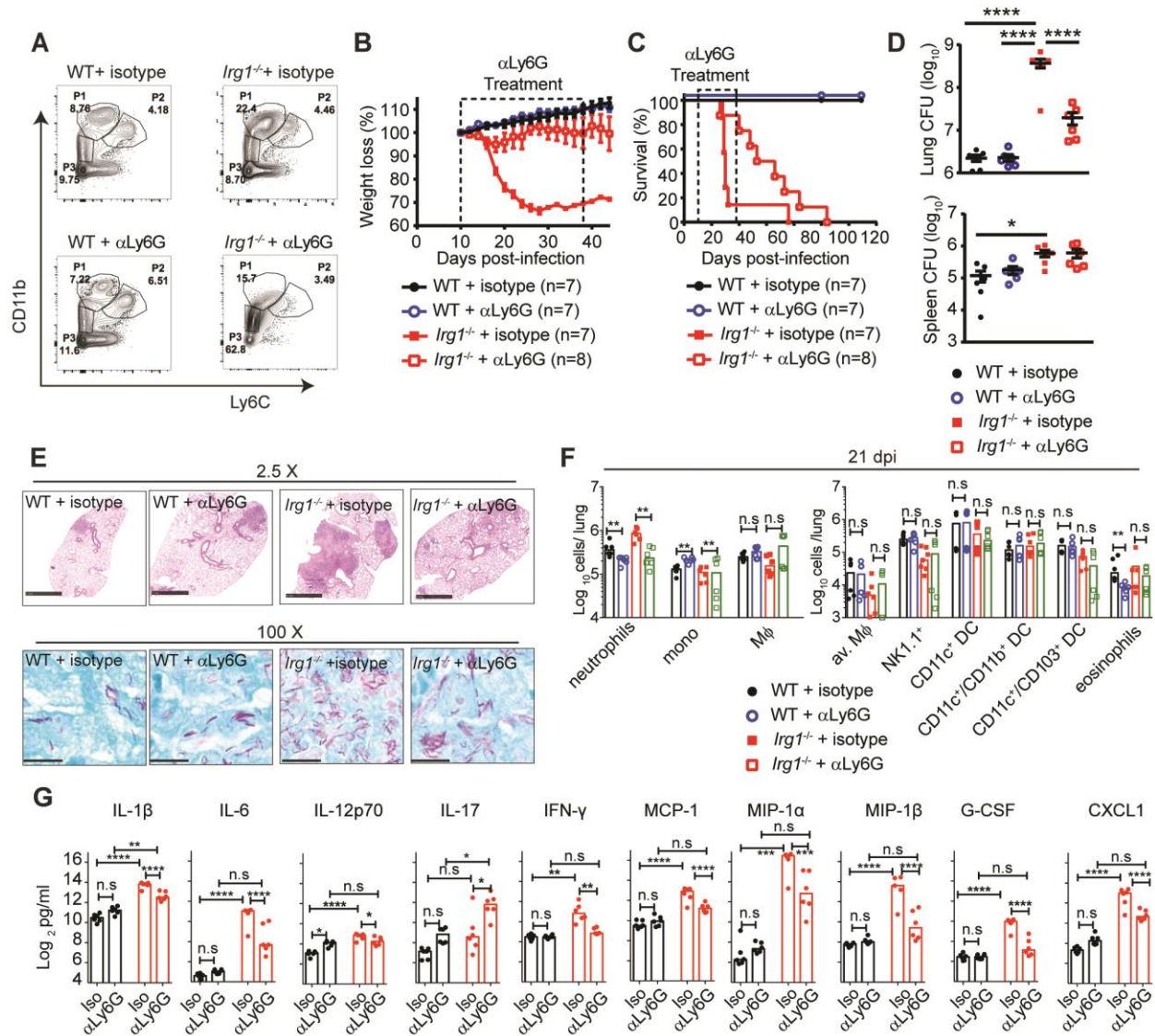


**Figure 21. Neutrophil depletion enhances the survival of *Irg1*<sup>-/-</sup> mice.**

(A-G) Mice were infected with *Mtb* and treated with anti-Ly6G (αLy6G) or isotype control antibodies beginning at 10 dpi. (A) Representative flow cytometry for lung neutrophils at 21 dpi. (B) Weight loss kinetics. (C) Survival analysis. (D) Lung and spleen *Mtb* burden at 21 dpi. (E) Lung histopathology and acid-fast bacilli at 21 dpi were visualized with H&E (top) and acid-fast (bottom) stains. Bars: 1 mm (top); 100 μm (bottom). (F) Innate immune cell populations in the lung at 21 dpi. (G) Lung cytokine levels at 21 dpi. Statistical differences were determined by one-way ANOVA with Tukey's post-test (D, F) and Mann-Whitney test (G). ns, not significant; \*, P < 0.05; \*\*, P < 0.01; \*\*\*, P < 0.001; \*\*\*\*, P < 0.0001. Data are from or representative of two (A-G) independent experiments. Panels (A, C-G) were previously published in Nair and Huynh et al., 2018.

after *Mtb* infection. Once neutrophil depletion was halted and neutrophils were allowed to accumulate in the lung, disease ensued and all *Irg1*<sup>-/-</sup> mice succumbed to infection (mean time to death for isotype control and anti-Ly6G-treated *Irg1*<sup>-/-</sup> mice was 30 and 62 days, respectively). This demonstrated that the excessive accumulation of neutrophils contributed to the early susceptibility of *Irg1*<sup>-/-</sup> mice and that *Irg1* is required to restrict neutrophilic inflammation during acute and chronic *Mtb* infection. Neutrophil depletion also reduced lung *Mtb* burden in *Irg1*<sup>-/-</sup> mice by 19-fold at 21 dpi, but had no effect on splenic *Mtb* burden (**Fig. 21D**). However, lung *Mtb* levels in neutrophil-depleted *Irg1*<sup>-/-</sup> mice remained higher (9-fold) than in anti-Ly6G-treated WT mice (**Fig. 21D**), indicating incomplete neutrophil depletion or that recruitment and infection of neutrophils only partially contributed to the higher bacterial burden in *Mtb* infected *Irg1*<sup>-/-</sup> mice. Correspondingly, diminished numbers of acid-fast bacilli were present in lung sections of neutrophil depleted *Irg1*<sup>-/-</sup> mice compared to controls (**Fig. 21E**). Histological analysis showed that lung lesions from infected, neutrophil depleted *Irg1*<sup>-/-</sup> mice were smaller than their isotype treated counterparts (**Fig. 21E**). Other than a 1.5-fold decrease in inflammatory monocytes, the recruitment of which could be altered by decreases in lung cytokine and chemokine expression caused by neutrophil depletion, all other innate immune cell subsets (infiltrating and alveolar macrophages, NK1.1<sup>+</sup> cells, DCs, eosinophils) were unaffected by neutrophil depletion in *Irg1*<sup>-/-</sup> mice (**Fig. 21F**). Cytokine (IL-1 $\beta$ , IL-6, IL-12p70, G-CSF, IFN- $\gamma$ ) and chemokine (CCL2, CCL3, CCL4, CXCL1) levels in the lung also were decreased in neutrophil depleted *Irg1*<sup>-/-</sup> mice at 21 dpi, demonstrating that neutrophils contributed to the heightened inflammatory response at this time point (**Fig. 21G**). Collectively, these experiments show that depletion of neutrophils mitigates the bacterial and pro-inflammatory pathological phenotypes observed at 21 dpi in

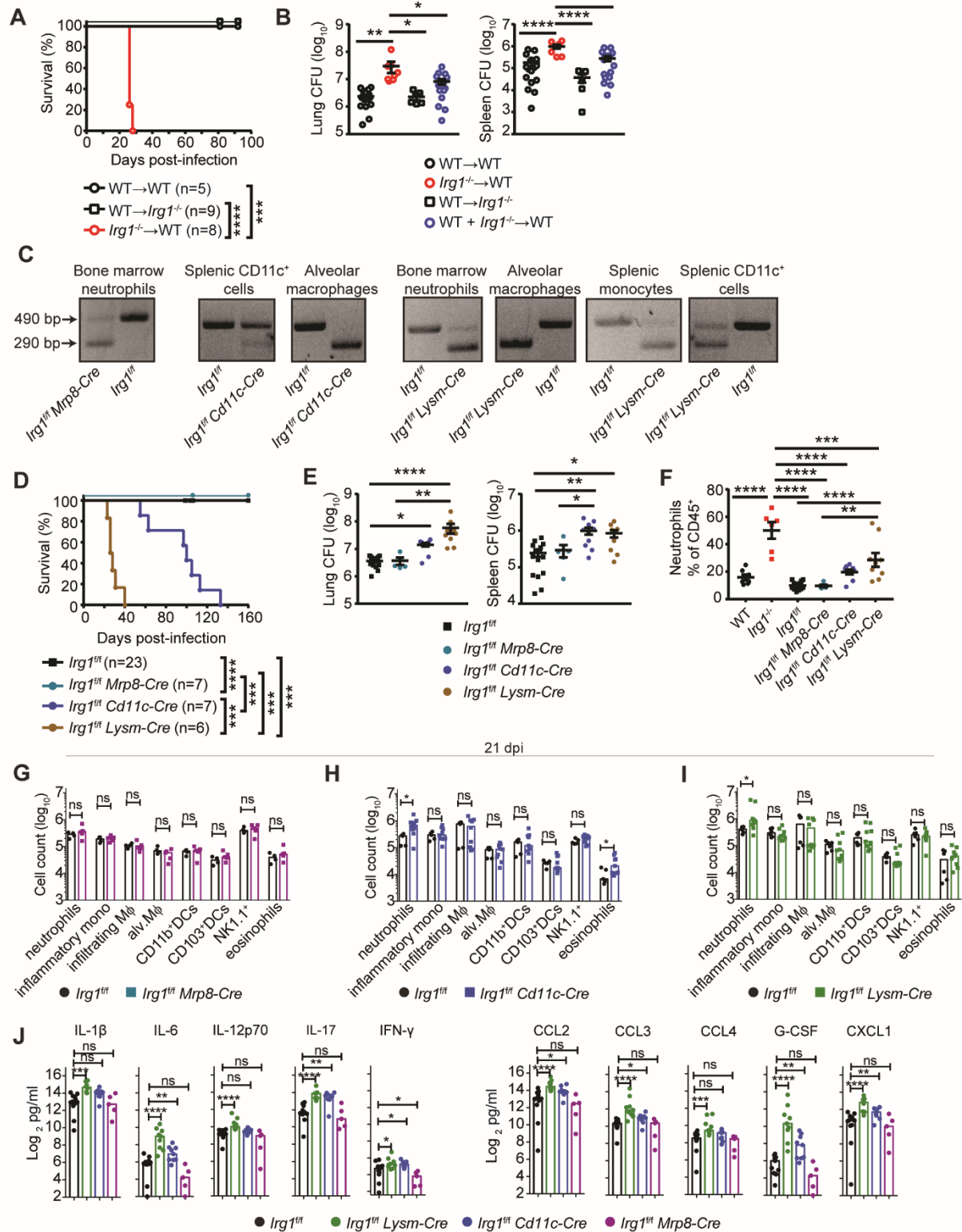


**Figure 22. Expression of Irg1 in myeloid cell subsets enables survival of *Mtb* infection.** (A, B, D-J) Mice were infected with *Mtb*. (A) Survival analysis of bone marrow chimeric mice. (B) Lung *Mtb* burden in one-way and mixed bone marrow chimeric mice at 21 dpi. (C) Cells

were isolated from naive *Irg1<sup>fl/fl</sup>* and *Irg1<sup>fl/fl</sup>-Cre*-expressing mice. mRNA was then extracted and reverse transcribed, and a section of the *Irg1* gene spanning exon 4 was amplified by PCR. Non-recombined transcript yields a 490 bp amplicon, whereas Cre recombinase-mediated excision of exon 4 results in a 290 bp amplicon. Recombined *Irg1* exon 4 in cells from Cre-negative *Irg1<sup>fl/fl</sup>*, *Irg1<sup>fl/fl</sup>-Mrp8-Cre* (bone marrow neutrophils), *Irg1<sup>fl/fl</sup>-Cd11c-Cre* (alveolar macrophages from BAL and total splenic CD11c<sup>+</sup> cells), and *Irg1<sup>fl/fl</sup>-Lysm-Cre* mice (bone marrow neutrophils, alveolar macrophages from BAL, splenic monocytes, and total splenic CD11c<sup>+</sup> cells). (D) Survival analysis of conditional deletion mice. (E) Lung and spleen *Mtb* burden at 21 dpi. (F) Neutrophils as a percentage of the total lung CD45<sup>+</sup> population. (G-I) Quantitation of lung myeloid cells at 21 dpi in (G) *Irg1<sup>fl/fl</sup>-Mrp8-Cre*, (H) *Irg1<sup>fl/fl</sup>-Cd11c-Cre*, and (I) *Irg1<sup>fl/fl</sup>-Lysm-Cre*. Mφ, macrophages. (J) Lung cytokine levels at 21 dpi. The median ± SEM is graphed. Statistical differences were determined by log-rank Mantel-Cox test (A, D), one-way ANOVA with Tukey's post-test (B, E, F, J), or Mann-Whitney test (G-I). n.s., not significant, \*, P < 0.05; \*\*, P < 0.01; \*\*\*, P < 0.001; \*\*\*\*, P < 0.0001. Data are from or representative of two (A-C, I-K) or one (D-H) independent experiments. Panels (A, C-E, G-J) and parts of panel (B) were previously published in Nair and Huynh et al., 2018.

*Irg1<sup>-/-</sup>* mice and suggest that a dysfunctional neutrophil response contributes to the susceptibility of these mice to *Mtb* infection.

### ***Expression of Irg1 in LysM<sup>+</sup> and CD11c<sup>+</sup> cells enables survival of Mtb infection.***

In order to define the cell types that require *Irg1* expression for control of *Mtb* infection, we generated reciprocal bone marrow chimeric mice, infected them with *Mtb*, and monitored survival (Fig. 22A). Whereas WT→WT and WT→*Irg1<sup>-/-</sup>* mice survived past 80 dpi, *Irg1<sup>-/-</sup>*→WT mice succumbed by 32 dpi, similar to the phenotype observed with *Irg1<sup>-/-</sup>* mice. This result demonstrated that the protective effects of *Irg1* were derived from radio-sensitive cells, likely in the hematopoietic compartment. Consistent with the survival data, *Mtb* titers in the lungs and the spleen of *Irg1<sup>-/-</sup>*→WT mice were higher than WT→WT mice at 21 dpi (lung, 10-fold; spleen, 3-fold) (Fig. 22B). Intriguingly, lung and spleen CFU counts in mixed WT + *Irg1<sup>-/-</sup>*→WT chimeras were similar to those of WT→WT chimeras and significantly lower than in *Irg1<sup>-/-</sup>*→WT

chimeras. This result suggested that the presence of Irg1-expressing cells could compensate for the defective ability of *Irg1*<sup>-/-</sup> cells to control *Mtb* infection. However, the proportions of WT and *Irg1*<sup>-/-</sup> cells in the lungs of mixed bone marrow chimera mice prior to infection were not assessed and phenotypes observed in these mice could be due to differences in the engraftment ability of WT and *Irg1*<sup>-/-</sup> cells.

Since bone marrow chimera experiments revealed a role for Irg1 in hematopoietic cells, we sought to identify the Irg1-expressing cell types that modulated neutrophil accumulation and *Mtb* disease pathogenesis. Because Irg1 is expressed principally in cells of myeloid lineage,<sup>134,138,143,152</sup> we used conditional deletion mice to test its role in myeloid cells during *Mtb* infection. Mice with a loxP site-flanked exon of *Irg1* (*Irg1*<sup>fl/fl</sup>) were crossed to mice that expressed Cre recombinase under the control of various myeloid cell-specific promoters and targeted cells were isolated and assessed for *Irg1* exon deletion (**Fig. 22C**). As expected, we did not detect *Irg1* exon deletion in Cre-negative *Irg1*<sup>fl/fl</sup> mice. The expected patterns of deletion were detected in *Irg1*<sup>fl/fl</sup>-*Mrp8-Cre* (deletion in neutrophils) and *Irg1*<sup>fl/fl</sup>-*Lysm-Cre* mice (deletion in monocytes, alveolar macrophages, neutrophils, and some DCs). However, we found that *Irg1*<sup>fl/fl</sup>-*Cd11c-Cre* mice exhibited strong deletion in alveolar macrophages and poor deletion in splenic DCs, suggesting that lung DCs might have a similarly low level of deletion. Conditional deletion mice were infected with *Mtb* and monitored for survival (**Fig. 22D**). All Cre-negative *Irg1*<sup>fl/fl</sup> and *Irg1*<sup>fl/fl</sup>-*Mrp8-Cre* mice survived past 150 dpi, but *Irg1*<sup>fl/fl</sup>-*Lysm-Cre* mice succumbed within 40 dpi, a phenotype similar to that of *Irg1*<sup>-/-</sup> mice (**Fig. 17A**). In comparison, all *Irg1*<sup>fl/fl</sup>-*Cd11c-Cre* mice succumbed by 135 dpi. Consistent with these survival results, *Mtb* levels in the lungs of *Irg1*<sup>fl/fl</sup>-*Mrp8-Cre* mice were similar to littermate Cre-negative *Irg1*<sup>fl/fl</sup> controls, whereas *Irg1*<sup>fl/fl</sup>-*Lysm-Cre* and *Irg1*<sup>fl/fl</sup>-*Cd11c-Cre* mice both had greater higher lung *Mtb* burden at 21 dpi

(14-fold and 4-fold respectively) (**Fig. 22E**). Splenic *Mtb* burdens were also higher in *Irg1<sup>fl/fl</sup>-Lysm-Cre* and *Irg1<sup>fl/fl</sup>-Cd11c-Cre* mice at 21 dpi compared to controls (**Fig. 22E**).

We next assessed cellular inflammation in the lung at 21 dpi and found that *Irg1<sup>fl/fl</sup>-Lysm-Cre* had a higher frequency (**Fig. 22F**) and absolute number (**Fig. 22I**) of neutrophils in the lung as compared to Cre-negative *Irg1<sup>fl/fl</sup>* controls, although their neutrophil frequency remained lower than that of *Irg1<sup>-/-</sup>* mice. *Irg1<sup>fl/fl</sup>-Cd11c-Cre* mice had greater numbers of lung neutrophils compared to Cre-negative *Irg1<sup>fl/fl</sup>* mice, but *Irg1<sup>fl/fl</sup>-Mrp8-Cre* mice did not (**Fig. 22G, H**). Loss of *Irg1* expression in myeloid cells (*Irg1<sup>fl/fl</sup>-Lysm-Cre* mice) resulted in higher levels of cytokines and chemokines in the lungs at 21 dpi (**Fig. 22J**). Loss of *Irg1* expression in alveolar macrophages and some DCs (*Irg1<sup>fl/fl</sup>-Cd11c-Cre* mice) also resulted in greater amounts of inflammatory cytokines and chemokines. In contrast, deletion of *Irg1* in neutrophils (*Irg1<sup>fl/fl</sup>-Mrp8-Cre* mice) had little effect on cytokine responses. These data show that *Irg1* expression in CD11c<sup>+</sup> and LysM<sup>+</sup> cell subsets regulates neutrophil recruitment and inflammation. Although neutrophils mediate *Mtb*-induced immunopathology in *Irg1<sup>-/-</sup>* mice, their cell-intrinsic expression of *Irg1* is dispensable for this process.

### ***Susceptibility of Irg1<sup>-/-</sup> mice is dependent on Mtb expression of PDIM and ESX-1, but not ICLI***

We next investigated the requirement for key *Mtb* virulence factors in the susceptibility of *Irg1<sup>-/-</sup>* mice. The ESX-1 secretion system and the *Mtb* membrane lipid phthiocerol dimycoserolate (PDIM) enable *Mtb* to modulate host immune responses<sup>195–197</sup> and thus may have important effects on the inflammatory response observed in *Irg1<sup>-/-</sup>* mice. *Irg1<sup>-/-</sup>* mice infected with isogenic *Mtb* strains lacking ESX-1 ( $\Delta$ ESX-1) or PDIM ( $\Delta$ PDIM) exhibited no

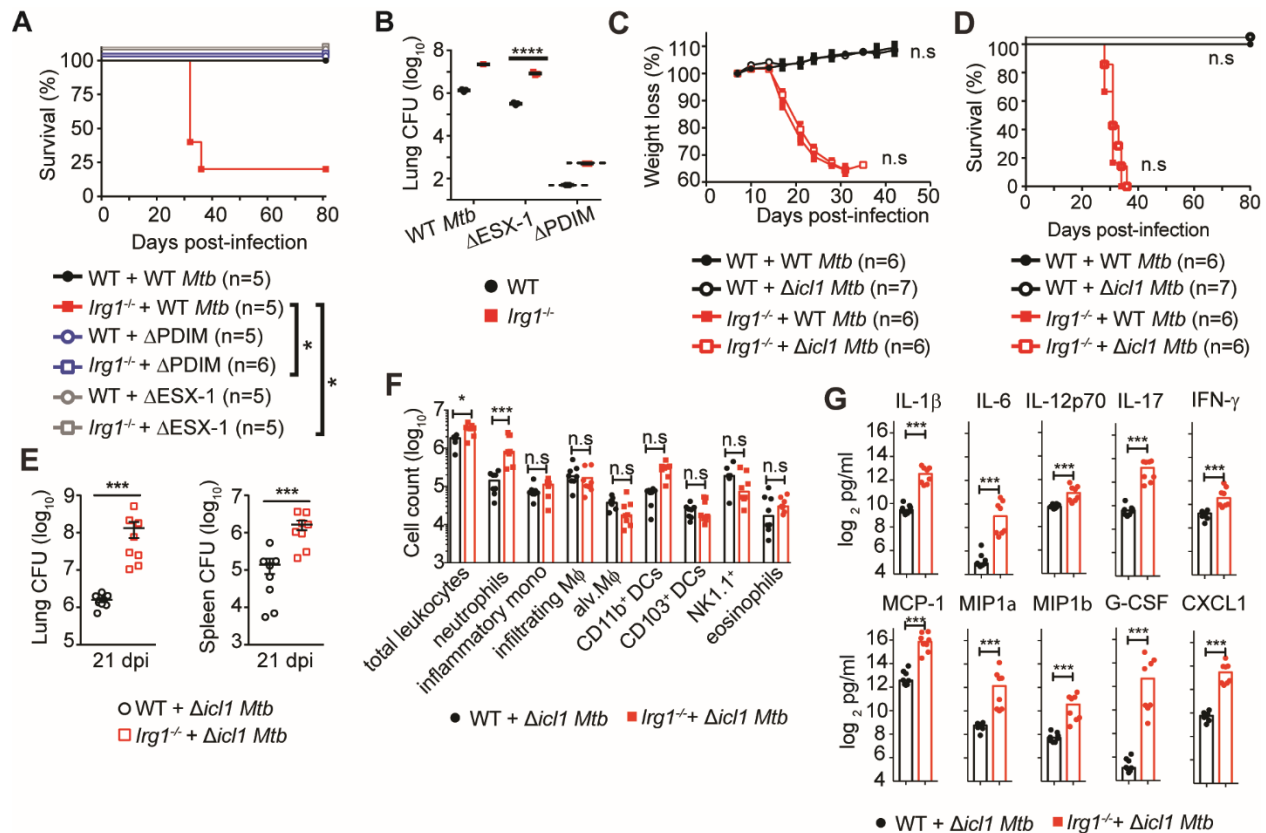


**Figure 23. Susceptibility of *Irg1*<sup>-/-</sup> mice is dependent on *Mtb* expression of PDIM and ESX-1, but not ICL1.**

(A-B) Mice were infected with WT,  $\Delta$ PDIM or  $\Delta$ ESX-1 *Mtb* and monitored for (A) survival or (B) lung *Mtb* burden at 81 dpi. Dotted lines in (B) indicate limit of detection (WT, 50 CFU; *Irg1*<sup>-/-</sup>, 500 CFU). (C-G) Mice were infected with WT or  $\Delta$ *icl1* *Mtb* and monitored for (C) weight loss kinetics, (D) survival, (E) lung and spleen burden at 21 dpi, (F) myeloid lung cell populations at 21 dpi, and (G) lung cytokines at 21 dpi. The median  $\pm$  SEM is graphed. Statistical differences were determined by log-rank Mantel-Cox test (A, D), one-way unpaired Student's t test (B), or Mann-Whitney test (C, E-G). n.s., not significant, \*,  $P < 0.05$ ; \*\*,  $P < 0.01$ ; \*\*\*,  $P < 0.001$ ; \*\*\*\*,  $P < 0.0001$ . Data are from or representative of one (A, B) or two (C-G) independent experiments.

susceptibility over 80 days of infection (Fig. 23A). At 81 dpi lung CFU counts for  $\Delta$ PDIM *Mtb* were below the limit of detection in *Irg1*<sup>-/-</sup> mice while  $\Delta$ ESX-1 *Mtb* counts were 25-fold higher in *Irg1*<sup>-/-</sup> lungs compared to WT mice (Fig. 23B). These experiments show that expression of

ESX-1 and PDIM by *Mtb* is required for the acute susceptibility of *Irg1*<sup>-/-</sup> mice, but ESX-1 is not required for defective control of *Mtb* by *Irg1*<sup>-/-</sup> mice.

Since Irg1 catalyzes the production of itaconate, a metabolite that can inhibit the glyoxylate shunt enzymes ICL1 and ICL2, it has been suggested that Irg1 restricts *Mtb* infection by blocking the glyoxylate shunt.<sup>143</sup> The strain of *Mtb* used in this study, Erdman, encodes two ICL genes, ICL1 and ICL2, although ICL1 is considered functionally dominant.<sup>145,150</sup> *In vivo*, *Δicl1* *Mtb* replicates normally during the acute phase but is attenuated during the chronic phase of infection, whereas *Δicl2* *Mtb* shows no defects during *in vivo* infection.<sup>145,150</sup> In comparison, *Δicl1/Δicl2* strains grow poorly in liquid culture and are completely avirulent *in vivo*.<sup>145</sup> To test the impact of Irg1 on restriction of ICL1 activity *in vivo*, we infected WT and *Irg1*<sup>-/-</sup> mice with WT and isogenic *Δicl1* *Mtb* strains. As anticipated, WT mice infected with WT or *Δicl1* *Mtb* showed no signs of morbidity (**Fig. 23C**) and survived past 80 dpi (**Fig. 23D**). In contrast, all *Irg1*<sup>-/-</sup> mice infected with *Δicl1* *Mtb* succumbed to infection with weight loss (**Fig. 23C**) and survival (**Fig. 23D**) patterns highly similar to that of *Irg1*<sup>-/-</sup> mice infected with an isogenic WT *Mtb* strain. Moreover, *Δicl1* *Mtb* titers were higher in the lung (83-fold) and spleen (12-fold) of *Irg1*<sup>-/-</sup> mice compared to WT mice (**Fig. 23E**). Our findings that *Δicl1* *Mtb* is still virulent in *Irg1*<sup>-/-</sup> mice suggest that the susceptibility of *Irg1*<sup>-/-</sup> mice is independent of ICL1 activity and that Irg1 likely restricts *in vivo* *Mtb* infection independently of its activity on ICL1.

Since *Irg1*<sup>-/-</sup> mice infected with WT or *Δicl1* *Mtb* succumbed to infection at equivalent rates (**Fig. 23D**), we asked whether the pattern of inflammatory responses in these mice also was similar. Indeed, *Irg1*<sup>-/-</sup> mice infected with WT or *Δicl1* *Mtb* showed similarly increased accumulation of neutrophils in their lungs at 21 dpi (**Fig. 23F**). Correspondingly, pro-inflammatory cytokines (IL-1β, IL-6, IL-12p70, IL-17, G-CSF, IFN-γ) and chemokines (CCL2,

CCL3, CCL4, CXCL1) were higher in  $\Delta icl1$  *Mtb*-infected *Irg1*<sup>-/-</sup> mice compared to WT mice (Fig. 23G). The similar inflammatory responses to WT and  $\Delta icl1$  *Mtb* in *Irg1*<sup>-/-</sup> mice further supports the hypothesis that the defective control of *Mtb* infection in these mice is independent of ICL1 activity.

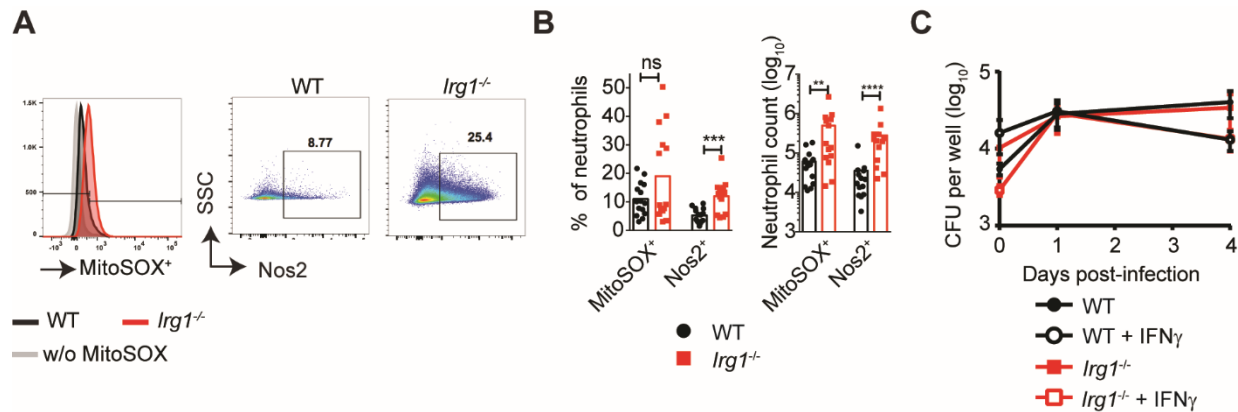


**Figure 24. *Irg1* is not required for induction of ROS, NOS2, or control of *Mtb* in BMDMs.** (A-B) Mice were infected with *Mtb* and at 21 dpi lung neutrophils were assessed for (A, B) reactive oxygen species by MitoSOX Red dye or intracellular NOS2 expression. (C) BMDMs were IFN- $\gamma$  pretreated or not, infected with *Mtb* (multiplicity of infection = 1), and CFUs were assessed at 0, 24, and 96 hpi. The median  $\pm$  SEM is graphed. Statistical differences were determined by Mann-Whitney test (B) or one-way ANOVA with Tukey's post-test (C). n.s., not significant, \*,  $P < 0.05$ ; \*\*,  $P < 0.01$ ; \*\*\*,  $P < 0.001$ ; \*\*\*\*,  $P < 0.0001$ . Data are from or representative of three (A, B) or two (C) independent experiments.

### *Irg1* is not required for induction of ROS and NOS2 or control of *Mtb* in macrophages

Reactive oxygen species (ROS) have been proposed as a cell autonomous antibacterial mechanism during *Mtb* infection<sup>198</sup> and *Irg1* has been reported to promote production of antibacterial reactive oxygen species during *Salmonella enterica* infection.<sup>152</sup> However, overproduction of ROS has been linked to inflammatory pathology and exogenous itaconate suppresses ROS production by macrophages *in vitro*.<sup>138,160</sup> We asked whether neutrophils might be contributing to susceptibility through altered ROS production and addressed this question by

quantifying ROS-producing lung neutrophils in WT and *Irg1*<sup>-/-</sup> mice at 21 dpi using a dye that reports ROS production, MitoSOX Red. We observed an increase in intracellular ROS (**Fig. 24A**) and a higher number of ROS<sup>+</sup> (MitoSOX<sup>+</sup>) neutrophils in *Irg1*<sup>-/-</sup> mice, but no difference in the frequency of ROS<sup>+</sup> neutrophils (**Fig. 24B**). The increased number of ROS<sup>+</sup> neutrophils was expected, given the higher number of neutrophils present in the lung at this time point (**Fig. 19E**). No differences in ROS expression were detected in Ly6G-negative immune cells (data not shown). These data suggest *Irg1*<sup>-/-</sup> neutrophils and macrophages are not failing to produce potentially bactericidal ROS and neutrophils may be contributing to lung pathology through overproduction of ROS.

Inducible nitric oxide synthase (NOS2) restricts pathologic, granulocyte-dominated inflammatory responses<sup>33,96</sup> that appear grossly similar to the neutrophil-dominated inflammation we observe in *Irg1*<sup>-/-</sup> mice. However, overexpression of NOS2 by macrophages has been associated with a hyperinflammatory state and tissue pathology.<sup>138</sup> We asked whether the susceptibility of *Irg1*<sup>-/-</sup> mice might be associated with alterations in NOS2 expression and addressed this by measuring expression of NOS2 in lung neutrophils at 21 dpi. The frequency and absolute number of NOS2<sup>+</sup> neutrophils were significantly higher in *Irg1*<sup>-/-</sup> mice (**Fig. 24A, B**). No differences in NOS2 expression were detected in Ly6G-negative immune cells (data not shown). These data suggest that *Irg1*<sup>-/-</sup> neutrophils may be in a pathologic, hyper-inflamed state.

We next investigated whether *Irg1* deficiency impacted control of *Mtb* by macrophages, a cell type identified as a key expresser of *Irg1* by the susceptibility of *Irg1*<sup>fl/fl</sup>-*Ly6G-Cre* mice (**Fig. 22D-J**). *Irg1* had no effect on IFN- $\gamma$ -independent or -dependent control of *Mtb* *in vitro*, as no differences in *Mtb* titer were detected in WT and *Irg1*<sup>-/-</sup> bone marrow-derived macrophages (BMDMs) (**Fig. 24C**). These data suggest that *Irg1* is dispensable for control of *Mtb* in

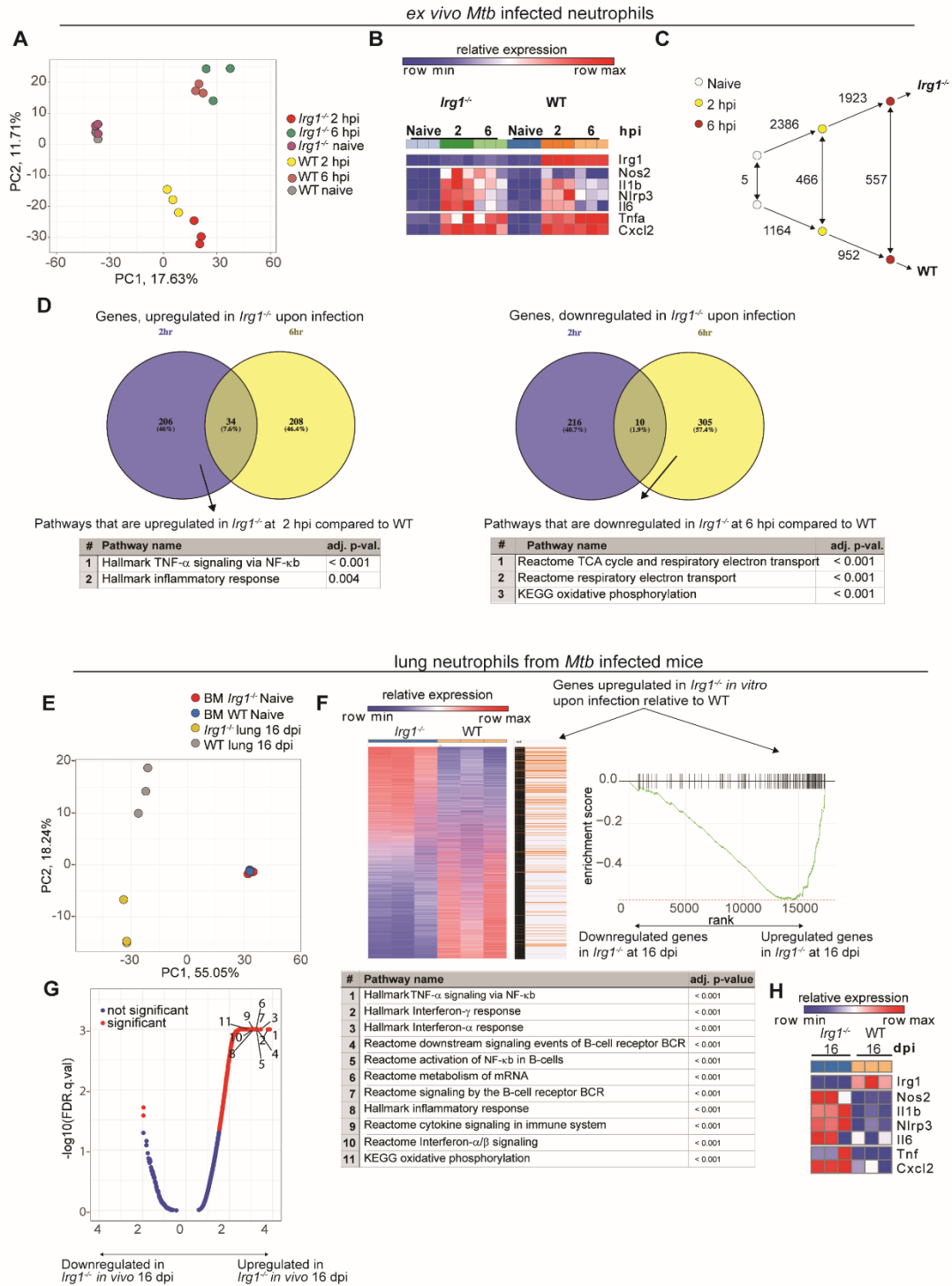


**Figure 25. *Irg1* alters transcription of inflammatory and metabolic genes in neutrophils during *Mtb* infection.**

Neutrophils were infected *ex vivo* and analyzed at 0 (naïve), 2, and 6 hpi. Experiments were performed in triplicate for each cohort. (A) PCA plot: PCA component 1 indicates difference between naïve and infected samples. PCA component 2 shows a time-dependent change in

infected samples. **(B)** Heat map shows the relative expression intensity of the indicated inflammatory genes in WT and *Irg1*<sup>-/-</sup> neutrophils. **(C)** Diagram shows the numbers of differentially expressed genes between WT and *Irg1*<sup>-/-</sup> neutrophils over the time course of *ex vivo* infection. **(D)** Venn diagrams show comparison of differentially expressed genes between WT and *Irg1*<sup>-/-</sup> neutrophils at 2 hpi versus those at 6 hpi. Tables show the top enriched pathways as indicated for each diagram. **(E-G)** Transcriptome data from WT and *Irg1*<sup>-/-</sup> neutrophils purified from lungs at 16 dpi or from the bone marrow of naïve mice (as baseline comparison) (n = 3 per cohort). **(E)** PCA plot. PCA component 1 indicates the difference between samples derived from infected lungs and naive bone marrow. The second component indicates difference between WT and *Irg1*<sup>-/-</sup> neutrophils after infection. **(F)** Data sets from WT and *Irg1*<sup>-/-</sup> neutrophils *in vivo* were compared to data sets from WT and *Irg1*<sup>-/-</sup> neutrophils *ex vivo* (2 and 6 hpi combined). Genes that are upregulated in *ex vivo* infected *Irg1*<sup>-/-</sup> neutrophils also are enriched in *Irg1*<sup>-/-</sup> neutrophils isolated from lung at 16 dpi. Left plot shows gene expression table of WT and *Irg1*<sup>-/-</sup> neutrophils from infected mice. Columns and rows show conditions and genes, respectively. Genes are ranked according to significance of differential expression and direction of change. Orange bars (right side) represent genes that become upregulated in the combined transcriptome of *Irg1*<sup>-/-</sup> neutrophils at 2 + 6 hpi. Right plot shows the running score for the gene set as the analysis moves down the ranked list. The score at the peak of the plot (the score furthest from 0.0) is the score for the gene set. **(G)** Gene set enrichment analysis comparison between WT and *Irg1*<sup>-/-</sup> neutrophils from infected lungs described above. Each dot on volcano plot (left) represents a pathway and is characterized by two values: NES (normalized enrichment score) shows direction and strength of change; minus logarithm of adjusted P value represents the significance of the pathway. Significantly enriched pathways are highlighted in red and listed on the table along with adjusted P values. **(H)** Heat map of selected inflammatory genes in neutrophils isolated from WT and *Irg1*<sup>-/-</sup> lungs at 16 dpi.

macrophages. Collectively, these findings indicate that *Irg1*<sup>-/-</sup> cells are in a hyper-inflamed state, rather than being defective in cell autonomous control of *Mtb*.

### ***Irg1 regulates inflammatory responses in myeloid cells during Mtb infection.***

To gain insight into why a lack of Irg1 expression in myeloid cells resulted in excessive accumulation of neutrophils and hyper-inflammation in *Irg1*<sup>-/-</sup> mice during *Mtb* infection we examined the expression profiles of *Mtb*-infected WT and *Irg1*<sup>-/-</sup> neutrophils and BMDMs.

*Ex vivo* analysis of naïve neutrophils isolated from WT and *Irg1*<sup>-/-</sup> bone marrow showed a highly overlapping gene expression profile (**Fig. 25A**), indicating that the basal gene expression pattern of both genotypes was similar. Within 2 hrs of *Mtb* infection *ex vivo*, *Irg1*<sup>-/-</sup> neutrophils had higher expression of *Nos2*, *Il6*, *Il1b*, and *Nlrp3* but not *Tnfa* and *Cxcl2* transcripts (**Fig. 25B**), indicating that *Irg1* expression in neutrophils controls expression of a subset of pro-inflammatory genes. Indeed, *Irg1*<sup>-/-</sup> neutrophils exposed to *Mtb* induced the differential expression of twice as many transcripts as WT cells (**Fig. 25C**). Pathway enrichment analysis of samples at 2 hours post-infection (hpi) revealed that infected *Irg1*<sup>-/-</sup> neutrophils had prominent inflammatory response transcriptional signatures compared to WT cells (**Fig. 25D**). At 6 hpi, *Irg1*<sup>-/-</sup> neutrophils had down-regulated transcripts of several genes involved in the electron transport chain, TCA cycle, and oxidative phosphorylation (**Fig. 25D**), which is consistent with the reported metabolic functions of *Irg1*.<sup>138,155</sup> We then analyzed neutrophils isolated directly from lungs of mice at 16 dpi (**Fig. 25E-G**). WT and *Irg1*<sup>-/-</sup> neutrophils were distinguished by global gene expression patterns (**Fig. 25E**), confirming a marked effect of *Irg1* on neutrophil responses during *Mtb* infection *in vivo*. Genes that were upregulated in *Irg1*<sup>-/-</sup> neutrophils *ex vivo* after *Mtb* infection were also upregulated in *Irg1*<sup>-/-</sup> neutrophils isolated from the lung at 16 dpi (**Fig. 25F**). Neutrophils in *Irg1*<sup>-/-</sup> mice at 16 dpi upregulated transcriptional signatures associated with inflammation, including NF-κB and pro-inflammatory signaling pathways downstream of cytokine receptors and interferons (**Fig. 25G, H**). This pronounced pro-inflammatory phenotype of *Irg1*<sup>-/-</sup> neutrophils isolated *in vivo* was accompanied by altered expression of genes involved in oxidative phosphorylation, which links the anti-inflammatory action of *Irg1* with its control of cellular metabolic activity.

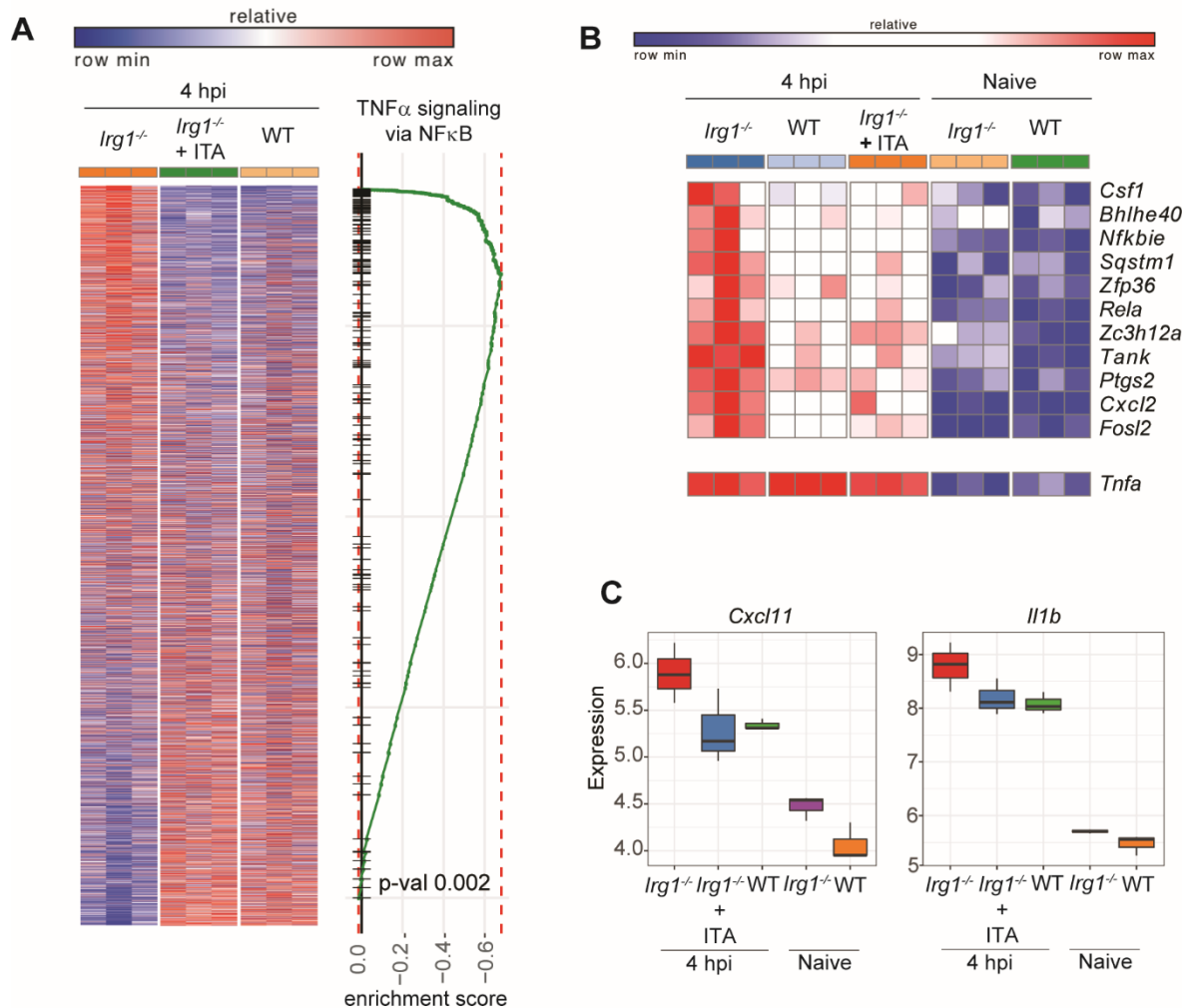


**Figure 26. *Irg1* alters the transcriptional signature of *Mtb* infected BMDMs.**

(A-C) Transcriptomic data from WT, *Irg1*<sup>-/-</sup>, and *Irg1*<sup>-/-</sup> + itaconate (ITA)-treated BMDMs infected with *Mtb* and analyzed at 4 hrs post-infection (hpi). (A, left) Heat map comparing the transcriptional changes that occur at 4 hpi in *Irg1*<sup>-/-</sup> BMDMs  $\pm$  ITA and WT BMDMs. Genes that are up-regulated in WT BMDMs also are enriched in *Irg1*<sup>-/-</sup> + ITA BMDMs at 4 hpi. Columns and rows show conditions and genes, respectively. Genes are ranked according to significance of differential expression and direction of change. (A, right) Plot shows the running score for NF- $\kappa$ B gene set as the analysis moves down the ranked list. (B) Gene set enrichment analysis comparison for genes in NF- $\kappa$ B signaling and (C) inflammatory chemokines *Cxcl11* and *Il1b* between WT versus *Irg1*<sup>-/-</sup>, WT versus *Irg1*<sup>-/-</sup> + ITA, and *Irg1*<sup>-/-</sup> versus *Irg1*<sup>-/-</sup> + ITA BMDMs. The median  $\pm$  SEM is graphed. Data is from one experiment.

We next compared the expression profiles of *Mtb* infected WT and *Irg1*<sup>-/-</sup> BMDMs.

Within just 4 hours of *Mtb* infection, the transcriptional signature in *Irg1*<sup>-/-</sup> BMDMs differed markedly from WT BMDMs. Many of the genes that were upregulated in *Irg1*<sup>-/-</sup> cells after *Mtb*

infection were reciprocally downregulated in WT BMDMs (**Fig. 26A, B**). Exogenous addition of itaconate (ITA) to *Mtb* infected *Irg1*<sup>-/-</sup> BMDMs switched their transcriptional signature to one similar to *Mtb* infected WT BMDMs (**Fig. 26A, B**), suggesting that the effect of *Irg1* deletion on transcriptional profiles was due principally to the loss of itaconate production. Pathway enrichment analysis indicated that a lack of *Irg1* expression in *Mtb* infected BMDMs resulted in induction of inflammatory and chemoattractant genes downstream of NF-κB signaling, and correspondingly, addition of itaconate to *Irg1*<sup>-/-</sup> BMDMs reverses this effect (**Fig. 26B, C**). Nonetheless, and consistent with our *in vivo* experiments (**Fig. 20D**), *Tnfa* expression levels were similar in *Mtb* infected WT and *Irg1*<sup>-/-</sup> BMDMs in the presence or absence of itaconate treatment. Collectively, this data shows that *Irg1* and its product itaconate function to limit inflammation during *Mtb* infection at the transcriptional level.

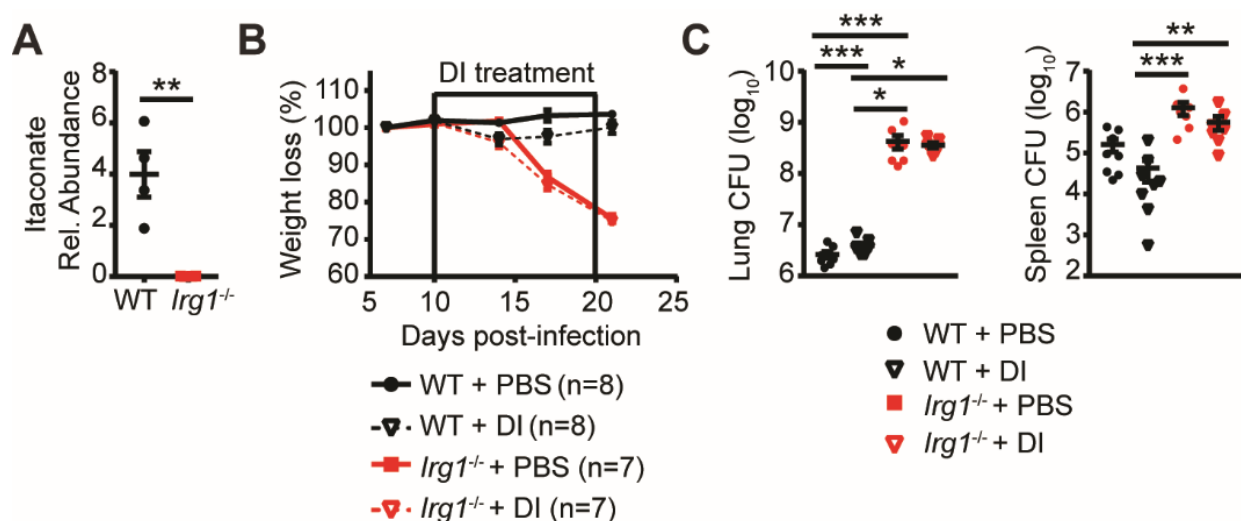


**Figure 27. *Irg1* is the sole source of lung itaconate during *Mtb* infection and i.p. administration of dimethyl itaconate fails to rescue *Irg1*<sup>-/-</sup> susceptibility.**

(A-C) Mice were infected with *Mtb*. (A) Relative abundance of itaconate in total lung samples from 21 dpi. (B-C) Mice were administered dimethyl itaconate (DI) i.p. daily from 10-20 dpi and monitored for (B) weight loss kinetics and (C) *Mtb* burden in lung and spleen. The mean ± SEM is graphed. Statistical differences were determined by two-tailed unpaired Student's t test (A) or unpaired Kruskal-Wallis test (C). \*, P < 0.05; \*\*, P < 0.01; \*\*\*, P < 0.001; \*\*\*\*, P < 0.0001. Data are from two independent experiments.

### ***Irg1 is the sole source of itaconate in the lung during Mtb infection***

The ability of exogenous itaconate to restore the transcriptional profile of *Irg1*<sup>-/-</sup> BMDMs to a profile resembling that of WT BMDMs raised the questions of whether there were *Irg1*-independent sources of itaconate during *Mtb* infection and if administration of an exogenous itaconate analog could rescue the susceptibility of *Irg1*<sup>-/-</sup> mice to *Mtb*. We performed liquid chromatography-tandem mass spectrometry (LC-MS/MS) on methanol-soluble extracts of total lung samples taken from *Mtb* infected mice to quantify relative levels of itaconate. Itaconate was not detected in WT mice at 7 dpi (data not shown) but was detected at 21 dpi. In contrast to WT mice, no itaconate was detected in any *Irg1*<sup>-/-</sup> lung samples, demonstrating that *Irg1* is the sole source of itaconate in the lung during *Mtb* infection (**Fig. 27A**).

We next attempted to complement the susceptibility associated phenotypes in *Irg1*<sup>-/-</sup> mice through exogenous delivery of dimethyl itaconate (DI), a more cell permeable analog of itaconate. Daily intraperitoneal administration of DI had no effect on weight loss kinetics (**Fig. 27B**) or *Mtb* burden in the lung or spleen (**Fig. 27C**). Additionally, DI administration was poorly tolerated by mice and induced hunching and temporary hind limb paralysis. Presence of DI in the lung was not evaluated and thus it is unclear whether it failed to rescue *Irg1*<sup>-/-</sup> susceptibility because DI did not reach the lung, was not consistently present at an effective concentration, did not have the same effect as itaconate in this context, or because *Irg1* is required for itaconate-independent functions. Experiments that utilize alternative routes of delivery (for example, intranasal) and monitor bioavailability of itaconate in the lung will be necessary to draw conclusions about the ability of exogenously administered itaconate to rescue *Irg1*<sup>-/-</sup> mouse susceptibility.

## Discussion

Active *Mtb* infection in humans induces a potent inflammatory response characterized by neutrophilia in the blood.<sup>199</sup> Studies in mice have shown that regulation of neutrophil recruitment to the lung during early stages of *Mtb* infection is a determinant of *Mtb* pathogenesis, as these cells can exert protective<sup>200,201</sup> or deleterious<sup>24,32</sup> effects. Our results demonstrate that Irg1 has an important role in hematopoietic cells in regulating inflammation to prevent neutrophil-mediated immunopathology during *Mtb* infection in mice. Whereas infection of WT mice with *Mtb* induced an inflammatory response that resulted in long-term survival, infection of mice lacking Irg1 led to heightened inflammation characterized by increased production of pro-inflammatory cytokines and chemokines and recruitment of granulocytes (neutrophils and eosinophils) by 14 dpi. By 21 dpi uncontrolled accumulation of neutrophils provided an expanded niche for *Mtb* replication that extended to infection of other myeloid cells subsets recruited to the lung. Loss of Irg1 expression in CD11c<sup>+</sup> and LysM<sup>+</sup> cells led to increased neutrophil accumulation in the lung by 21 dpi. Together, these bacterial and immune consequences contributed to the severe lung pathology and subsequent death of *Irg1*<sup>-/-</sup> mice within 40 days. As depletion of neutrophils in *Irg1*<sup>-/-</sup> mice reduced bacterial burden, prolonged survival, and dampened lung inflammation, we suggest that neutrophils are a principal cell type contributing to the immunopathology of *Irg1*<sup>-/-</sup> mice after *Mtb* infection.

Several groups have reported Irg1 as a highly induced protein in activated macrophages.<sup>131,134,138</sup> We observed that Irg1 regulates expression of pro-inflammatory and chemoattractant genes in macrophages within 4 hours of *Mtb* infection. Irg1 may be regulating inflammation during *Mtb* infection in several ways. Irg1 has been reported to suppress production of Toll-like receptor (TLR)-triggered NF-κB-dependent cytokines by promoting the

activity of anti-inflammatory factors such as TNFAIP3 (also known as A20), Nrf2, and Atf3.<sup>153,154,156</sup> Although an increased inflammatory response was detected in the lungs of *Irg1*<sup>-/-</sup> mice at 14 dpi, we failed to detect differences in TNF- $\alpha$ , a cytokine regulated by TNFAIP3,<sup>154,157</sup> compared to WT lung homogenates. Thus, in the context of *Mtb* infection Irg1 appears to modulate inflammatory responses by dampening expression of a selected subset of NF- $\kappa$ B regulated genes in both macrophage and neutrophils, perhaps through Nrf2- or Atf3-dependent mechanisms. Irg1 also has been implicated in inducing the production of reactive oxygen species, which can have antibacterial or immunomodulatory effects *in vivo*.<sup>152,160</sup> The neutrophil-dependent pathology in *Irg1*<sup>-/-</sup> mice infected with *Mtb* could be due to overproduction of NOS2 production in neutrophils or the increased number of ROS-producing neutrophils.

An established function of Irg1 is its *cis*-aconitate decarboxylase activity, which produces itaconate through the decarboxylation of the TCA intermediate, *cis*-aconitate.<sup>143</sup> Irg1 has been proposed to have an important protective role in *Mtb* infection through production of itaconate, which blocks the glyoxylate shunt by inhibiting ICL1 and ICL2.<sup>143,144,202</sup> Our experiments with *Δicl1 Mtb* suggest that *in vivo*, Irg1 exerts its action against *Mtb* by regulating inflammatory responses, rather than by inhibiting ICL1. The *Δicl1 Mtb* strain was as virulent as WT *Mtb* in *Irg1*<sup>-/-</sup> mice even though its glyoxylate shunt capacity is suboptimal.<sup>150</sup> However, we cannot rule out an effect of Irg1 on the glyoxylate shunt because *Mtb* Erdman encodes a second ICL enzyme, ICL2, which could compensate for loss of ICL1. Nonetheless, our immunologic and transcriptional profiling data are more consistent with a model where the dominant role for Irg1 is to restrict production of pro-inflammatory chemokines and accumulation of myeloid cells that provide a niche for *Mtb* replication. Consistent with this hypothesis, we observed no difference in the ability of WT and *Irg1*<sup>-/-</sup> BMDMs to restrict *Mtb* growth *in vitro*. Intriguingly, *Mtb*, *M.*

*abscessus*, and *M. avium* all possess ICL homologs<sup>151,203</sup> but the susceptibility and degree of bacterial control observed in *Irg1*<sup>-/-</sup> mice varied dramatically by species. This suggests that the protective function of Irg1 may vary by mycobacterial species. Future studies can address this topic by comparing host inflammatory responses and species-specific requirements for the glyoxylate shunt.

Our data support a model (**Fig. 28**) where CD11c<sup>+</sup> and LysM<sup>+</sup> cells requires Irg1 to dampen pro-inflammatory cytokine production and subsequent neutrophil inflammation. Our transcriptomic analysis after *Mtb* infection of *Irg1*<sup>-/-</sup> BMDMs revealed a pro-inflammatory signature that was reversed by the addition of exogenous itaconate. Thus, the distinct gene expression profiles in Irg1-sufficient and Irg1-deficient cells likely are due to differences in the production of itaconate, a metabolite that is absent in the lung homogenates of *Mtb* infected *Irg1*<sup>-/-</sup> mice. Collectively, our data suggest a key role for Irg1 and itaconate in regulating inflammation in the context of *Mtb* infection. Infection studies in gene-edited mice expressing forms of Irg1 that lack the ability to generate itaconate will be the focus of future work to confirm this hypothesis.

In summary, our experiments establish an essential role for Irg1 in regulating neutrophil-dependent inflammation during *Mtb* infection of the lung. We show that Irg1, likely through its ability to convert the TCA cycle intermediate *cis*-aconitate to itaconate, shapes the host immune responses through an immunometabolism axis to curtail *Mtb*-induced lung disease. As murine Irg1 is ~80% identical in amino acid sequence to human IRG1 with all five predicted *cis*-aconitate decarboxylase domains fully conserved,<sup>143</sup> the development of pharmacological agents that enhance Irg1 function or promote itaconate production might minimize pathological

inflammatory responses that cause severe lung injury associated with tuberculosis disease progression.

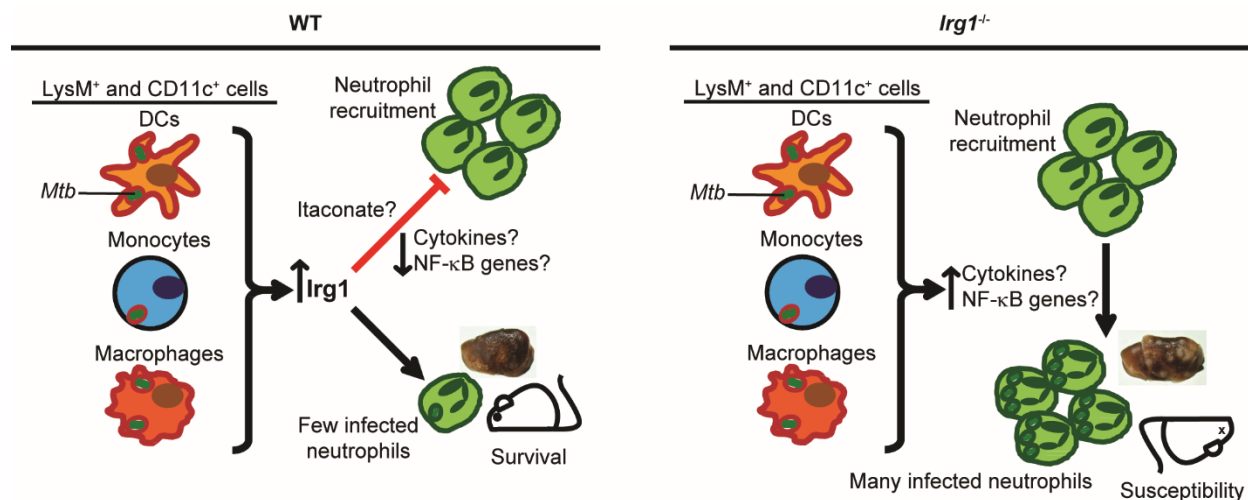


**Figure 28. Model of Irg1 function during *Mtb* infection.**

During *Mtb* infection of WT mice, Irg1 is induced in LysM<sup>+</sup> and CD11c<sup>+</sup> cells such as macrophages, monocytes, and DCs. Irg1 acts to suppress transcriptional upregulation of pro-inflammatory cytokines and NK-κB-regulated genes, likely through production of itaconate. This prevents recruitment of pathologic neutrophils and enables survival. In *Irg1*<sup>-/-</sup> mice, *Mtb* infection strongly induces pro-inflammatory cytokine production by LysM<sup>+</sup> and CD11c<sup>+</sup> cells, resulting in excessive neutrophil recruitment that promotes *Mtb* growth and causes lung pathology, ultimately resulting in susceptibility.

## Experimental Procedures

### *Ethics statement*

All procedures involving animals were conducted following the National Institutes of Health (NIH) guidelines for housing and care of laboratory animals and performed in accordance with institutional regulations after protocol review and approval by the Institutional Animal Care and Use Committee of the Washington University in St. Louis School of Medicine (protocol no. 20160118). Washington University is registered as a research facility with the United States Department of Agriculture and is fully accredited by the American Association of Accreditation of Laboratory Animal Care. The Animal Welfare Assurance is on file with Office for Protection

from Research Risks–NIH. All animals used in these experiments were subjected to no or minimal discomfort. All mice were euthanized by CO<sub>2</sub> asphyxiation, which is approved by the American Veterinary Association Panel on Euthanasia.

### *Mouse strains*

C57BL/6N (WT) mice were either purchased from Charles River or bred in-house. No differences in survival or disease progression during Mtb infection were observed in *IrgI*<sup>+/+</sup> littermate controls or *IrgI*<sup>+/+</sup> C57BL/6N mice obtained from Charles River in three independent experiments. B6.SJL (CD45.1) mice were obtained from Jackson Laboratories. *IrgI*<sup>-/-</sup> mice (embryonic stem cells obtained from KOMP [C57BL/6N background reporter-tagged insertion with conditional potential, MGI: 103206]) were generated at Washington University and have been described previously.<sup>138</sup> Adult mice (6–13 weeks of age) of both sexes were used, and sex was randomized between experiments. Cre-negative *IrgI*<sup>fl/fl</sup> mice were generated as described previously<sup>204</sup> with two loxP sites flanking exon 4 of *IrgI*. *IrgI*<sup>-/-</sup> mice were bred with *FLPe* “deleter” mice<sup>205</sup> to facilitate deletion of *lacZ* and neomycin resistance cassettes between FRT sites and create *IrgI*<sup>fl/+</sup> founder mice. The founder mice were backcrossed to C57BL/6J background using speed congenic approaches (>99% purity) and then interbred to generate *IrgI*<sup>fl/fl</sup> mice. These animals were crossed with *Mrp8-Cre*<sup>+</sup>, *Lysm-Cre*<sup>+</sup>, and *Cd11c-Cre*<sup>+</sup> (Jackson Laboratory) mice to delete exon 4 of *IrgI* from specific subsets of myeloid cells.

### *Generation of bone marrow chimeric mice*

Bone marrow chimeric mice were generated by irradiation (900 Gy) of WT or *IrgI*<sup>-/-</sup> recipients and reconstitution with 10<sup>7</sup> bone marrow cells from WT or *IrgI*<sup>-/-</sup> donors. 6-8 weeks

after bone marrow transplantation, *IrgI*<sup>-/-</sup> (CD45.2) → WT (CD45.1), WT (CD45.1) → *IrgI*<sup>-/-</sup> and WT (CD45.1) → WT (CD45.2), and WT (CD45.1) + *IrgI*<sup>-/-</sup> (CD45.2) → WT (CD45.1) mice were bled to confirm chimerism by flow cytometry before *Mtb* infection.

### *Mouse infections*

*Mtb* cultures in logarithmic growth phase (OD<sub>600 nm</sub> = 0.5-0.8) were washed with PBS + 0.05% Tween 80, sonicated to disperse clumps, and diluted in sterile water. Mice were exposed to  $1.6 \times 10^8$  CFUs of *Mtb*, a dose chosen to deliver 100-200 CFUs of aerosolized *Mtb* per lung using an inhalation exposure system (Glas-Col). For each infection, lungs were harvested from at least two control mice, homogenized, and plated on 7H11 agar to confirm the input CFU dose. The mean dose determined at this time point was assumed to be representative of the dose received by all other mice infected concurrently. *Mtb* burden was determined after homogenizing the superior, middle, and inferior lobes of the lung or the entire spleen and plating serial dilutions on 7H11 agar. Colonies were counted after 3 weeks of incubation at 37°C in 5% CO<sub>2</sub>.

*M. abscessus* (strain L948) and *M. avium* (strain TMC724) cultures in logarithmic growth phase (OD<sub>600</sub> = 0.5-0.8) were washed with PBS + 0.05% Tween 80, passaged through a 27 G needle three times to disperse clumps, and diluted in sterile water. Mice were sedated with ketamine (Henry Schein) and xylazine (Akorn), then infected by intranasal inoculation of  $1.5 \times 10^7$  CFU. For each infection, lungs were harvested from at least two control mice, homogenized, and plated on 7H11 agar to confirm the input CFU dose. The mean dose determined at this time point was assumed to be representative of the dose received by all other mice infected concurrently. Bacterial burden was determined after homogenizing the superior, middle, and

inferior lobes of the lung and plating serial dilutions on 7H11 agar. Colonies were counted after 5 days (*M. abscessus*) or 3 weeks (*M. avium*) of incubation at 37°C in 5% CO<sub>2</sub>.

*Listeria monocytogenes* (strain EGD) was stored at mid-logarithmic growth as frozen glycerol stocks. Thawed bacteria were diluted into pyrogen-free saline for intravenous injection into mice at a dose of 10<sup>5</sup> bacteria/mouse in 200 µl.

Mice were infected with IAV strain A/California/04/2009 H1N1 by intranasal inoculation of 10<sup>5</sup> or 10<sup>6</sup> tissue culture dose. At 5 dpi viral titer was assessed from bronchoalveolar (BAL) fluid by tissue culture dose.

#### *Neutrophil depletions*

Mice were administered 200 µg of anti-Ly6G monoclonal antibody (clone 1A8; BioXCell) or rat IgG2a isotype control antibody (clone 2A3; BioXCell) diluted in sterile PBS (Hyclone) by intraperitoneal injection every 48 hrs, beginning at 10 dpi and ending at 20 or 34 dpi, depending on the experiment. For confirmation of depletion during survival experiments, lungs from one anti-Ly6G treated *Irg1*<sup>-/-</sup> control mouse and one isotype treated *Irg1*<sup>-/-</sup> control mouse were harvested from each independent experiment and analyzed by flow cytometry for reduction in CD45<sup>+</sup>/CD11b<sup>+</sup>/Ly6C<sup>mid</sup> cells.

#### *In vivo itaconate administration*

Mice were intraperitoneally administered 500 µl of 250 mM dimethyl itaconate (Alfa Aesar) daily, beginning at 10 dpi and ending at 20 dpi.

### *Metabolomics profiling of Mtb infected lung cells*

The superior, middle, and inferior lobes of the lung were left unperfused, minced with a razor blade, and placed into 800  $\mu$ l 80% HPLC-grade methanol/20% deionized water. Samples were bead-beaten three times and kept on ice between cycles. Cell debris were pelleted by centrifugation at 17,000 x g for 5 min at room temp. Supernatants were sterilized by filtration through two 0.22  $\mu$ m Spin-X cellulose acetate filters (Costar) and stored at -80°C until analysis by liquid chromatography-tandem mass spectrometry.

### *Infection of neutrophils*

Neutrophils were purified from bone marrow of naïve mice by negative selection using magnetic-activated cell sorting beads (Miltenyi). Neutrophil purity (>95%) was assessed by flow cytometry as the percentage of Ly6G<sup>+</sup>CD11b<sup>+</sup> cells. Neutrophils were cultured in RPMI-1640 supplemented with 10% heat-inactivated FBS, 1% non-essential amino acids at 37°C, 5% CO<sub>2</sub>. *Mtb* was grown to mid-log phase, washed with PBS, sonicated to disperse clumps, and resuspended in neutrophil culture media. *Mtb* was then was opsonized prior to infection by mixing with an equal volume of normal mouse sera (Sigma) and incubation at room temperature for 30 min. Neutrophils were mock-infected or infected with opsonized *Mtb* at MOI 1 and incubated at 37°C, 5% CO<sub>2</sub>.

### *Infection of BMDMs*

Macrophages were obtained by culturing bone marrow cells in RPMI-1640 (Invitrogen) supplemented with 10% heat-inactivated FBS, 2 mM L-glutamine, 1% nonessential amino acids, 100 U penicillin per ml, 100  $\mu$ g streptomycin per ml, and 22 ng M-CSF (Peprotech)/ml for 6

days at 37°C, 5% CO<sub>2</sub>. Fresh media was added on day 3 of culture. After 6 days of culture, nonadherent cells were discarded. Adherent macrophages were switched into antibiotic-free media and seeded at 10<sup>5</sup> cells per well and 9 x 10<sup>5</sup> cells per well in tissue culture-treated 96- and 6-well plates, respectively. In some cases, macrophages were treated with physiologically relevant concentrations of 0.25 mM itaconic acid (Sigma) or 50 ng IFN-γ (Peprotech)/ml for 12 hrs before infection with *Mtb*.<sup>143</sup> *Mtb* was grown to OD<sub>600</sub>=0.6-0.8, washed with PBS, sonicated to disperse clumps, and resuspended in antibiotic-free macrophage culture media. Macrophage cultures were infected by adding *Mtb*-containing media at a multiplicity of infection of 1 and centrifuging for 10 min at 200 x g. Cells were washed twice with PBS to remove unbound *Mtb*, fresh culture media was added, and cells were incubated at 37°C, 5% CO<sub>2</sub>. In some cases, culture media was supplemented with 0.25 mM itaconic acid.

### *Bacterial cultures*

*Mtb* strain Erdman, mutant *Mtb* strains, *M. abscessus*, and *M. avium* were cultured at 37°C in 7H9 broth (Sigma) or on 7H11 agar (BD Difco) medium supplemented with 10% oleic acid/albumin/dextrose/catalase, 0.5% glycerol, and 0.05% Tween 80 (broth only).

*Listeria monocytogenes* was grown in a shaking culture in brain-heart infusion broth at 37°C to mid-logarithmic growth phase, washed in PBS, and frozen as glycerol stocks at -80°C.

### *Generation of Mtb mutants*

*Mtb*-GFP was generated by transforming *Mtb* strain Erdman with a plasmid (pMV261-kan-GFP) that drives constitutive expression of GFP under the control of the *hsp60* promoter. Cultures were grown in the presence of kanamycin to ensure plasmid retention.  $\Delta icl1$  *Mtb* was

generated by transducing *Mtb* strain Erdman with a phage containing homology to nucleotides 556805–557527 and 558797–559447.  $\Delta$ PDIM *Mtb* was generated by transducing *Mtb* strain Erdman with a phage containing homology to nucleotides 3243062-3243567 and 3272196-3272718.  $\Delta$ ESX-1 *Mtb* was generated by transducing *Mtb* strain Erdman with a phage containing homology to nucleotides 4349945-4350677 and 4356534-4357206. Phage transduction was used to replace the endogenous *icl1* ( $\Delta$ *icl1* strain); *fadD26* and *ppsABCDE* ( $\Delta$ PDIM strain); and *pe35*, *ppe68*, *esxAB*, *espI*, and *eccD1* ( $\Delta$ ESX-1 strain) genes with a hygromycin resistance cassette. Mutants were selected by culture on hygromycin-containing 7H11 agar. Individual hygromycin-resistant colonies were expanded by inoculation into hygromycin-supplemented 7H9 media. Replacement of the target genes with the hygromycin resistance cassette was confirmed by Southern blotting of genomic DNA from expanded cultures.

#### *Viral cultures*

A/California/04/2009 H1N1 influenza viral stocks were prepared as previously described.<sup>206</sup>

#### *Bronchoalveolar lavage (BAL) of IAV infected mice*

For analysis of BAL fluid, mice were sacrificed by Avertin overdose, followed by anterior neck dissection and cannulation of the trachea with a 22-G catheter. BAL was performed with three washes of 0.8 ml of sterile Hanks' balanced salt solution. BAL fluid was centrifuged and the cell-free supernatant was collected and stored for viral titer analysis.

### *Flow cytometry*

Lungs were perfused with sterile PBS and left lobes of lungs were digested at 37°C with 630 µg/ml collagenase D (Roche) and 75 U/ml DNase I (Sigma). All antibodies were used at a dilution of 1:200. Single cell suspensions were preincubated with Fc Block antibody (BD Pharmingen) in PBS + 2% heat-inactivated FBS for 10 min at room before staining. Cells were incubated with antibodies against the following markers: V500 anti-CD45.1 (clone A20), AF700 anti-CD45.2 (clone 104; eBioscience), AF700 anti-CD45 (clone 30 F-11), APC-Cy7 anti-CD11c (clone N418), PE anti-SiglecF (clone E50-2440; BD), PE-Cy7 anti-Ly6G (clone 1A8), PB or Qdot605 anti-Ly6C (clone AL-21/HK1.4; Biolegend/ BD), PerCP-Cy5.5 anti-CD11b (clone M1/70), APC anti-CD103 (clone 2E7; eBioscience), PB anti-CD3 (clone 17A2), PE-Cy7, APC anti-CD4 (clone RM4-5), PE-Cy7 anti-CD8 (clone53-6.7), anti-NK1.1 (clone PK136), and APC anti-Nos2 (clone CXN FT; all from eBioscience). Intracellular ROS were stained with MitoSOX red dye (Thermo Fisher). Absolute cell counts were determined using TruCount beads (BD). Cells were stained for 20 min at 4°C, washed, and fixed in 4% paraformaldehyde (Electron Microscopy Sciences) in PBS for 20 min at 4°C. Flow cytometry data were acquired on a cytometer (LSR Fortessa; BD Biosciences) and analyzed using FlowJo software (Tree Star). Gating strategies are depicted in **Figure 29**.

### *Cytokine/chemokine quantification*

Lungs were homogenized in 5 ml of PBS supplemented with 0.05% Tween 80. Homogenates were filtered (0.22 µm) twice and analyzed by BioPlex-Pro Mouse Cytokine 23-Plex Immunoassay (Bio-Rad).

*Histology and imaging*

Lung samples were fixed in 10% buffered formalin (Thermo Fisher). Gross pathology images were acquired using a Power Shot G9 camera (Canon). For detailed histological analysis, lung lobes were embedded in paraffin, sectioned, and stained with H&E (Pulmonary Morphology Core, Washington University). Acid-fast bacilli were stained with Ziehl-Neelsen

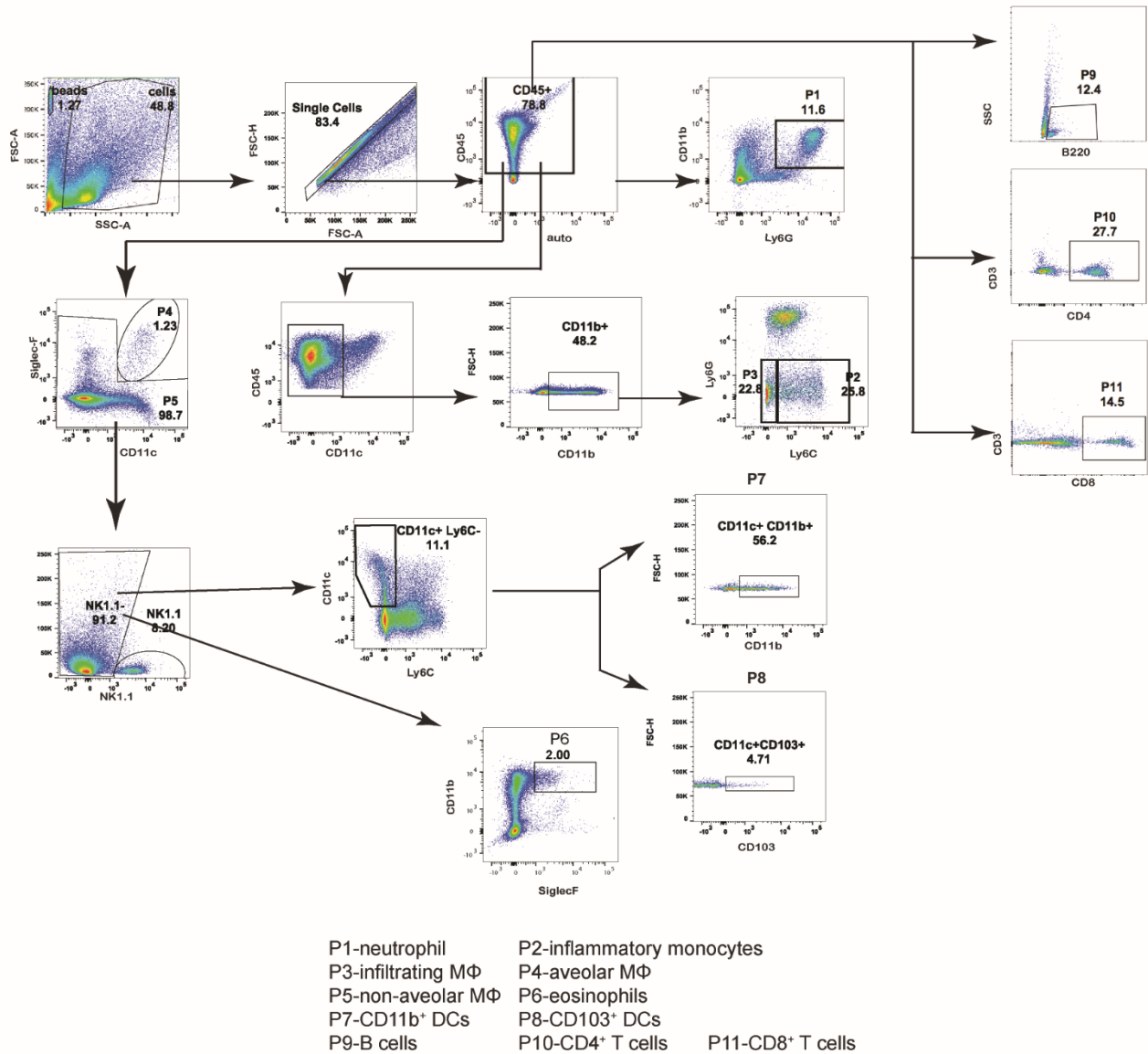


**Figure 29. Flow cytometry gating strategy used in Irg1 experiments.**

stain (Pulmonary Morphology Core). Images were acquired using NanoZoomer 2.0-HT System (Hamamatsu) or an Eclipse E400 camera (Nikon).

### *RNA-seq*

Neutrophils were purified by magnetic-activated cell sorting from the bone marrow of naïve mice (negative selection) or whole lungs of *Mtb* infected mice at 16 dpi (selection for Ly6G<sup>+</sup> cells) (Miltenyi). Neutrophil purity was defined by flow cytometry as the percentage of Ly6G<sup>+</sup>CD11b<sup>+</sup> cells (negatively selected samples) or Gr-1<sup>high</sup>CD11b<sup>+</sup> cells (positively selected samples). BMDMs were harvested at 4 h after *Mtb* infection, and RNA was extracted using TriZol reagent (Invitrogen).

Total RNA was isolated from TriZol by chloroform extraction, precipitated with isopropanol and high salt buffer (0.8 M sodium citrate, 1.2 M NaCl in RNase-free water), washed with 80% ethanol/20% RNase-free water, dried for 10 min at room temp, and resuspended in 20 µl RNase-free water.

mRNA was extracted with oligo-dT beads (Invitrogen) and cDNA synthesized using custom oligo-dT primer with a barcode and adaptor-linker sequence (CCT ACA CGA CGC TCT TCC GAT CT-XXX XXX XX-T15). Samples were pooled based on *Actb* qPCR values, RNA-DNA hybrids degraded with acid-alkali treatment and a second sequencing linker (5'-AGA TCG GAA GAG CAC ACG TCTG- 3') was ligated with T4 ligase (NEB). After SPRI bead cleanup (Agencourt AMPure XP; Beckman Coulter), the mixture was PCR-enriched (12 cycles) and SPRI-purified, yielding final strand-specific RNA-seq libraries. Libraries were sequenced on a HiSeq 2500 (Illumina) using 40 x 10 bp paired-end sequencing. Second read (read-mate) was used for sample demultiplexing. Files obtained from the sequencing center were demultiplexed

with fastq-multx tool. Fastq files for each sample were aligned to mm10 genome (Release M8 Gencode; GRCm38.p4) using STAR. Each sample was evaluated according to a variety of both pre- and postalignment quality control measures with Picard tools. Aligned reads were quantified using a quant3p script (Computer Technologies Laboratory, 2016) to account for specifics of 3' sequencing: higher dependency on good 3' annotation and lower level of sequence specificity close to 3' end. Actual read counts were performed by HTSeq with enriched genome annotation and alignment with fixed multimapper flags. DESeq2 was used for analysis of differential gene expression. Preranked GSEA analysis was used to identify pathway enrichments in hallmark and canonical pathways.

#### *Quantification and statistical analysis*

All data are from at least two independent biological experiments with multiple mice in each group. No blinding was performed during animal experiments. Statistical differences were calculated using Prism 7 (GraphPad) using log-rank Mantel-Cox tests (survival), unpaired two-tailed Mann-Whitney tests (to compare two groups with non-normal data distribution), and one-way ANOVA with Tukey's multiple comparisons tests (to compare more than two groups with normal data distribution). Differences with a p-value of  $<0.05$  were defined as statistically significant.

#### *Data and software availability*

RNA-seq data are available in the Gene Expression Omnibus repository under reference series number GSE98458.

## **Chapter 4**

## **Conclusions**

## **Introduction**

Protective immune responses to *Mycobacterium tuberculosis* (*Mtb*) must induce bactericidal functions while minimizing damage to the lung. Such responses require precise control of pro- and anti-inflammatory factors to regulate the recruitment and function of protective immune cells but the mechanisms by which this control is exerted remain incompletely defined. Bhlhe40 is a transcription factor known to regulate production of pro- and anti-inflammatory cytokines that affect protective immunity to *Mtb*. Irg1 is an enzyme that generates itaconate, a metabolite with potential anti-inflammatory and antibacterial roles during *Mtb* infection.

We found that Bhlhe40 enables protective immune responses to *Mtb* in T cells and CD11c<sup>+</sup> cells and enables resistance to acute infection by restricting expression of the anti-inflammatory cytokine IL-10. Bhlhe40 does so by repressing *Il10* transcription, likely by direct binding to the *Il10* locus. Additionally, we discovered that Irg1 functions in LysM<sup>+</sup> and CD11c<sup>+</sup> cells to prevent neutrophil-mediated immunopathology. Irg1 expression restricts inflammatory responses in myeloid cells at a transcriptional level, likely through production of the metabolite itaconate. The impact of Bhlhe40 and Irg1 on protective immunity to *Mtb* was unknown prior to the studies detailed in this dissertation.

## **Discussion and Future Directions**

### ***Bhlhe40* expression patterns**

Using *Bhlhe40*<sup>GFP</sup> transgenic reporter mice that express green fluorescent protein (GFP) under the control of the genomic regions flanking the *Bhlhe40* gene we demonstrated that Bhlhe40 is expressed in multiple innate and adaptive lung immune cell types before infection

and during acute infection. Mice with conditional deletions of *Bhlhe40* in T cells and CD11c<sup>+</sup> cells were susceptible to *Mtb*, indicating that these are the key cell types that require Bhlhe40 expression. Studies in other model systems have demonstrated that Bhlhe40 expression is dynamic and regulated by multiple stimuli. Given the importance of Bhlhe40 for control of *Mtb* infection, it is possible that these dynamics impact control of *Mtb* infection. *Bhlhe40*<sup>GFP</sup> mice could be highly useful in future studies that seek to answer questions about where Bhlhe40-expressing cells localize within the *Mtb* infected lung, the infection status of Bhlhe40-expressing cells, and patterns of Bhlhe40 expression in specific cell types over a prolonged course of *Mtb* infection. These questions could be answered by flow cytometry and immunohistochemistry studies on lung lesions in *Bhlhe40*<sup>GFP</sup> mice infected with a *Mtb* strain that expresses a non-GFP fluorescent marker and flow cytometric analysis of *Bhlhe40*<sup>GFP</sup> mice at later points in infection. Additionally, we did not address the importance of Bhlhe40 in chronic *Mtb* infection but could do so using *Bhlhe40*<sup>fl/fl</sup> mice that express Cre recombinase under the control of a tamoxifen-inducible promoter, such as *ERT2-Cre* mice.

Bhlhe40 expression patterns could also be modulated by diet, with potentially important effects on control of *Mtb* infection. Epidemiological<sup>207,208</sup> and *in vitro*<sup>209</sup> studies have suggested that vitamin A levels are associated with resistance to *Mtb* and all-*trans* retinoic acid, the biologically available form of vitamin A, is known to induce Bhlhe40 expression.<sup>106,123</sup> Together with our findings on the importance of Bhlhe40 in control of murine tuberculosis and lower *BHLHE40* expression in patients with active tuberculosis, these reports raise the possibility of a Bhlhe40-mediated link between micronutrient availability, disease severity, and variation in long-term control of disease. Experiments characterizing how vitamin A availability modulates Bhlhe40 expression and associated control of *Mtb* in mice in conjunction with prospective

studies in humans tracking serum metabolites, Bhlhe40 expression, and progression to active tuberculosis could address this relationship.

### ***Bhlhe40 and IL-10-dependent control of Mtb infection***

We assessed the role of Bhlhe40 expression on control of *in vivo Mtb* infection using genetically deficient mice. Bhlhe40 was required in T cells and CD11c<sup>+</sup> cells and enabled protective immune responses to acute *Mtb* infection by restricting expression of IL-10. Bhlhe40 does so by repressing *Il10* transcription, likely by direct binding to the *Il10* locus. Multiple groups had previously demonstrated that IL-10 has detrimental effects on control of *Mtb* infection but these phenotypes were mild or occurred late in infection. Our findings show for the first time that IL-10 can have major impacts on control of *Mtb* and that Bhlhe40 is an essential regulator of IL-10. However, it remains unclear exactly how increased IL-10 production causes susceptibility in *Bhlhe40*<sup>-/-</sup> mice. Our observations of decreased *Il12b* and *Ifng* transcript aligns with a large body of literature demonstrating that IL-10 interferes with mechanisms involved in inducing and responding to IFN- $\gamma$ , but studies comparing the transcriptional and functional state of WT and *Bhlhe40*<sup>-/-</sup> cells *in vivo* will be necessary to fully prove that this is the case. *Bhlhe40*<sup>-/-</sup> cells would be expected to exhibit a transcriptional profile characterized by reduced expression of IFN- $\gamma$ -stimulated genes after the induction of *Mtb*-specific adaptive immune responses.

We have identified multiple immune cell populations that overexpress IL-10 as well as the key cell types that must express Bhlhe40 during *Mtb* infection. We also observed increased IL-10 expression in non-Bhlhe40-expressing cell types in the context of global Bhlhe40 deficiency which raises the possibility that non-Bhlhe40-expressing cells may be important sources of IL-10. It remains to be determined which of these cell types mediate IL-10 dependent

susceptibility. Cell types that cause susceptibility by overproducing IL-10 in a globally *Bhlhe40*-deficient setting can be identified by generating *Bhlhe40*<sup>-/-</sup>*Il10*<sup>fl/fl</sup> mice that express Cre recombinase in the cell types we found to be over-producers of IL-10 in our analysis of *Bhlhe40*<sup>-/-</sup> 10BiT<sup>+</sup> mice. Cell types in which *Bhlhe40* is essential to regulate IL-10 production can be identified by generating *Bhlhe40*<sup>fl/fl</sup>*Il10*<sup>fl/fl</sup> mice that express Cre recombinase in the cell types we identified as expressing *Bhlhe40* in our analysis of *Bhlhe40*<sup>GFP</sup> mice. Susceptibility-associated phenotypes such as survival, *Mtb* burden, and inflammation can then be compared in Cre-positive and Cre-negative *Bhlhe40*<sup>-/-</sup>*Il10*<sup>fl/fl</sup> mice or *Bhlhe40*<sup>fl/fl</sup>*Il10*<sup>WT/WT</sup> mice with the same Cre expression pattern. Cre-positive *Bhlhe40*<sup>-/-</sup>*Il10*<sup>fl/fl</sup> and *Bhlhe40*<sup>fl/fl</sup>*Il10*<sup>fl/fl</sup> mice that show improvement in susceptibility-associated phenotypes will reveal key cell types that mediate IL-10-dependent susceptibility.

Additionally, we have yet to identify the cell types that mediate susceptibility by responding to the increased IL-10. Such cell types can be identified by comparing susceptibility-associated phenotypes in Cre-positive and Cre-negative *Bhlhe40*<sup>-/-</sup>*Il10ra*<sup>fl/fl</sup> mice. Key cell types will be identified by Cre-positive mice that show improvements in susceptibility associated phenotypes as compared to Cre-negative mice.

While we have established that *Bhlhe40* is a direct regulator of IL-10, the pathway of IL-10 induction in which *Bhlhe40* functions remains to be determined. IL-10 can be induced by a wide variety of extracellular signals during *Mtb* infection<sup>75,165</sup> and the ability of *Bhlhe40* to repress IL-10 may vary according to the induction pathway. We found that *Bhlhe40*<sup>-/-</sup> cells and mice do not overexpress *Il10* prior to infection which strongly implies that a transcriptional activator is triggered by *Mtb* infection. The identity of this putative activator is currently unknown and there are many possibilities, but c-Maf, AP-1 family members, and IRF4 stand out

by virtue of their reported ability to bind the *Il10* locus close to the *Bhlhe40* binding site we identified at *Il10* +6 kb. c-Maf (encoded by the *Maf* gene) is induced in T cells by cytokine signals<sup>210,211</sup> and promotes T cell production of IL-10 in infectious disease, allergy, and autoimmune contexts.<sup>212</sup> *Bhlhe40* expression was found to be upregulated in c-Maf-deficient T cells<sup>212</sup> and *Maf* expression is increased in *Bhlhe40*-deficient T cells,<sup>129</sup> suggesting that these transcription factors regulate each other. In support of this idea, our ChIP-seq data identified *Maf* as a gene predicted to be regulated by *Bhlhe40* in T<sub>H</sub>1 cells. Binding sites for c-Maf have been reported in the *Il10* promoter and near the *Il10* +6 kb site bound by *Bhlhe40*.<sup>212</sup> Interferon regulatory factor 4 (IRF4) promotes IL-10 production after T cell activation and has been shown to bind a *Il10* +6.45 kb enhancer site in T<sub>H</sub>2 cells.<sup>213</sup> Several members of the activator protein (AP)-1 family of transcription factors have also been reported to bind the *Il10* +6.45 kb site in T cells after T cell receptor stimulation, including JunB and c-Jun.<sup>181,214</sup> The AP-1 family member c-fos promotes IL-10 production in myeloid DCs after stimulation with toll-like receptor (TLR) agonists and could potentially bind to the same AP-1 site as JunB or c-Jun in DCs, but direct binding has yet to be demonstrated.<sup>215</sup> *Bhlhe40* has also been reported to interact with histone deacetylases (HDACs)<sup>102</sup> and could be preventing binding of an activator elsewhere in the *Il10* locus by controlling chromatin accessibility. Thus, these transcription factors represent likely candidates for the activator of *Il10* transcription that is restricted by *Bhlhe40*.

CRISPR or small-interfering RNA knock-down approaches could be used to target the activator protein candidates mentioned above in *Bhlhe40*<sup>-/-</sup> T cells and GM-CSF cultured cells. *Il10* transcript levels could then be measured after treatment with IL-10-inducing stimuli such as anti-CD3/anti-CD28 and PMA/Ionomycin or heat-killed *Mtb* antigen. Knock-down of the activator protein will result in reduced *Il10* transcription in *Bhlhe40*<sup>-/-</sup> cells. Activator protein

redundancy is also a possibility and multiple activator candidates may need to be targeted simultaneously. HDAC-dependent mechanisms could be identified through treatment with trichostatin A, a pan-HDAC inhibitor, profiling of histone acetylation status, and co-immunoprecipitation mass spectrometry to identify HDAC interactions or potential activators that Bhlhe40 represses through direct binding. The importance of activator candidates in *Mtb* infection can then be tested by generation of *Bhlhe40*<sup>-/-</sup> mice that also lack the protein of interest and comparison of susceptibility-associated phenotypes with *Bhlhe40*<sup>-/-</sup> mice. Once an activator protein is identified, the key upstream signaling pathways that trigger it can be identified by genetic knock-out or antibody blockade and treatment with IL-10-inducing stimuli.

Another IL-10-dependent role for Bhlhe40 concerns clinical tuberculosis diagnostics. IFN- $\gamma$  release assays (IGRAs) are a commonly used method of diagnosing *Mtb* exposure, but more than 10% of culture-positive tuberculosis patients test negative by IGRA.<sup>216</sup> These patients tend to have worse disease outcomes, likely due to delayed treatment. IGRAs work by stimulating a sample of peripheral blood with *Mtb* antigens and measuring IFN- $\gamma$  production.<sup>216</sup> We found that Bhlhe40-deficiency leads to increased production of IL-10 and that patients with active tuberculosis had lower *BHLHE40* expression in their peripheral blood. Since IL-10 is well established as a suppressor of IFN- $\gamma$ , our findings suggest that patients with lower expression of Bhlhe40 in peripheral blood could produce increased IL-10 with a suppressive effect on IFN- $\gamma$  production. Thus, lower Bhlhe40 expression levels could have an adverse effect on IGRA specificity and patient outcomes. Future studies could address this question by obtaining peripheral blood samples from discordant active tuberculosis patients who tested negative for tuberculosis by IGRA, but positive by bacterial culture and concordant patients who were positive by IGRA and culture. *Bhlhe40* expression levels in unstimulated and stimulated

peripheral blood samples could then be compared in concordant and discordant active tuberculosis patients to determine if lower *BHLHE40* expression before stimulation is correlated with a false negative IGRA result. Stimuli that induce *Bhlhe40* expression, such as retinoic acid, could be used to treat blood samples from discordant patients and demonstrate an active role for *Bhlhe40*. IL-10-neutralizing antibodies could be used to test the role of IL-10 in any observed effects.

### ***IL-10-independent roles for Bhlhe40 in Mtb infection***

We have demonstrated that the acute susceptibility of *Bhlhe40*<sup>-/-</sup> mice is largely IL-10-dependent, but loss of IL-10 does not confer complete restoration of WT phenotypes. *Il10*<sup>-/-</sup>*Bhlhe40*<sup>-/-</sup> mice have more neutrophilic inflammation at 21 dpi and significantly shorter survival time compared to WT mice. These findings demonstrate that *Bhlhe40* has IL-10-independent functions that are important during *Mtb* infection. The key cell types mediating IL-10-independent functions of *Bhlhe40* can be identified by comparison of Cre-positive *Bhlhe40*<sup>fl/fl</sup> and Cre-positive *Bhlhe40*<sup>fl/fl</sup>*Il10*<sup>fl/fl</sup>. Susceptibility associated phenotypes found in both strains with the same Cre expression pattern would be due to IL-10-independent functions of *Bhlhe40* in Cre-expressing cells. Identification of IL-10-independent functions for *Bhlhe40* could be identified in an unbiased manner by transcriptomic comparison of WT, *Bhlhe40*<sup>-/-</sup>, and *Il10*<sup>-/-</sup>*Bhlhe40*<sup>-/-</sup> lung hematopoietic cells at 21 dpi, a time point at which *Il10*<sup>-/-</sup>*Bhlhe40*<sup>-/-</sup> mice already have a higher frequency of neutrophils compared to WT mice.

We have also identified genes that *Bhlhe40* is predicted to regulate based on DNA binding sites and this data could also be used to address IL-10-independent roles. *Bhlhe40* has been reported to function in a wide variety of biological processes including cell death and

regulation of non-IL-10 cytokine production. Our studies of *Irg1* and *Bhlhe40* have demonstrated the importance of inflammatory control for infection and cell death modalities are known to impact control of *Mtb*.<sup>217</sup> Perturbation of these processes in *Bhlhe40*<sup>-/-</sup> cells could adversely affect control of inflammation and *Mtb* growth in the absence of IL-10. Additionally, we have observed that *Il10*<sup>-/-</sup>*Bhlhe40*<sup>-/-</sup> mice have a stronger neutrophil response than WT mice as early as 21 dpi. Based on literature reports and our data, investigation of *Bhlhe40*-regulated genes that are likely to regulate cytokine production, cell death, or have previously been identified as important for control of *Mtb* should be prioritized. Three candidate genes, all of which were identified as potentially regulated by *Bhlhe40* in both myeloid and lymphoid cells, are discussed below.

Tristetraprolin (TTP, encoded by *Zfp36*) is an RNA-binding protein that regulates mRNA stability. TTP has been reported to repress production of IL-12<sup>218</sup> and IFN- $\gamma$ ,<sup>219</sup> and transcript levels for both of these cytokines trend downward in *Il10*<sup>-/-</sup>*Bhlhe40*<sup>-/-</sup> compared to WT mice. TTP can also regulate other proinflammatory cytokines of potential importance in *Il10*<sup>-/-</sup>*Bhlhe40*<sup>-/-</sup> mouse susceptibility during chronic infection.<sup>220</sup> TTP also regulates RIP1 kinase activity,<sup>221</sup> and decreased RIP1 activity could lead to detrimental cell death pathways.<sup>90</sup> Forkhead box protein O3 (*Foxo3*) is a transcription factor that exerts predominantly anti-inflammatory effects on immune cells. *Foxo3* has been reported to promote T cell apoptosis<sup>222</sup> and to repress pro-inflammatory responses by DCs and T cells.<sup>223,224</sup> Dysregulated *Foxo3* activity could lead to over or underproduction of inflammatory cytokines or be detrimental for survival of effector T cells during *Mtb* infection. Hypoxia inducible factor-1 $\alpha$  (*Hif-1 $\alpha$* ) is a transcription factor that mediates a wide variety of IFN- $\gamma$ -stimulated responses and is essential for control of *Mtb* infection.<sup>225</sup> However, over-expression of *Hif-1 $\alpha$*  can cause proteinase-mediated tissue pathology.<sup>226</sup> Dysregulated *Hif-1 $\alpha$*  activity could compromise protective functions of IFN- $\gamma$  during *Mtb*

infection or promote immunopathology. Thus TTP, Foxo3, and Hif-1 $\alpha$  all modulate key immune cell processes involved in control of *Mtb* and could promote IL-10-independent susceptibility if dysregulated in *Bhlhe40*<sup>-/-</sup> mice.

### ***Irg1 and restriction of neutrophil-mediated immunopathology***

We have discovered that Irg1 expression restricts neutrophil-dominated inflammatory responses in myeloid cells at a transcriptional level, likely through production of the metabolite itaconate. In support of itaconate as an anti-inflammatory mediator, we found that exogenous itaconate treatment was sufficient to revert *Irg1*<sup>-/-</sup> macrophages to a less inflammatory, WT-like transcriptional profile and suppressed transcription of the neutrophil recruitment signal CXCL2 and the broadly inflammatory gene *Il1b*. Intriguingly, we found that levels of IL-17, a cytokine that triggers and sustains neutrophilic inflammation, were also highly upregulated in the lungs of *Irg1*<sup>-/-</sup> mice. This suggests that Irg1 restricts neutrophilic inflammatory responses by limiting production of cytokines such as CXCL2, IL-1 $\beta$ , and IL-17.

However, the mechanism by which Irg1 exerts its anti-inflammatory effects during *Mtb* infection remains unclear. Studies in other models of immunopathology have reported that Irg1 or itaconate promotes the activity of anti-inflammatory factors such as TNFAIP3 (also known as A20), Nrf2, and Atf3, leading to the repression of a subset of pro-inflammatory cytokines that includes IFN- $\beta$ , IL-1 $\beta$ , IL-6, and IL-12.<sup>153,154,156</sup> Unpublished data from our co-authors suggests that itaconate may also regulate IL-17 production by interfering with expression of the transcription factor BATF (Lampropolou & Artyomov, in preparation). Our findings that IL-1 $\beta$ , IL-6, and IL-17 are more highly expressed in *Mtb* infected *Irg1*<sup>-/-</sup> lungs a 14 dpi suggest that they might lead to neutrophilic inflammation. Future studies could test this by blockade or genetic

deletion of IL-6R and IL-17R and treatment with the IL-1R antagonist anakinra, followed by assessment of neutrophil accumulation and other susceptibility-associated phenotypes in *Irg1*<sup>-/-</sup> mice.

Our studies implicate Irg1-derived itaconate as a key suppressor of neutrophilic inflammation. Since neutrophil-dominated responses to *Mtb* are associated with active tuberculosis in humans, itaconate supplementation is a potential therapeutic approach for limiting neutrophil-mediated immunopathology in humans. Our efforts to modulate the pulmonary response to *Mtb* through intraperitoneal delivery of dimethyl itaconate were unsuccessful, but this may be due to insufficient bioavailability in the lung. Itaconate or an analog could be delivered intravenously or intranasally and *Irg1*<sup>-/-</sup> mice could be assessed for reduction neutrophil recruitment or inflammatory mediators such as IL-6 and IL-17. It is also possible that Irg1 has itaconate-independent effects *in vivo*. Future studies utilizing comparing *Irg1*<sup>-/-</sup> mice with mice that express a catalytically-inactivated version of Irg1 during *Mtb* infection will be required to identify such effects.

### ***Myeloid cell-specific requirements for Irg1***

We found that although the susceptibility of *Irg1*<sup>-/-</sup> mice is mediated by neutrophils, neutrophil-specific loss of Irg1 expression was not sufficient for susceptibility to *Mtb* infection. In contrast, loss of Irg1 expression in LysM<sup>+</sup> and CD11c<sup>+</sup> cells was sufficient to cause susceptibility. These susceptibility patterns point to a requirement for Irg1 in macrophages, monocytes, and DCs during *Mtb* infection. Irg1 deficiency in LysM<sup>+</sup> cells led to an earlier susceptibility than deficiency in CD11c<sup>+</sup> cells, demonstrating that expression in macrophages and monocytes enables survival of acute infection. Neutrophils also express LysM and Irg1-

deficient neutrophils are likely an important contributor to the acute susceptibility of *Irg1*<sup>fl/fl</sup>-*Lysm-Cre* mice, despite being insufficient for susceptibility when other myeloid cells express Irg1. We do not yet know why loss of Irg1 in neutrophils alone has no impact on susceptibility but it may be due to the ability of Irg1-expressing cell types to secrete itaconate and thereby provide *in trans* complementation to Irg1-deficient neutrophils.<sup>138</sup> Transcriptomic comparison of neutrophils isolated from *Mtb*-infected Cre-negative *Irg1*<sup>fl/fl</sup>, *Irg1*<sup>fl/fl</sup>-*Mrp8-Cre*, and *Irg1*<sup>-/-</sup> lungs would reveal whether Irg1-deficient neutrophils take on a less inflammatory profile when other Irg1-sufficient cells are present.

### ***Impact of Irg1 on adaptive immunity***

Irg1 and itaconate exert host-protective effects on innate immune cell function during *Mtb* infection, but no studies have yet examined their impact on adaptive immune cells. The lungs of *Mtb* infected *Irg1*<sup>-/-</sup> mice contained increased amounts of IFN- $\gamma$  and IL-17 at 21 dpi, cytokines produced in large quantities by T helper (T<sub>H</sub>) 1 and T<sub>H</sub>17-polarized CD4<sup>+</sup> T cells, respectively. IFN- $\gamma$  and IL-17 have important protective functions in primary- and vaccine-elicited responses that control *Mtb* infection<sup>34,35,227</sup> but both can cause pathology and susceptibility if over-produced.<sup>37,228</sup> The ability of IL-17-producing CD4<sup>+</sup> T cells to drive pathologic granulocyte-dominated inflammation during *Mtb* infection<sup>228</sup> is of particular interest given that the susceptibility of *Irg1*<sup>-/-</sup> mice is mediated by neutrophils, a type of granulocyte strongly associated with failure to control *Mtb* infection.<sup>24,32,33</sup> Our observations of increased IFN- $\gamma$  and IL-17 and neutrophil-mediated susceptibility in *Mtb* infected *Irg1*<sup>-/-</sup> mice suggest that Irg1 may restrict the generation of pathologic T cell responses that contribute to susceptibility.

Irg1 could be regulating T cell survival, recruitment, polarization, or effector function. Our studies focused on the role of Irg1 in myeloid cells and thus we did not test any of these possibilities. Still, some of our observations are suggestive of potential effects. Our finding that *Irg1*<sup>-/-</sup> mice had no differences in the absolute number of lung CD4<sup>+</sup> T cells at 21 dpi suggests that T cell survival and recruitment are unaffected. The fold increase in IL-17 levels in infected *Irg1*<sup>-/-</sup> lungs compared to WT was much greater than the fold increase in IFN- $\gamma$  levels, implicating over-production of IL-17 as the dominant effector cytokine and a cause of neutrophil-mediated immunopathology. Recently generated data from our co-authors shows that secreted itaconate from myeloid cells inhibits T<sub>H</sub>17 cell effector function (Lampropoulou & Artyomov, in preparation). This raises the possibility that loss of itaconate in *Irg1*<sup>-/-</sup> mice leads to unrestrained T<sub>H</sub>17 cell production of IL-17 and recruitment of pathologic neutrophils. Future studies should assess the role of T cells in *Irg1*<sup>-/-</sup> mouse susceptibility by characterizing *in vivo* expression of lineage-defining transcription factors, ability to generate antigen-specific responses, antigen-specific cytokine production, and T cell transcriptional profiles.

If Irg1 is found to be important for regulating T cell responses, follow-up studies could utilize *Irg1*<sup>fl/fl</sup>-*Cd4-Cre* mice examine a requirement for T cell-intrinsic Irg1 expression and the ability of secreted itaconate to modulate T cell metabolism and effector function during *Mtb* infection.

### ***Direct antibacterial roles for Irg1 in Mtb infection***

A direct antibacterial role for Irg1 has been hypothesized based on the ability of itaconate to inhibit *Mtb* ICLs *in vitro*. We have demonstrated that neutrophil depletion reduces WT *Mtb* burden in *Irg1*<sup>-/-</sup> mice but does not restore it to levels observed in WT mice. This partial rescue

could be due to incomplete neutrophil depletion, cytokine-mediated reductions in bactericidal capacity, or a direct antibacterial role for Irg1. We have also shown that the susceptibility of *Irg1*<sup>-/-</sup> mice is ICL1-independent and that *Irg1*<sup>-/-</sup> BMDMs have no defect in control of WT *Mtb*. These results do not support a direct antibacterial role for Irg1 during *Mtb* infection but are not definitive. Further studies are required and must account for the redundancy of ICL1 and ICL2 as well as confounding factors such as host-mediated pathology, the potential for *Mtb* to degrade itaconate, and the involvement of ICLs in other metabolic pathways.

The compensatory effects of ICL2 in  $\Delta icl1$  *Mtb* limit our ability to identify an inhibitory role for Irg1. Comparison of bacterial burden and susceptibility in WT and *Irg1*<sup>-/-</sup> mice infected with  $\Delta icl1/\Delta icl2$  *Mtb* will be necessary to draw more comprehensive conclusions on a role for Irg1 in restricting the glyoxylate shunt. However, it is likely that interpreting the results of such an experiment will be complicated by the severe *in vivo* attenuation of  $\Delta icl1/\Delta icl2$  *Mtb*.<sup>145</sup> This attenuation has attributed to the dual functionality of ICL1 and ICL2 in the glyoxylate shunt for carbon assimilation and the methylcitrate cycle for detoxification of propionate.<sup>146</sup> The finding that *Irg1*<sup>-/-</sup> mice are equally susceptible to WT and  $\Delta icl1/\Delta icl2$  *Mtb* would demonstrate that susceptibility is independent of the glyoxylate shunt and support restraint of inflammation as the crucial function for Irg1 in acute infection but would not rule out a simultaneous defect in antibacterial activity. An antibacterial role for Irg1 would be supported if  $\Delta icl1/\Delta icl2$  *Mtb* in an *Irg1*<sup>-/-</sup> mouse is cleared at rates equivalent to a WT mouse, but only if confounding inflammatory effects are avoided by limiting neutrophilic inflammation in the *Irg1*<sup>-/-</sup> mice to levels comparable to a WT mouse. This could be accomplished by neutrophil-specific depletion and antibody-mediated reduction of over-produced pro-inflammatory cytokines such as IL-17 in the *Irg1*<sup>-/-</sup> mice. Measurement of glyoxylate levels during *in vitro* or *in vivo* infection of WT and *Irg1*<sup>-/-</sup>

macrophages and mice by mass spectrometry would also provide a direct assessment of whether Irg1 restricts glyoxylate shunt activity since the glyoxylate cycle is absent from mammals.<sup>147</sup>

It is also unclear whether the potentially antibacterial activity of itaconate is being blocked by itaconate-degrading enzymes in *Mtb*. Mammals and several *Yersinia*, *Pseudomonas*, and *Salmonella* species encode three enzymes that enable detoxification of itaconate: succinyl-CoA:itaconyl-CoA transferase (ICT), itaconyl-CoA hydratase (ICH), and citramalyl-CoA lyase (CCL).<sup>149</sup> Genes that may provide the same functionality in *Mtb* include *scoAB* and *Rv3551/Rv3552* for ICT; *echA1-echA21*, *Rv1136*, and *Rv3538* for ICH; and *citE* for CCL. Future studies could test the ability of *Mtb* to degrade itaconate by radiolabeling itaconate and performing mass spectrometry to look for its breakdown products. The necessity of the genes listed above for itaconate degradation could be determined by genetic knock-out. However, these genes are likely to have roles in multiple processes and the likelihood of pleiotropic effects is high. For example, CitE is predicted to generate acetyl-CoA for fatty acid biosynthesis based on its genomic location,<sup>229</sup> and fatty acid biosynthesis is essential for survival of *Mtb* within macrophages.<sup>230</sup>

### ***Explanations for virulence of $\Delta icl1$ *Mtb* in *Irg1*<sup>-/-</sup> mice***

The persistence defect of  $\Delta icl1$  *Mtb* during chronic infection demonstrates that glyoxylate shunt function is suboptimal in this strain.<sup>145</sup> Since Irg1 is hypothesized to inhibit the glyoxylate shunt through itaconate, we asked whether  $\Delta icl1$  *Mtb*, a strain with suboptimal glyoxylate shunt function, might phenocopy the inhibitory effects of itaconate on the glyoxylate shunt and exhibit reduced virulence in *Irg1*<sup>-/-</sup> mice and if the susceptibility of *Irg1*<sup>-/-</sup> mice was independent of ICL1 function. ICL1-deficient *Mtb* proved not to be attenuated in *Irg1*<sup>-/-</sup> mice and we found that *Irg1*<sup>-/-</sup>

mice were equally susceptible to WT and  $\Delta icl1$  *Mtb*. There are several possible explanations for this lack of a difference. First, it is possible that the glyoxylate shunt is not active during acute infection and thus inhibition by itaconate would have no effect on virulence. The essentiality of malate synthase (*glcB*) to detoxify ICL-generated glyoxylate during acute infection suggests that ICLs and the glyoxylate shunt are active during acute infection and argues against this possibility.<sup>231</sup> Second, it is possible that ICL2 is compensating for loss of ICL1 during acute infection. This is very likely because  $\Delta icl1/\Delta icl2$  *Mtb* is severely attenuated during acute infection, while  $\Delta icl1$  *Mtb* is not.<sup>145</sup> Third, *Irg1*<sup>-/-</sup> mice may succumb to inflammatory defects at a time point before effects of glyoxylate shunt inhibition by itaconate can be observed. This is suggested by the observations that *Irg1*<sup>-/-</sup> mice succumb 5-6 weeks post-infection but the persistence defect of  $\Delta icl1$  *Mtb* is first seen at 8 weeks post-infection. Fourth, the neutrophil-dominated inflammation observed in *Irg1*<sup>-/-</sup> mice may generate a nutrient rich, growth-permissive environment<sup>33</sup> in which the glyoxylate shunt is not needed. Such an environment could compensate for any attenuation caused by loss of ICL1. A fifth and final possibility is that during acute infection itaconate does not inhibit ICL1 or ICL2 enough to affect *Mtb* growth or survival. This idea is supported by the report that  $\Delta icl1$  *Mtb* in WT mice is attenuated in chronic infection, but we and others find that WT and  $\Delta icl1$  *Mtb* reach similar titers by 21 dpi in WT and *Irg1*<sup>-/-</sup> mice. This lack of an inhibitory effect could be due to the presence of a degradative pathway for itaconate in *Mtb*, as mentioned previously.

### ***Itaconate catabolism and vitamin B12 deficiency***

An intermediate in the metabolic pathway responsible for itaconate catabolism has been shown to cause vitamin B12 depletion in human cells.<sup>232</sup> Since mammals and bacteria utilize a

similar pathway for itaconate break down,<sup>149</sup> vitamin B12 deficiency is likely to occur in bacteria as well. As stated previously, it is unclear whether or not *Mtb* can catabolize itaconate. If so, this process could lead to vitamin B12 deficiency that inhibits the methylmalonyl-CoA cycle,<sup>233,234</sup> one of several processes used by *Mtb* to detoxify propionate generated during metabolism of host fatty acids. If allowed to accumulate, propionate causes defects in intrabacterial pH and membrane potential.<sup>146</sup> Thus, itaconate could limit vitamin B12 availability, metabolic flexibility, and homeostasis in *Mtb* through its breakdown products.

Itaconate catabolism-driven consumption of vitamin B12 may also cause localized vitamin B12 depletion in host cells. Vitamin B12 is used as a coenzyme by two human enzymes, MUT, which recycles carbon from the methylmalonyl cycle back into the TCA cycle and MTR, which synthesizes methionine.<sup>232</sup> Lower circulating vitamin B12 levels are associated with increased expression of inflammatory biomarkers.<sup>235,236</sup> The effect of vitamin B12 deficiency on inflammatory responses is currently unclear, but may be important for understanding the progression of itaconate-mediated effects. Future studies could address this by treating mice with itaconyl-CoA, the vitamin B12-depleting itaconate metabolite, to deplete vitamin B12 in the absence of other itaconate-derived effects and analyzing its impact on *Mtb*-elicited inflammation.

### ***Possible cross-talk between Bhlhe40 and Irg1***

Irg1-sufficient (*Irg1*<sup>+/+</sup>) bone marrow-derived macrophages generated by culture of bone marrow cells with M-CSF (BMDMs) do not express *Bhlhe40* before or after *Mtb* infection. However, we found that *Bhlhe40* transcript is highly induced in *Irg1*<sup>-/-</sup> BMDMs as early as four hours after *Mtb* infection and that itaconate treatment blocks *Bhlhe40* induction in *Irg1*<sup>-/-</sup> BMDMs. This demonstrates that expression of *Bhlhe40* in certain macrophage subsets is

repressed by Irg1 and itaconate. In conjunction with previous reports that Irg1 and itaconate are highly expressed by activated macrophages, these observations may explain why minimal Bhlhe40 expression is detected in CD11b<sup>+</sup> macrophages during *in vivo Mtb* infection. By extension, Irg1 expression in LysM<sup>+</sup> cells, such as macrophages, during *in vivo* infection may repress Bhlhe40 and explain why loss of Bhlhe40 expression in LysM<sup>+</sup> cells had no effect on *in vivo* control of *Mtb*. *Irg1* is not predicted to be regulated by Bhlhe40 based on binding site data, although it could still be regulated through DNA binding-independent functions of Bhlhe40. Future studies could determine whether itaconate suppresses transcription of *Bhlhe40 in vivo* by comparing *Mtb* infected *Bhlhe40*<sup>GFP</sup> and *Irg1*<sup>-/-</sup>*Bhlhe40*<sup>GFP</sup> mice. *In vitro* studies of GM-CSF-cultured cells treated with itaconate could use Western blotting and mass spectrometry to determine whether itaconate might directly repress Bhlhe40 through post-translational modification leading to degradation, as has been shown for KEAP1.<sup>156</sup> Comparison of the resulting transcriptomic changes in WT, *Bhlhe40*<sup>-/-</sup>, and *Irg1*<sup>-/-</sup> cells of the same type would enable large scale conclusions on how their effects synergize to promote protective responses to *Mtb*. DCs may be an appropriate starting cell type for such a transcriptional comparison since we have demonstrated that expression of both Bhlhe40 and Irg1 in CD11c<sup>+</sup> cells is essential for resistance to *Mtb*.

### **Closing remarks**

The work presented in this dissertation has relied heavily on insights gained from studies on the functions of Bhlhe40 in neuroinflammation and Irg1 in macrophage activation. The unexpected roles that these genes had in regulating inflammatory responses provided a rationale for investigation of their function during *Mtb* infection. Using mice with global and conditional

deletions of *Bhlhe40* and *Irg1* in conjunction with *in vitro* models we have discovered novel and essential components of aspects of protective immunity to *Mtb*.

Prior to these studies it was unclear why the broadly anti-inflammatory cytokine IL-10 had such mild effects on control of *Mtb* infection. A multitude of reports in other disease models had demonstrated the potential of IL-10 to suppress protective immune responses but its effects on *Mtb* infection appeared to be limited to chronic infection and varied by genetic background. The work presented here has revealed that IL-10 can compromise protective immunity to *Mtb* if overexpressed during acute infection and has identified *Bhlhe40* as an essential transcriptional regulator that prevents over-expression of IL-10. This regulatory function of *Bhlhe40* is one mechanism by which the immune system promotes host-protective responses by suppressing non-protective responses.

*Irg1* had gained a great deal of interest for its ability to generate a potentially antibacterial effector but little attention was given to its immunomodulatory capabilities. We demonstrate here that *Irg1* has an unexpected and essential role in preventing pathologic inflammation by limiting neutrophil recruitment. This selective immunosuppression allows the immune system to avoid responses that fail to limit *Mtb* replication and severely damage the lung.

These studies establish the ability of *Bhlhe40* and *Irg1* to directly and indirectly tune the inflammatory response to *Mtb* at a transcriptional level. In summation, my dissertation work advances understanding of protective immunity to *Mtb* by revealing novel mechanisms used by specific innate and adaptive immune cell types to promote bactericidal activity and suppress pathologic inflammation.

## References

1. Comas, I. *et al.* Out-of-Africa migration and Neolithic coexpansion of *Mycobacterium tuberculosis* with modern humans. *Nat. Genet.* **45**, 1176–1182 (2013).
2. Sakula, A. Robert Koch: centenary of the discovery of the tubercle bacillus, 1882. *Thorax* **37**, 246–251 (1982).
3. WHO. *Global Tuberculosis Report 2017*. Who (2017). doi:WHO/HTM/TB/2017.23
4. Pai, M. *et al.* Tuberculosis. *Nat. Rev. Dis. Prim.* **2**, 16077 (2016).
5. Vynnycky, E. & Fine, P. E. M. The natural history of tuberculosis: The implications of age-dependent risks of disease and the role of reinfection. *Epidemiol. Infect.* **119**, 183–201 (1997).
6. Barry, C. E. *et al.* The spectrum of latent tuberculosis: Rethinking the biology and intervention strategies. *Nat. Rev. Microbiol.* **7**, 845–855 (2009).
7. Liu, J., Tran, V., Leung, A. S., Alexander, D. C. & Zhu, B. BCG vaccines: their mechanisms of attenuation and impact on safety and protective efficacy. *Hum. Vaccin.* **5**, 70–78 (2009).
8. Colditz, A., Berkey, S., Wilson, E., Brewer, F. & Fineberg, V. The Efficacy of Bacillus Calmette-Guerin Vaccination of Newborns and Infants in the Prevention of Tuberculosis: Meta-Analyses of the Published Literature. *Pediatrics* **96**, 29–35 (1995).
9. Trunz, B. B., Fine, P. & Dye, C. Effect of BCG vaccination on childhood tuberculous meningitis and miliary tuberculosis worldwide: a meta-analysis and assessment of cost-effectiveness. *Lancet* **367**, 1173–1180 (2006).
10. Comstock, G. & Palmer, C. Long-Term Results of BCG Vaccination in the Southern United States. *Am. Rev. Respir. Dis.* **93**, 171–183 (1966).
11. Hart, P. & Sutherland, I. BCG and vole bacillus vaccines in the prevention of tuberculosis in adolescence and early adult life. *Br. Med. J.* **2**, 293–295 (1977).
12. Baily, G. Tuberculosis Prevention Trial, Madras. *Indian J. Med. Res.* **72**, 1–75 (1980).
13. Sauer, B. & Henderson, N. Site-specific DNA recombination in mammalian cells by the Cre recombinase of bacteriophage P1. *Proc. Natl. Acad. Sci.* **85**, 5166–5170 (1988).
14. Gu, H., Marth, J., Orban, P., Mossman, H. & Rajewsky, K. Deletion of a DNA polymerase beta gene segment in T cells using cell type-specific gene targeting. *Science*. **265**, 103–6 (1994).
15. Sonnenberg, P. *et al.* How soon after infection with HIV does the risk of tuberculosis start to increase? A retrospective cohort study in South African gold miners. *J. Infect. Dis.* **191**, 150–8 (2005).
16. Badri, M., Wilson, D. & Wood, R. Effect of highly active antiretroviral therapy on incidence of tuberculosis in South Africa: a cohort study. *Lancet* **359**, 2059–64 (2002).
17. Ramakrishnan, L. Revisiting the role of the granuloma in tuberculosis. *Nat. Rev. Immunol.* **12**, 352–66 (2012).
18. Lee, S. W. *et al.* Time interval to conversion of interferon- $\gamma$  release assay after exposure to tuberculosis. *Eur. Respir. J.* **37**, 1447–1452 (2011).
19. Altare, F. *et al.* Interleukin-12 receptor  $\beta$ 1 deficiency in a patient with abdominal tuberculosis. *J. Infect. Dis.* **184**, 231–236 (2001).
20. Jouanguy, E. *et al.* Partial interferon- $\gamma$  receptor 1 deficiency in a child with tuberculoid bacillus Calmette-Guerin infection and a sibling with clinical tuberculosis. *J. Clin. Invest.* **100**, 2658–2664 (1997).

21. Boisson-Dupuis, S. *et al.* IL-12R $\beta$ 1 deficiency in two of fifty children with severe tuberculosis from Iran, Morocco, and Turkey. *PLoS One* **6**, 1–7 (2011).
22. Bustamante, J., Boisson-Dupuis, S., Abel, L. & Casanova, J. L. Mendelian susceptibility to mycobacterial disease: Genetic, immunological, and clinical features of inborn errors of IFN- $\gamma$  immunity. *Semin. Immunol.* **26**, 454–470 (2014).
23. MacMicking, J. D., Taylor, G. a & McKinney, J. D. Immune control of tuberculosis by IFN- $\gamma$ -inducible LRG-47. *Science.* **302**, 654–659 (2003).
24. Nandi, B. & Behar, S. M. Regulation of neutrophils by interferon- $\gamma$  limits lung inflammation during tuberculosis infection. *J. Exp. Med.* **208**, 2251–62 (2011).
25. Feng, C. G. *et al.* The immunity-related GTPase Irgm1 promotes the expansion of activated CD4<sup>+</sup> T cell populations by preventing interferon- $\gamma$ -induced cell death. *Nat. Immunol.* **9**, 1279–1287 (2008).
26. Fabri, M. *et al.* Vitamin D is required for IFN-gamma-mediated antimicrobial activity of human macrophages. *Sci. Transl. Med.* **3**, 104ra102 (2011).
27. Alonso, S., Pethe, K., Russell, D. G. & Purdy, G. E. Lysosomal killing of *Mycobacterium* mediated by ubiquitin-derived peptides is enhanced by autophagy. *Proc. Natl. Acad. Sci.* **104**, 6031–6036 (2007).
28. Ng, V. H., Cox, J. S., Sousa, A. O., MacMicking, J. D. & McKinney, J. D. Role of KatG catalase-peroxidase in mycobacterial pathogenesis: Countering the phagocyte oxidative burst. *Mol. Microbiol.* **52**, 1291–1302 (2004).
29. Wagner, D. *et al.* Elemental Analysis of *Mycobacterium avium*-, *Mycobacterium tuberculosis*-, and *Mycobacterium smegmatis*-Containing Phagosomes Indicates Pathogen-Induced Microenvironments within the Host Cell's Endosomal System. *J. Immunol.* **174**, 1491–1500 (2005).
30. Botella, H. *et al.* Mycobacterial P1-Type ATPases mediate resistance to Zinc poisoning in human macrophages. *Cell Host Microbe* **10**, 248–259 (2011).
31. Zhang, Y. J. *et al.* Tryptophan biosynthesis protects mycobacteria from CD4 T-Cell-mediated Killing. *Cell* **155**, 1296–1308 (2013).
32. Kimmey, J. M. *et al.* Unique role for ATG5 in neutrophil-mediated immunopathology during *M. tuberculosis* infection. *Nature.* **528**, 565–569 (2015).
33. Mishra, B. B. *et al.* Nitric oxide prevents a pathogen-permissive granulocytic inflammation during tuberculosis. *Nat. Microbiol.* **2**, 17072 (2017).
34. Cooper, A. M. *et al.* Disseminated tuberculosis in interferon gamma gene-disrupted mice. *J. Exp. Med.* **178**, 2243–7 (1993).
35. Flynn, J. L. *et al.* An essential role for interferon gamma in resistance to *Mycobacterium tuberculosis* infection. *J. Exp. Med.* **178**, 2249–2254 (1993).
36. Green, A. M., Difazio, R. & Flynn, J. L. IFN- $\gamma$  from CD4 T cells is essential for host survival and enhances CD8 T cell function during *Mycobacterium tuberculosis* infection. *J. Immunol.* **190**, 270–7 (2013).
37. Sakai, S. *et al.* CD4 T Cell-Derived IFN- $\gamma$  Plays a Minimal Role in Control of Pulmonary *Mycobacterium tuberculosis* Infection and Must Be Actively Repressed by PD-1 to Prevent Lethal Disease. *PLoS Pathog.* **12**, 1–22 (2016).
38. Feng, C. G. *et al.* NK cell-derived IFN- $\gamma$  differentially regulates innate resistance and neutrophil response in T cell-deficient hosts infected with *Mycobacterium tuberculosis*. *J. Immunol.* **177**, 7086–7093 (2006).
39. Gazzinelli, R. T. *et al.* IL-10 inhibits parasite killing and nitrogen oxide production by

- IFN-gamma-activated macrophages. *J. Immunol.* **148**, 1792–1796 (1992).
40. Turner, J. *et al.* *In vivo* IL-10 production reactivates chronic pulmonary tuberculosis in C57BL/6 mice. *J. Immunol.* **169**, 6343–6351 (2002).
  41. O’Leary, S., O’Sullivan, M. P. & Keane, J. IL-10 blocks phagosome maturation in *Mycobacterium tuberculosis*-infected human macrophages. *Am. J. Respir. Cell Mol. Biol.* **45**, 172–180 (2011).
  42. Beamer, G. L. *et al.* Interleukin-10 Promotes *Mycobacterium tuberculosis* Disease Progression in CBA/J Mice. *J. Immunol.* **181**, 5545–5550 (2008).
  43. Redford, P. S. *et al.* Enhanced protection to *Mycobacterium tuberculosis* infection in IL-10-deficient mice is accompanied by early and enhanced T<sub>H</sub>1 responses in the lung. *Eur. J. Immunol.* **40**, 2200–2210 (2010).
  44. Moreira-Teixeira, L. *et al.* T Cell-Derived IL-10 Impairs Host Resistance to *Mycobacterium tuberculosis* Infection. *J. Immunol.* [ji1601340](#) (2017).
  45. McNab, F. W. *et al.* Type I IFN Induces IL-10 Production in an IL-27-Independent Manner and Blocks Responsiveness to IFN- $\gamma$  for Production of IL-12 and Bacterial Killing in *Mycobacterium tuberculosis*-Infected Macrophages. *J. Immunol.* **193**, 3600–3612 (2014).
  46. Duan, L., Yi, M., Chen, J., Li, S. & Chen, W. *Mycobacterium tuberculosis* EIS gene inhibits macrophage autophagy through up-regulation of IL-10 by increasing the acetylation of histone H3. *Biochem. Biophys. Res. Commun.* **473**, 1229–1234 (2016).
  47. Lai, R. *et al.* CD11b<sup>+</sup> Dendritic Cell-Mediated Anti-*Mycobacterium tuberculosis* T<sub>H</sub>1 Activation Is Counterregulated by CD103<sup>+</sup> Dendritic Cells via IL-10. *J. Immunol.* [ji1701109](#) (2018).
  48. Roach, D. R. *et al.* Endogenous inhibition of antimycobacterial immunity by IL-10 varies between mycobacterial species. *Scand. J. Immunol.* **54**, 163–170 (2001).
  49. Demangel, C., Bertolino, P. & Britton, W. J. Autocrine IL-10 impairs dendritic cell (DC)-derived immune responses to mycobacterial infection by suppressing DC trafficking to draining lymph nodes and local IL-12 production. *Eur. J. Immunol.* **32**, 994–1002 (2002).
  50. Schreiber, T. *et al.* Autocrine IL-10 induces hallmarks of alternative activation in macrophages and suppresses antituberculosis effector mechanisms without compromising T cell immunity. *J. Immunol.* **183**, 1301–1312 (2009).
  51. Khader, S. a *et al.* Interleukin 12p40 is required for dendritic cell migration and T cell priming after *Mycobacterium tuberculosis* infection. *J. Exp. Med.* **203**, 1805–1815 (2006).
  52. de Waal Malefyt, R., Abrams, J., Bennett, B., Figdor, C. G. & de Vries, J. E. Interleukin 10 (IL-10) inhibits cytokine synthesis by human monocytes: an autoregulatory role of IL-10 produced by monocytes. *J. Exp. Med.* **174**, 1209–20 (1991).
  53. Mayer-Barber, K. & Sher, A. Innate and adaptive interferons suppress IL-1 $\alpha$  and IL-1 $\beta$  production by distinct pulmonary myeloid subsets during *Mycobacterium tuberculosis* infection. *Immunity* **18**, 1199–1216 (2011).
  54. Areeshi, M. Y. *et al.* *IL10* -1082 A>G (rs1800896) polymorphism confers susceptibility to pulmonary tuberculosis in Caucasians but not in Asians and Africans: a meta-analysis. *Biosci. Rep.* **37**, BSR20170240 (2017).
  55. Ke, Z. *et al.* IL-10 polymorphisms and tuberculosis susceptibility: An updated meta-analysis. *Yonsei Med. J.* **56**, 1274–1287 (2015).
  56. Liang, B., Guo, Y., Li, Y. & Kong, H. Association between IL-10 gene polymorphisms and susceptibility of tuberculosis: Evidence based on a meta-analysis. *PLoS One* **9**,

- (2014).
57. Zhang, J. *et al.* Interleukin-10 polymorphisms and tuberculosis susceptibility: A meta-analysis. *Int. J. Tuberc. Lung Dis.* **15**, 594–601 (2011).
  58. Gao, X. *et al.* Interleukin-10 promoter gene polymorphisms and susceptibility to tuberculosis: A meta-analysis. *PLoS One* **10**, 1–16 (2015).
  59. Pacheco, A. G., Cardoso, C. C. & Moraes, M. O. *IFNG* +874T/A, *IL10* -1082G/A and *TNF* -308G/A polymorphisms in association with tuberculosis susceptibility: A meta-analysis study. *Hum. Genet.* **123**, 477–484 (2008).
  60. Liu, Q., Li, W., Li, D., Feng, Y. & Tao, C. The association of interleukin-10 -1082, -819, -592 polymorphisms and tuberculosis risk. *Saudi Med. J.* **36**, 407–417 (2015).
  61. Barnes, P. F. *et al.* Cytokine production at the site of disease in human tuberculosis. *Infect. Immun.* **61**, 3482–9 (1993).
  62. Bonecini-Almeida, M. G. *et al.* Down-modulation of lung immune responses by interleukin-10 and transforming growth factor  $\beta$  (TGF- $\beta$ ) and analysis of TGF- $\beta$  receptors I and II in active tuberculosis. *Infect. Immun.* **72**, 2628–2634 (2004).
  63. Almeida, A. S. *et al.* Tuberculosis Is Associated with a Down-Modulatory Lung Immune Response That Impairs T<sub>H</sub>1-Type Immunity. *J. Immunol.* **183**, 718–731 (2009).
  64. Huard, R. C. *et al.* The *Mycobacterium tuberculosis* complex-restricted gene *cfp32* encodes an expressed protein that is detectable in tuberculosis patients and is positively correlated with pulmonary interleukin-10. *Infect. Immun.* **71**, 6871–83 (2003).
  65. Verbon, A. *et al.* Serum concentrations of cytokines in patients with active tuberculosis (TB) and after treatment. *Clin. Exp. Immunol.* **115**, 110–3 (1999).
  66. Olobo, J. O. *et al.* Circulating TNF- $\alpha$ , TGF- $\beta$ , and IL-10 in tuberculosis patients and healthy contacts. *Scand. J. Immunol.* **53**, 85–91 (2001).
  67. Gong, J. *et al.* Induced T<sub>H</sub>1 Responses and CTLA-4 Expression. *Microbiology* **64**, 913–918 (1996).
  68. Zhang, M. *et al.* T cell cytokine responses in persons with tuberculosis and human immunodeficiency virus infection. *J. Clin. Invest.* **94**, 2435–42 (1994).
  69. Rojas, R. E., Balaji, K. N., Subramanian, a & Boom, W. H. Regulation of human CD4<sup>+</sup>  $\alpha\beta$  T-cell-receptor-positive (TCR<sup>+</sup>) and  $\gamma\delta$  TCR<sup>+</sup> T-cell responses to *Mycobacterium tuberculosis* by interleukin-10 and transforming growth factor beta. *Infect. Immun.* **67**, 6461–6472 (1999).
  70. North, R. J. Mice incapable of making IL-4 or IL-10 display normal resistance to infection with *Mycobacterium tuberculosis*. *Clin. Exp. Immunol.* **113**, 55–58 (1998).
  71. Jung, Y. J., Ryan, L., Lacourse, R. & North, R. J. Increased interleukin-10 expression is not responsible for failure of T helper 1 immunity to resolve airborne *Mycobacterium tuberculosis* infection in mice. *Immunology* **109**, 295–299 (2003).
  72. Richardson, E. T. *et al.* TLR2-dependent ERK signaling in *Mycobacterium tuberculosis* -infected macrophages drives anti-inflammatory responses and inhibits T<sub>H</sub>1 polarization of responding T cells. *Infect. Immun.* **83**, IAI.00135-15 (2015).
  73. Jang, S., Uematsu, S., Akira, S. & Salgame, P. IL-6 and IL-10 Induction from Dendritic Cells in Response to *Mycobacterium tuberculosis* Is Predominantly Dependent on TLR2-Mediated Recognition. *J. Immunol.* **173**, 3392–3397 (2004).
  74. Geijtenbeek, T. B. H. *et al.* Mycobacteria Target DC-SIGN to Suppress Dendritic Cell Function. *J. Exp. Med.* **197**, 7–17 (2003).
  75. Gabryšová, L., Howes, A., Saraiva, M. & O’Garra, A. The Regulation of IL-10

- Expression. *Curr. Top. Microbiol. Immunol.* **380**, 157–190 (2014).
76. Saraiva, M. & O’Garra, A. The regulation of IL-10 production by immune cells. *Nat. Rev. Immunol.* **10**, 170–181 (2010).
  77. Hörber, S. *et al.* The atypical inhibitor of NF- $\kappa$ B, I $\kappa$ B $\zeta$ , controls macrophage interleukin-10 expression. *J. Biol. Chem.* **291**, 12851–12961 (2016).
  78. Riemann, M., Endres, R., Liptay, S., Pfeffer, K. & Schmid, R. M. The I $\kappa$ B Protein Bcl-3 Negatively Regulates Transcription of the IL-10 Gene in Macrophages. *J. Immunol.* **175**, 3560–3568 (2005).
  79. Villagra, A. *et al.* The histone deacetylase HDAC11 regulates the expression of interleukin 10 and immune tolerance. *Nat. Immunol.* **10**, 92–100 (2009).
  80. Kang, X., Kim, H.-J., Ramirez, M., Salameh, S. & Ma, X. The Septic Shock-Associated *IL-10* -1082 A >G Polymorphism Mediates Allele-Specific Transcription via Poly(ADP-Ribose) Polymerase 1 in Macrophages Engulfing Apoptotic Cells. *J. Immunol.* **184**, 3718–3724 (2010).
  81. Chandra, V. *et al.* Human *IL10* Gene Repression by Rev-erba ameliorates *Mycobacterium tuberculosis* clearance. *J. Biol. Chem.* **288**, 10692–10702 (2013).
  82. Van Den Bosch, M. W. M., Palsson-Mcdermott, E., Johnson, D. S. & O’Neill, L. A. J. LPS induces the degradation of programmed cell death protein 4 (PDCD4) to release Twist2, activating c-Maf transcription to promote interleukin-10 production. *J. Biol. Chem.* **289**, 22980–22990 (2014).
  83. Krausgruber, T. *et al.* IRF5 promotes inflammatory macrophage polarization and T<sub>H</sub>1-TH17 responses. *Nat. Immunol.* **12**, 231–238 (2011).
  84. Yee, C. S. K. *et al.* Enhanced Production of IL-10 by Dendritic Cells Deficient in CIITA. *J. Immunol.* **174**, 1222–1229 (2005).
  85. Lee, C.-G. *et al.* Interaction of Ets-1 with HDAC1 Represses IL-10 Expression in T<sub>H</sub>1 Cells. *J. Immunol.* **188**, 2244–2253 (2012).
  86. Chang, H. C. *et al.* PU.1 expression delineates heterogeneity in primary T<sub>H</sub>2 cells. *Immunity* **22**, 693–703 (2005).
  87. Zhang, Y. *et al.* Foxd3 suppresses interleukin-10 expression in B cells. *Immunology* **150**, 478–488 (2017).
  88. Lai, R. P. J., Meintjes, G. & Wilkinson, R. J. HIV-1 tuberculosis-associated immune reconstitution inflammatory syndrome. *Semin. Immunopathol.* **38**, 185–198 (2016).
  89. Barber, D. L., Mayer-Barber, K. D., Feng, C. G., Sharpe, A. H. & Sher, A. CD4 T Cells Promote Rather than Control Tuberculosis in the Absence of PD-1-Mediated Inhibition. *J. Immunol.* **186**, 1598–1607 (2011).
  90. Roca, F. J. & Ramakrishnan, L. TNF dually mediates resistance and susceptibility to mycobacteria via mitochondrial reactive oxygen species. *Cell* **153**, 521–534 (2013).
  91. Eum, S. Y. *et al.* Neutrophils are the predominant infected phagocytic cells in the airways of patients with active pulmonary TB. *Chest* **137**, 122–128 (2010).
  92. Berry, M. P. R. *et al.* An interferon-inducible neutrophil-driven blood transcriptional signature in human tuberculosis. *Nature* **466**, 973–7 (2010).
  93. Panteleev, A. V. *et al.* Severe Tuberculosis in Humans Correlates Best with Neutrophil Abundance and Lymphocyte Deficiency and Does Not Correlate with Antigen-Specific CD4 T Cell Response. *Front. Immunol.* **8**, 1–16 (2017).
  94. Lowe, D. M. *et al.* Neutrophilia independently predicts death in tuberculosis. *Eur. Respir. J.* **42**, 1752–1757 (2013).

95. Dorhoi, A. *et al.* The adaptor molecule CARD9 is essential for tuberculosis control. *J. Exp. Med.* **207**, 777–792 (2010).
96. Mishra, B. B. *et al.* Nitric oxide controls the immunopathology of tuberculosis by inhibiting NLRP3 inflammasome-dependent processing of IL-1 $\beta$ . *Nat. Immunol.* **14**, 52–60 (2013).
97. Ong, C. W. M. *et al.* Neutrophil-Derived MMP-8 Drives AMPK-Dependent Matrix Destruction in Human Pulmonary Tuberculosis. *PLoS Pathog.* **11**, 1–21 (2015).
98. Snelgrove, R., Patel, D., Patel, T. & Lloyd, C. The enigmatic role of the neutrophil in asthma: friend, foe or indifferent? *Clin. Exp. Allergy* 1–11 (2018).  
doi:doi:10.1111/cea.13191
99. Yamada, K. & Miyamoto, K. Basic Helix-Loop-Helix transcription factors BHLHB2 and BHLHB3; their gene expressions are regulated by multiple extracellular stimuli. *Front. Biosci.* 3151–3171 (2005).
100. Rossner, M. J., Dörr, J., Gass, P., Schwab, M. H. & Nave, K. A. SHARPs: Mammalian enhancer-of-split-and hairy-related proteins coupled to neuronal stimulation. *Mol. Cell. Neurosci.* **9**, 460–475 (1997).
101. Shen, M. *et al.* Molecular characterization of the novel basic helix-loop-helix protein DEC1 expressed in differentiated human embryo chondrocytes. *Biochem. Biophys. Res. Commun.* **236**, 294–8 (1997).
102. Sun, H. & Taneja, R. Stra13 expression is associated with growth arrest and represses transcription through histone deacetylase (HDAC)-dependent and HDAC-independent mechanisms. *Proc. Natl. Acad. Sci. U. S. A.* **97**, 4058–63 (2000).
103. Miyazaki, K. *et al.* Identification of functional hypoxia response elements in the promoter region of the DEC1 and DEC2 genes. *J. Biol. Chem.* **277**, 47014–47021 (2002).
104. Chen, C.-R., Kang, Y. & Massague, J. Defective repression of c-myc in breast cancer cells: A loss at the core of the transforming growth factor growth arrest program. *Proc. Natl. Acad. Sci.* **98**, 992–999 (2001).
105. Ivanova, A. V. *et al.* STRA13 interacts with STAT3 and modulates transcription of STAT3-dependent targets. *J. Mol. Biol.* **340**, 641–653 (2004).
106. Gosselin, D. *et al.* Environment Drives Selection and Function of Enhancers Controlling Tissue-Specific Macrophage Identities. *Cell* **159**, 1327–1340 (2014).
107. Lavin, Y. *et al.* Tissue-Resident Macrophage Enhancer Landscapes Are Shaped by the Local Microenvironment. *Cell* **159**, 1312–1326 (2014).
108. Lin, C.-C. *et al.* IL-1–induced Bhlhe40 identifies pathogenic T helper cells in a model of autoimmune neuroinflammation. *J. Exp. Med.* **213**, 251–271 (2016).
109. Sun, H., Lu, B., Li, R. Q., Flavell, R. A. & Taneja, R. Defective T cell activation and autoimmune disorder in Stra13-deficient mice. *Nat. Immunol.* **2**, 1040–1047 (2001).
110. Seimiya, M. *et al.* Clast5/Stra13 is a negative regulator of B lymphocyte activation. *Biochem. Biophys. Res. Commun.* **292**, 121–127 (2002).
111. Kanda, M. *et al.* Transcriptional regulator Bhlhe40 works as a cofactor of T-bet in the regulation of IFN- $\gamma$  production in iNKT cells. *Proc. Natl. Acad. Sci.* **113**, E3394–E3402 (2016).
112. Honma, S. *et al.* Dec1 and Dec2 are regulators of the mammalian molecular clock. *Nature* **419**, 841–844 (2002).
113. Ivanova, A. V., Ivanov, S. V., Danilkovitch-Miagkova, A. & Lerman, M. I. Regulation of STRA13 by the von Hippel-Lindau Tumor Suppressor Protein, Hypoxia, and the

- UBC9/Ubiquitin Proteasome Degradation Pathway. *J. Biol. Chem.* **276**, 15306–15315 (2001).
114. Martínez-Llordella, M. *et al.* CD28-inducible transcription factor DEC1 is required for efficient autoreactive CD4<sup>+</sup> T cell response. *J. Exp. Med.* **210**, 1603–19 (2013).
  115. Shen, M. *et al.* Induction of basic helix-loop-helix protein DEC1 (BHLHB2)/Stra13/Sharp2 in response to the cyclic adenosine monophosphate pathway. *Eur. J. Cell Biol.* **80**, 329–334 (2001).
  116. Yamada, K. *et al.* Gene expression of basic helix-loop-helix transcription factor, SHARP-2, is regulated by gonadotropins in the rat ovary and MA-10 cells. *Biol. Reprod.* **70**, 76–82 (2004).
  117. Yamada, K. *et al.* Insulin induces the expression of the SHARP-2/Stra13/DEC1 gene via a phosphoinositide 3-kinase pathway. *J. Biol. Chem.* **278**, 30719–30724 (2003).
  118. Nakayama, Y., Iwamoto, Y., Maher, S. E., Tanaka, Y. & Bothwell, A. L. M. Altered gene expression upon BCR cross-linking in Burkitt's lymphoma B cell line. *Biochem. Biophys. Res. Commun.* **277**, 124–127 (2000).
  119. Qian, Y., Zhang, J., Yan, B. & Chen, X. DEC1, a basic helix-loop-helix transcription factor and a novel target gene of the p53 family, mediates p53-dependent premature senescence. *J. Biol. Chem.* **283**, 2896–2905 (2008).
  120. Thin, T. H., Li, L., Chung, T. K., Sun, H. & Taneja, R. Stra13 is induced by genotoxic stress and regulates ionizing-radiation-induced apoptosis. *EMBO Rep.* **8**, 401–407 (2007).
  121. Kreslavsky, T. *et al.* Essential role for the transcription factor Bhlhe41 in regulating the development, self-renewal and BCR repertoire of B-1a cells. *Nat. Immunol.* **18**, 442–455 (2017).
  122. Wu, Y. *et al.* The BHLH transcription factor DEC1 plays an important role in the epithelial-mesenchymal transition of pancreatic cancer. *Int. J. Oncol.* **41**, 1337–1346 (2012).
  123. Boudjelal, M. *et al.* Overexpression of Stra13, a novel retinoic acid-inducible gene of the basic helix-loop-helix family, inhibits mesodermal and promotes neuronal differentiation of P19 cells. *Genes Dev.* **11**, 2052–2065 (1997).
  124. Li, Y. *et al.* DEC1 negatively regulates the expression of DEC2 through binding to the E-box in the proximal promoter. *J. Biol. Chem.* **278**, 16899–16907 (2003).
  125. Dhar, M. & Taneja, R. Cross-regulatory interaction between Stra13 and USF results in functional antagonism. *Oncogene* **20**, 4750–4756 (2001).
  126. Chung, S. Y. *et al.* Bhlhe40 Represses PGC-1 $\alpha$  Activity on Metabolic Gene Promoters in Myogenic Cells. *Mol. Cell. Biol.* **35**, 2518–2529 (2015).
  127. Qian, Y., Zhang, J., Jung, Y. S. & Chen, X. DEC1 coordinates with HDAC8 to differentially regulate TAp73 and  $\Delta$ Np73 expression. *PLoS One* **9**, (2014).
  128. Lin, C.-C. *et al.* Bhlhe40 controls cytokine production by T cells and is essential for pathogenicity in autoimmune neuroinflammation. *Nat. Commun.* **5**, 3551 (2014).
  129. Yu, F. *et al.* The transcription factor Bhlhe40 is a switch of inflammatory versus anti-inflammatory T<sub>H</sub>1 cell fate determination. *J. Exp. Med.* **215**, 1813–1821 (2018).
  130. Miyazaki, K. *et al.* The Role of the Basic Helix-Loop-Helix Transcription Factor Dec1 in the Regulatory T Cells. *J. Immunol.* **185**, 7330–7339 (2010).
  131. Lee, C. G. L., Jenkins, N. A., Gilbert, D. J., Copeland, N. G. & O'Brien, W. E. Cloning and analysis of gene regulation of a novel LPS-inducible cDNA. *Immunogenetics* **41**, 263–270 (1995).

132. Li, H. *et al.* Different Neurotropic Pathogens Elicit Neurotoxic CCR9- or Neurosupportive CXCR3-Expressing Microglia. *J. Immunol.* **177**, 3644–3656 (2006).
133. Németh, T., Futosi, K., Sitaru, C., Ruland, J. & Mócsai, A. Neutrophil-specific deletion of the CARD9 gene expression regulator suppresses autoantibody-induced inflammation in vivo. *Nat. Commun.* **7**, 1–13 (2016).
134. Degrandi, D., Hoffmann, R., Beuter-Gunia, C. & Pfeffer, K. The proinflammatory cytokine-induced IRG1 protein associates with mitochondria. *J. Interf. Cytokine Res.* **29**, 55–67 (2009).
135. Naujoks, J. *et al.* IFNs Modify the Proteome of *Legionella*-Containing Vacuoles and Restrict Infection Via IRG1-Derived Itaconic Acid. *PLoS Pathog.* **12**, e1005408 (2016).
136. Cheon, Y.-P., Xu, X., Bagchi, M. K. & Bagchi, I. C. Immune-Responsive Gene 1 Is a Novel Target of Progesterone Receptor and Plays a Critical Role during Implantation in the Mouse. *Endocrinology* **144**, 5623–5630 (2003).
137. Cho, H. *et al.* Differential innate immune response programs in neuronal subtypes determine susceptibility to infection in the brain by positive-stranded RNA viruses. *Nat. Med.* **19**, 458–464 (2013).
138. Lampropoulou, V. *et al.* Itaconate Links Inhibition of Succinate Dehydrogenase with Macrophage Metabolic Remodeling and Regulation of Inflammation. *Cell Metab.* **0**, 1–9 (2016).
139. Preusse, M., Tantawy, M. A., Klawonn, F., Schughart, K. & Pessler, F. Infection- and procedure-dependent effects on pulmonary gene expression in the early phase of influenza A virus infection in mice. *BMC Microbiol* **13**, 293 (2013).
140. Gautam, A. *et al.* Interleukin-10 alters effector functions of multiple genes induced by *Borrelia burgdorferi* in macrophages to regulate lyme disease inflammation. *Infect. Immun.* **79**, 4876–4892 (2011).
141. Shi, S. *et al.* Expression of Many Immunologically Important Genes in *Mycobacterium tuberculosis*-Infected Macrophages Is Independent of Both TLR2 and TLR4 but Dependent on IFN- Receptor and STAT1. *J. Immunol.* **175**, 3318–3328 (2005).
142. Basler, T., Jeckstadt, S., Valentin-Weigand, P. & Goethe, R. *Mycobacterium paratuberculosis*, *Mycobacterium smegmatis*, and lipopolysaccharide induce different transcriptional and post-transcriptional regulation of the IRG1 gene in murine macrophages. *J. Leukoc. Biol.* **79**, 628–638 (2006).
143. Michelucci, A. *et al.* Immune-responsive gene 1 protein links metabolism to immunity by catalyzing itaconic acid production. *Proc. Natl. Acad. Sci. U. S. A.* **110**, 7820–5 (2013).
144. Mcfadden, B. A. & Purohit, S. Itaconate, an Isocitrate Lyase-Directed Inhibitor in *Pseudomonas indigofera*. *J. Bacteriol.* **131**, 136–144 (1977).
145. Muñoz-Elías, E. J. & McKinney, J. D. *Mycobacterium tuberculosis* isocitrate lyases 1 and 2 are jointly required for *in vivo* growth and virulence. *Nat. Med.* **11**, 638–44 (2005).
146. Eoh, H. & Rhee, K. Y. Methylcitrate cycle defines the bactericidal essentiality of isocitrate lyase for survival of *Mycobacterium tuberculosis* on fatty acids. *Proc. Natl. Acad. Sci.* **111**, 4976–4981 (2014).
147. Cordes, T., Michelucci, A. & Hiller, K. Itaconic Acid: The Surprising Role of an Industrial Compound as a Mammalian Antimicrobial Metabolite. *Annu. Rev. Nutr.* **35**, 451–473 (2015).
148. Muñoz-Elías, E. J., Upton, A. M., Cherian, J. & McKinney, J. D. Role of the methylcitrate cycle in *Mycobacterium tuberculosis* metabolism, intracellular growth, and virulence.

- Mol. Microbiol.* **60**, 1109–1122 (2006).
149. Sasikaran, J., Ziemski, M., Zadora, P. K., Fleig, A. & Berg, I. A. Bacterial itaconate degradation promotes pathogenicity. *Nat. Chem. Biol.* **10**, 371–377 (2014).
  150. McKinney, J. D. *et al.* Persistence of *Mycobacterium tuberculosis* in macrophages and mice requires the glyoxylate shunt enzyme isocitrate lyase. *Nature* **406**, 735–738 (2000).
  151. Höner zu Bentrup, K., Miczak, A., Swenson, D. L. & Russell, D. G. Characterization of activity and expression of isocitrate lyase in *Mycobacterium avium* and *Mycobacterium tuberculosis*. *J. Bacteriol* **181**, 7161–7167 (1999).
  152. Hall, C. J. *et al.* Immunoresponsive Gene 1 Augments Bactericidal Activity of Macrophage-Lineage Cells by Regulating  $\beta$ -Oxidation-Dependent Mitochondrial ROS Production. *Cell Metab.* **18**, 265–278 (2013).
  153. Bambouskova, M. *et al.* Electrophilic properties of itaconate and derivatives regulate the I $\kappa$ B $\zeta$ –ATF3 inflammatory axis. *Nature* (2018). doi:10.1038/s41586-018-0052-z
  154. Li, Y. *et al.* Immune Responsive Gene 1 (IRG1) promotes endotoxin tolerance by increasing A20 expression in macrophages through reactive oxygen species. *J. Biol. Chem.* **288**, 16225–16234 (2013).
  155. Cordes, T. *et al.* Immunoresponsive gene 1 and itaconate inhibit succinate dehydrogenase to modulate intracellular succinate levels. *J. Biol. Chem.* **291**, jbc.M115.685792 (2016).
  156. Mills, E. L. *et al.* Itaconate is an anti-inflammatory metabolite that activates Nrf2 via alkylation of KEAP1. *Nature* **556**, 113–117 (2018).
  157. Uddin, M. J. *et al.* IRG1 induced by heme oxygenase-1/carbon monoxide inhibits LPS-mediated sepsis and pro-inflammatory cytokine production. *Cell. Mol. Immunol.* **13**, 170–179 (2016).
  158. Zhou, R., Yazdi, A. S., Menu, P. & Tschopp, J. A role for mitochondria in NLRP3 inflammasome activation. *Nature* **469**, 221–226 (2011).
  159. Formentini, L. *et al.* Mitochondrial ROS Production Protects the Intestine from Inflammation through Functional M2 Macrophage Polarization. *Cell Rep.* **19**, 1202–1213 (2017).
  160. Ren, K. *et al.* Suppression of IRG-1 Reduces Inflammatory Cell Infiltration and Lung Injury in Respiratory Syncytial Virus Infection by Reducing. *J. Virol.* **90**, 7313–7322 (2016).
  161. Sugimoto, M. *et al.* Non-targeted metabolite profiling in activated macrophage secretion. *Metabolomics* **8**, 624–633 (2012).
  162. Strelko, C. L. *et al.* Itaconic acid is a mammalian metabolite induced during macrophage activation. *J. Am. Chem. Soc.* **133**, 16386–16389 (2011).
  163. Murray, P. J. & Young, R. a. Increased antimycobacterial immunity in interleukin-10-deficient mice. *Infect. Immun.* **67**, 3087–3095 (1999).
  164. Feng, C. *et al.* Transgenic Mice Expressing Human Interleukin-10 in the Antigen-Presenting Cell Compartment Show Increased Susceptibility to Infection with *Mycobacterium avium* Associated with Decreased Macrophage Effector Function and Apoptosis. *Infect. Immun.* **70**, 6672–6679 (2002).
  165. Redford, P. S., Murray, P. J. & O’Garra, A. The role of IL-10 in immune regulation during *M. tuberculosis* infection. *Mucosal Immunol.* **4**, 261–270 (2011).
  166. Iyer, S. S. & Cheng, G. Role of Interleukin 10 Transcriptional Regulation in Inflammation and Autoimmune Disease. *Crit Rev Immunol.* **32**, 23–63 (2012).
  167. Maertzdorf, J. *et al.* Functional correlations of pathogenesis-driven gene expression

- signatures in tuberculosis. *PLoS One* **6**, e26938 (2011).
168. Bloom, C. I. *et al.* Transcriptional Blood Signatures Distinguish Pulmonary Tuberculosis, Pulmonary Sarcoidosis, Pneumonias and Lung Cancers. *PLoS One* **8**, e70630 (2013).
  169. Yamada, H., Mizuno, S. & Reza-Gholizadeh, M. Relative Importance of NF- $\kappa$ B p50 in Mycobacterial Infection. *Infect. Immun.* **69**, 7100–7105 (2001).
  170. Liu, F., Wu, H. Y., Wesselschmidt, R., Kornaga, T. & Link, D. C. Impaired production and increased apoptosis of neutrophils in granulocyte colony-stimulating factor receptor-deficient mice. *Immunity* **5**, 491–501 (1996).
  171. Scott, H. M. & Flynn, J. L. *Mycobacterium tuberculosis* in Chemokine Receptor 2-Deficient Mice: Influence of Dose on Disease Progression. *Infect. Immun.* **70**, 5946–5954 (2002).
  172. Ow, J. R., Tan, Y. H., Jin, Y., Bahirvani, A. G. & Taneja, R. Stra13 and Sharp-1, the non-grouchy regulators of development and disease. *Curr. Top. Dev. Biol.* **110**, 317–338 (2014).
  173. Schmidt, E. F., Kus, L., Gong, S. & Heintz, N. BAC transgenic mice and the GENSAT database of engineered mouse strains. *Cold Spring Harb. Protoc.* **8**, 200–206 (2013).
  174. Abram, C. L., Roberge, G. L., Hu, Y. & Lowell, C. A. Comparative analysis of the efficiency and specificity of myeloid-Cre deleting strains using ROSA-EYFP reporter mice. *J. Immunol. Methods* **408**, 89–100 (2014).
  175. Maynard, C. L. *et al.* Regulatory T cells expressing interleukin 10 develop from Foxp3<sup>+</sup> and Foxp3<sup>-</sup> precursor cells in the absence of interleukin 10. *Nat. Immunol.* **8**, 931–941 (2007).
  176. Helft, J. *et al.* GM-CSF Mouse Bone Marrow Cultures Comprise a Heterogeneous Population of CD11c<sup>+</sup>MHCII<sup>+</sup> Macrophages and Dendritic Cells. *Immunity* **42**, 1197–1211 (2015).
  177. Poon, G. F. T. *et al.* Hyaluronan Binding Identifies a Functionally Distinct Alveolar Macrophage-like Population in Bone Marrow-Derived Dendritic Cell Cultures. *J. Immunol.* **195**, 632–642 (2015).
  178. Heng, T. S. P. & Painter, M. W. The Immunological Genome Project: networks of gene expression in immune cells. *Nat. Immunol.* **9**, 1091–4 (2008).
  179. Kopf, M., Schneider, C. & Nobs, S. P. The development and function of lung-resident macrophages and dendritic cells. *Nat. Immunol.* **16**, 36–44 (2015).
  180. St-Pierre, B., Flock, G., Zacksenhaus, E. & Egan, S. E. Stra13 homodimers repress transcription through class B E-box elements. *J. Biol. Chem.* **277**, 46544–46551 (2002).
  181. Jones, E. A. & Flavell, R. A. Distal Enhancer Elements Transcribe Intergenic RNA in the IL-10 Family Gene Cluster. *J. Immunol.* **175**, 7437–7446 (2005).
  182. Feng, C. G. *et al.* Maintenance of pulmonary Th1 effector function in chronic tuberculosis requires persistent IL-12 production. *J. Immunol.* **174**, 4185–92 (2005).
  183. Cooper, A. & Magram, J. Interleukin 12 (IL-12) is crucial to the development of protective immunity in mice intravenously infected with *Mycobacterium tuberculosis*. *J. Exp. Med.* **186**, (1997).
  184. Holscher, C. *et al.* A Protective and Agonistic Function of IL-12p40 in Mycobacterial Infection. *J. Immunol.* **167**, 6957–6966 (2001).
  185. Bonecini-Almeida, M. G. *et al.* Down-modulation of lung immune responses by interleukin-10 and transforming growth factor beta (TGF-beta) and analysis of TGF-beta receptors I and II in active tuberculosis. *Infect. Immun.* **72**, 2628–2634 (2004).

186. Chou, C. *et al.* The Transcription Factor AP4 Mediates Resolution of Chronic Viral Infection through Amplification of Germinal Center B Cell Responses. *Immunity* **45**, 570–582 (2016).
187. Zhang, Y. *et al.* Model-based Analysis of ChIP-Seq (MACS). *Genome Biol.* **9**, R137 (2008).
188. Machanick, P. & Bailey, T. L. MEME-ChIP: Motif analysis of large DNA datasets. *Bioinformatics* **27**, 1696–1697 (2011).
189. McLean, C. Y. *et al.* GREAT improves functional interpretation of cis-regulatory regions. *Nat. Biotechnol.* **28**, 495–501 (2010).
190. Sia, J. K., Georgieva, M. & Rengarajan, J. Innate Immune Defenses in Human Tuberculosis: An Overview of the Interactions between *Mycobacterium tuberculosis* and Innate Immune Cells. *J. Immunol. Res.* **2015**, 1–12 (2015).
191. Segal, W. & Bloch, H. Biochemical Differentiation of *Mycobacterium tuberculosis* grown in vivo and in vitro. *J. Bacteriol.* **72**, 132–141 (1955).
192. Tallam, A. *et al.* Gene Regulatory Network Inference of Immunoresponsive Gene 1 (IRG1) Identifies Interferon Regulatory Factor 1 (IRF1) as Its Transcriptional Regulator in Mammalian Macrophages. *PLoS One* **11**, 1–28 (2016).
193. Howard, S. T. *et al.* Spontaneous reversion of *Mycobacterium abscessus* from a smooth to a rough morphotype is associated with reduced expression of glycopeptidolipid and reacquisition of an invasive phenotype. *Microbiology* **152**, 1581–1590 (2006).
194. Clary, G. *et al.* *Mycobacterium abscessus* Smooth And Rough Morphotypes Form Antimicrobial-Tolerant Biofilm Phenotypes But Are Killed by Acetic Acid. *Antimicrob. Agents Chemother.* **62**, AAC.01782-17 (2018).
195. Stanley, S. a., Johndrow, J. E., Manzanillo, P. & Cox, J. S. The Type I IFN response to infection with *Mycobacterium tuberculosis* requires ESX-1-mediated secretion and contributes to pathogenesis. *J. Immunol.* **178**, 3143–3152 (2007).
196. Manzanillo, P., Shiloh, M., Portnoy, D. & Cox, J. *Mycobacterium tuberculosis* activates the DNA-dependent cytosolic surveillance pathway within macrophages. *Cell Host Microbe* **11**, 469–480 (2012).
197. Cambier, C. J. *et al.* Mycobacteria manipulate macrophage recruitment through coordinated use of membrane lipids. *Nature* **505**, 218–222 (2014).
198. Edwards, K. M. *et al.* Iron-cofactored Superoxide Dismutase Inhibits Host Responses to *Mycobacterium tuberculosis*. *Am. J. Respir. Crit. Care Med.* **164**, 2213–2219 (2001).
199. Martineau, A. R. *et al.* Neutrophil-mediated innate immune resistance to mycobacteria. *J. Clin. Invest.* **117**, 1988–1994 (2007).
200. Blomgran, R. & Ernst, J. D. Lung neutrophils facilitate activation of naive antigen-specific CD4<sup>+</sup> T cells during *Mycobacterium tuberculosis* infection. *J. Immunol.* **186**, 7110–7119 (2011).
201. Lowe, D. M., Redford, P. S., Wilkinson, R. J., O’Garra, A. & Martineau, A. R. Neutrophils in tuberculosis: friend or foe? *Trends Immunol.* **33**, 14–25 (2012).
202. Dunn, M. F., Ramírez-Trujillo, J. A. & Hernández-Lucas, I. Major roles of isocitrate lyase and malate synthase in bacterial and fungal pathogenesis. *Microbiology* **155**, 3166–3175 (2009).
203. Pawlik, A. *et al.* Identification and characterization of the genetic changes responsible for the characteristic smooth-to-rough morphotype alterations of clinically persistent *Mycobacterium abscessus*. *Mol. Microbiol.* **90**, 612–629 (2013).

204. Coleman, J. L. J., Brennan, K., Ngo, T. & Balaji, P. Rapid knockout and reporter mouse line generation and breeding colony establishment using eUCoMM conditional-ready embryonic stem cells: a case study. *Front. Endocrinol.* **6**, 1–13 (2015).
205. Kanki, H., Suzuki, H. & Itohara, S. High-efficiency CAG-FLPe Deleter Mice in C57BL/6J Background. *Exp. Anim.* **55**, 137–141 (2006).
206. Williams, G. D., Pinto, A. K., Doll, B. & Boon, A. C. M. A North American H7N3 Influenza Virus Supports Reassortment with 2009 Pandemic H1N1 and Induces Disease in Mice without Prior Adaptation. *J. Virol.* **90**, 4796–4806 (2016).
207. Mugusi, F. M., Rusizoka, O., Habib, N. & Fawzi, W. Vitamin A status of patients presenting with pulmonary tuberculosis and asymptomatic HIV-infected individuals, Dar es Salaam, Tanzania. *Int. J. Tuberc. Lung Dis.* **7**, 804–807 (2003).
208. Ramachandran, G. *et al.* Vitamin A levels in sputum-positive pulmonary tuberculosis patients in comparison with household contacts and healthy ‘normals’. *Int. J. Tuberc. Lung Dis.* **8**, 1130–1133 (2004).
209. Wheelwright, M. *et al.* All-trans retinoic acid-triggered antimicrobial activity against *Mycobacterium tuberculosis* is dependent on NPC2. *J. Immunol.* **192**, 2280–90 (2014).
210. Pot, C. *et al.* Cutting Edge: IL-27 Induces the Transcription Factor c-Maf, Cytokine IL-21, and the Costimulatory Receptor ICOS that Coordinately Act Together to Promote Differentiation of IL-10-Producing Tr1 Cells. *J. Immunol.* **183**, 797–801 (2009).
211. Rutz, S. *et al.* Transcription factor c-Maf mediates the TGF- $\beta$ -dependent suppression of IL-22 production in TH17 cells. *Nat. Immunol.* **12**, 1238–1245 (2011).
212. Gabryšová, L. *et al.* C-Maf controls immune responses by regulating disease-specific gene networks and repressing IL-2 in CD4<sup>+</sup> T cells. *Nat. Immunol.* **19**, 497–507 (2018).
213. Ahyi, A.-N. N., Chang, H.-C., Dent, A. L., Nutt, S. L. & Kaplan, M. H. IFN Regulatory Factor 4 Regulates the Expression of a Subset of TH2 Cytokines. *J. Immunol.* **183**, 1598–1606 (2009).
214. Wang, Z.-Y. *et al.* Regulation of IL-10 Gene Expression in TH2 Cells by Jun Proteins. *J. Immunol.* **174**, 2098–2105 (2005).
215. Kaiser, F. *et al.* TPL-2 negatively regulates interferon- $\beta$  production in macrophages and myeloid dendritic cells. *J. Exp. Med.* **206**, 1863–1871 (2009).
216. Nguyen, D. T., Teeter, L. D., Graves, J. & Graviss, E. A. Characteristics Associated with Negative Interferon-gamma Release Assay Results in Culture-Confirmed Tuberculosis Patients, Texas, USA, 2013–2015. *Emerg. Infect. Dis.* **24**, 534–540 (2018).
217. Divangahi, M. *et al.* *Mycobacterium tuberculosis* evades macrophage defenses by inhibiting plasma membrane repair. *Nat. Immunol.* **10**, 899–906 (2009).
218. Gu, L. *et al.* Suppression of IL-12 production by tristetraprolin through blocking NF- $\kappa$ B nuclear translocation. *J. Immunol.* **191**, 3922–30 (2013).
219. Ogilvie, R. L. *et al.* Tristetraprolin mediates interferon- $\gamma$  mRNA decay. *J. Biol. Chem.* **284**, 11216–11223 (2009).
220. Guo, J., Qu, H., Chen, Y. & Xia, J. The role of RNA-binding protein tristetraprolin in cancer and immunity. *Med. Oncol.* **34**, 1–12 (2017).
221. Selmi, T. *et al.* ZFP36 stabilizes RIP1 via degradation of XIAP and cIAP2 thereby promoting ripoptosome assembly. *BMC Cancer* **15**, 1–7 (2015).
222. Stahl, M. *et al.* The Forkhead Transcription Factor FoxO Regulates Transcription of p27Kip1 and Bim in Response to IL-2. *J. Immunol.* **168**, 5024–5031 (2002).
223. Lin, L., Hron, J. D. & Peng, S. L. Regulation of NF- $\kappa$ B, TH activation, and

- autoinflammation by the forkhead transcription factor Foxo3a. *Immunity* **21**, 203–213 (2004).
224. Dejean, A. S. *et al.* Transcription factor Foxo3 controls the magnitude of T cell immune responses by modulating the function of dendritic cells. *Nat. Immunol.* **10**, 504–513 (2009).
225. Braverman, J., Sogi, K. M., Benjamin, D., Nomura, D. K. & Stanley, S. A. HIF-1 $\alpha$  is an Essential Mediator of IFN- $\gamma$ -Dependent Immunity to *Mycobacterium tuberculosis*. *J. Immunol.* **197**, 1287–1297 (2016).
226. Belton, M. *et al.* Hypoxia and tissue destruction in pulmonary TB. *Thorax* **71**, 1145–1153 (2016).
227. Khader, S. a *et al.* IL-23 and IL-17 in the establishment of protective pulmonary CD4<sup>+</sup> T cell responses after vaccination and during *Mycobacterium tuberculosis* challenge. *Nat. Immunol.* **8**, 369–77 (2007).
228. Cruz, A. *et al.* Pathological role of interleukin 17 in mice subjected to repeated BCG vaccination after infection with *Mycobacterium tuberculosis*. *J. Exp. Med.* **207**, 1609–1616 (2010).
229. Goulding, C. W. *et al.* The Structure and Computational Analysis of *Mycobacterium tuberculosis* Protein CitE Suggest a Novel Enzymatic Function. *J. Mol. Biol.* **365**, 275–283 (2007).
230. Sasseti, C. M. & Rubin, E. J. Genetic requirements for mycobacterial survival during infection. *Proc. Natl. Acad. Sci.* **100**, 12989–12994 (2003).
231. Puckett, S. *et al.* Glyoxylate detoxification is an essential function of malate synthase required for carbon assimilation in *Mycobacterium tuberculosis*. *Proc. Natl. Acad. Sci.* **114**, E2225–E2232 (2017).
232. Shen, H. *et al.* The Human Knockout Gene CLYBL Connects Itaconate to Vitamin B12. *Cell* **171**, 771–782.e11 (2017).
233. Savvi, S. *et al.* Functional characterization of a vitamin B12-dependent methylmalonyl pathway in *Mycobacterium tuberculosis*: Implications for propionate metabolism during growth on fatty acids. *J. Bacteriol.* **190**, 3886–3895 (2008).
234. Lee, W., VanderVen, B. C., Fahey, R. J. & Russell, D. G. Intracellular *Mycobacterium tuberculosis* exploits host-derived fatty acids to limit metabolic stress. *J. Biol. Chem.* **288**, 6788–6800 (2013).
235. Al-Daghri, N. M. *et al.* Association of vitamin B12 with pro-inflammatory cytokines and biochemical markers related to cardiometabolic risk in Saudi subjects. *Nutrients* **8**, 1–8 (2016).
236. Lee, Y. J., Wang, M. Y., Lin, M. C. & Lin, P. T. Associations between vitamin B-12 status and oxidative stress and inflammation in diabetic vegetarians and omnivores. *Nutrients* **8**, 118 (2016).